

Synthesis of Magnetic Carbon Nanotubes via Co-Pyrolysis of
Eucalyptus Oil with Bimetallic Ni-Fe Catalyst

Mr. Tanapat Rodruangnon



A Thesis Submitted in Partial Fulfillment of the Requirements
for the Degree of Master of Engineering in Chemical Engineering
Department of Chemical Engineering
FACULTY OF ENGINEERING
Chulalongkorn University
Academic Year 2021
Copyright of Chulalongkorn University

การสังเคราะห์ท่อนานาโนคาร์บอนที่มีคุณสมบัติแม่เหล็กด้วยวิธีโคไฟโรไลซิสของน้ำมันยูคาลิปตัส
และตัวเร่งปฏิกิริยาไบเมทัลลิกของนิกเกิลและเหล็ก



วิทยานิพนธ์นี้เป็นส่วนหนึ่งของการศึกษาตามหลักสูตรปริญญาวิศวกรรมศาสตรมหาบัณฑิต
สาขาวิชาวิศวกรรมเคมี ภาควิชาวิศวกรรมเคมี
คณะวิศวกรรมศาสตร์ จุฬาลงกรณ์มหาวิทยาลัย
ปีการศึกษา 2564
ลิขสิทธิ์ของจุฬาลงกรณ์มหาวิทยาลัย

Thesis Title	Synthesis of Magnetic Carbon Nanotubes via Co-Pyrolysis of Eucalyptus Oil with Bimetallic Ni-Fe Catalyst
By	Mr. Tanapat Rodruangnon
Field of Study	Chemical Engineering
Thesis Advisor	Professor TAWATCHAI CHARINPANITKUL, D.Eng.
Thesis Co Advisor	Kritapas Laohhasurayotin, Ph.D.

Accepted by the FACULTY OF ENGINEERING, Chulalongkorn University
in Partial Fulfillment of the Requirement for the Master of Engineering

Dean of the FACULTY OF
ENGINEERING
(Professor SUPOT TEACHAVORASINSKUN, D.Eng.)

THESIS COMMITTEE

----- Chairman
(Professor SARAWUT RIMDUSIT, Ph.D.)
----- Thesis Advisor
(Professor TAWATCHAI CHARINPANITKUL,
D.Eng.)
----- Thesis Co-Advisor
(Kritapas Laohhasurayotin, Ph.D.)
----- Examiner
(Assistant Professor CHALIDA KLAYSOM, Ph.D.)
----- External Examiner
(Assistant Professor Weerawut Chaiwat, Ph.D.)

จุฬาลงกรณ์มหาวิทยาลัย
CHULALONGKORN UNIVERSITY

รศ.ดร.โรจน์เรืองนนท์ : การสังเคราะห์ท่อนาโนคาร์บอนที่มีคุณสมบัติแม่เหล็กด้วยวิธีโคไพโรไลซิสของน้ำมันยูคาลิปตัสและตัวเร่งปฏิกิริยาไบเมทัลลิกของนิกเกิลและเหล็ก. (Synthesis of Magnetic Carbon Nanotubes via Co-Pyrolysis of Eucalyptus Oil with Bimetallic Ni-Fe Catalyst) อ.ที่ปรึกษาหลัก : ศ. ดร.รัชชัช ฐรินพาณิชกุล, อ.ที่ปรึกษาร่วม : ดร.กฤตภาส เลาหสุรโยธิน

อนุภาคนาโนคาร์บอนที่มีคุณสมบัติแม่เหล็กเป็นวัสดุนาโนชนิดหนึ่งที่น่าสนใจนำไปประยุกต์ใช้ในงานต่าง ๆ อย่างแพร่หลาย เนื่องจากมีคุณสมบัติพิเศษหลายประการ เช่น คุณสมบัติการนำไฟฟ้า คุณสมบัติเชิงกล และความเสถียรทางเคมี นอกจากนี้อนุภาคนาโนคาร์บอนที่มีคุณสมบัติแม่เหล็กยังสามารถควบคุมการใช้งานได้ง่ายด้วยสนามแม่เหล็ก จึงมีการพัฒนากระบวนการผลิตอนุภาคเพื่อให้ได้ร้อยละผลได้และคุณภาพของอนุภาคนาโนคาร์บอนที่มีคุณสมบัติแม่เหล็กที่สูงขึ้น โดยงานนี้ได้ศึกษาการปรับปรุงการสังเคราะห์อนุภาคนาโนคาร์บอนดังกล่าวโดยใช้ตัวเร่งปฏิกิริยาไบเมทัลลิกของนิกเกิลและเหล็ก โดยองค์ประกอบของนิกเกิลจากนิกเกิลไนเตรตจะถูกฝังเป็กลบนผิวของเฟอร์โรซีนซึ่งเป็นแหล่งของเหล็ก โดยตัวเร่งปฏิกิริยาแบบใหม่นี้เรียกว่าเฟอร์โรซีนที่ฝังเป็กลด้วยนิกเกิลไนเตรต (ferrocene impregnated with nickel nitrate) การสังเคราะห์อนุภาคนาโนคาร์บอนที่มีคุณสมบัติแม่เหล็กใช้น้ำมันยูคาลิปตัสซึ่งมียูคาลิปตอลเป็นองค์ประกอบหลักเป็นสารตั้งต้นคาร์บอน จากการศึกษาผลกระทบของตัวเร่งปฏิกิริยา อุณหภูมิการสังเคราะห์และสัดส่วนเชิงโมลของยูคาลิปตอลต่อตัวเร่งปฏิกิริยา พบว่าสภาวะที่เหมาะสมที่สุดต่อการสังเคราะห์ท่อนาโนคาร์บอนที่มีคุณสมบัติแม่เหล็กคือการใช้ตัวเร่งปฏิกิริยาเฟอร์โรซีนที่ฝังเป็กลด้วยนิกเกิลไนเตรตที่เตรียมจากการใช้สัดส่วนเชิงโมลของเหล็กต่อนิกเกิลที่สัดส่วนเชิงโมล 4:1 อุณหภูมิสังเคราะห์ 800 °C และใช้สัดส่วนเชิงโมลน้ำมันยูคาลิปตัสต่อตัวเร่งปฏิกิริยาที่ 5:1 สภาวะนี้ให้ร้อยละผลได้โดยน้ำหนักของผลิตภัณฑ์สูงสุดอยู่ที่ 17.1 % และความเป็นผลึกของคาร์บอน (สัดส่วน I_D/I_G) สูงสุดอยู่ที่ 0.82 และ นอกจากนั้นจากผลของ VSM ยืนยันได้ว่าอนุภาคนาโนของคาร์บอนมีคุณสมบัติแม่เหล็กแบบเฟอร์โร และพบว่าการใช้ตัวเร่งปฏิกิริยาดังกล่าวสามารถเพิ่มความเป็นผลึกของคาร์บอนเมื่อเปรียบเทียบกับการใช้เฟอร์โรซีนจาก 1.19 เป็น 0.82 อีกทั้งยังมีความเสถียรทางความร้อนของผลิตภัณฑ์เพิ่มขึ้นจากอุณหภูมิออกซิเดชันจาก 519 °C เป็น 559 °C อีกทั้งยังให้ร้อยละผลได้ของผลิตภัณฑ์ที่สูงกว่าเมื่อเปรียบเทียบกับการใช้นิกเกิลไนเตรตเป็นตัวเร่งปฏิกิริยาจาก 7.7% เป็น 17.1% และจากผล XRD ยืนยันได้ว่าอนุภาคของตัวเร่งปฏิกิริยาในผลิตภัณฑ์อนุภาคนาโนคาร์บอนที่มีคุณสมบัติแม่เหล็กเป็นแบบไบเมทัลลิกของนิกเกิลและเหล็ก

จุฬาลงกรณ์มหาวิทยาลัย
CHULALONGKORN UNIVERSITY

สาขาวิชา วิศวกรรมเคมี
ปีการศึกษา 2564

ลายมือชื่อนิสิต
ลายมือชื่อ อ.ที่ปรึกษาหลัก
ลายมือชื่อ อ.ที่ปรึกษาร่วม

6270107421 : MAJOR CHEMICAL ENGINEERING

KEYWORD Carbon nanotube, Eucalyptus oil, Ferrocene impregnated with nickel nitrate, Co-pyrolysis, Magnetic carbon nanotube

D: Tanapat Rodruangnon : Synthesis of Magnetic Carbon Nanotubes via Co-Pyrolysis of Eucalyptus Oil with Bimetallic Ni-Fe Catalyst. Advisor: Prof. TAWATCHAI CHARINPANITKUL, D.Eng. Co-advisor: Kritapas Laohhasurayotin, Ph.D.

Magnetic carbon nanotubes (MCNTs) have been specified one of the most promising nanomaterials. They have been applied in many applications due to special electrical, mechanical, and chemical properties. Additionally, magnetic carbon nanotubes could be easily handled by using magnetic field. There are many production developments for increasing in yield and quality of MCNTs. In this thesis, bimetallic Ni-Fe catalyst was investigated for its possibility to improve MCNT synthesis. Nickel content was impregnated on the surface of ferrocene which is the source of Fe content. The catalyst is called 'ferrocene impregnated with nickel nitrate'. Eucalyptus oil, which mainly contains eucalyptol, was used as carbon precursor for MCNT synthesis. Experimental investigation on influence of catalyst types, synthesis temperature, and molar ratio of eucalyptus oil to catalyst demonstrated was conducted. It was found that MCNT synthesis with the highest total mass yield of 17.1% and the highest crystallinity (I_D/I_G ratio) of 0.82 could be achieved under the condition of 4:1 ferrocene impregnated with nickel nitrate, synthesis temperature of 800 °C and 5:1 molar ratio of eucalyptus oil to catalyst. Additionally, the CNTs had ferromagnetic properties as VSM results. From experimental, ferrocene impregnated with nickel nitrate could provide higher crystallinity degree of MCNTs than use of ferrocene from 1.19 to 0.82. Thermal stability also increased from oxidation temperature of 515 °C to 559 °C. Moreover, the new catalyst also achieved higher yield than using nickel nitrate from 7.7% to 17.1%. Ni-Fe bimetallic particles in MCNT products were also observed by XRD results.

จุฬาลงกรณ์มหาวิทยาลัย
CHULALONGKORN UNIVERSITY

Field of Study: Chemical Engineering

Student's Signature

Academic 2021

.....
Advisor's Signature

Year:

.....
Co-advisor's Signature

.....

ACKNOWLEDGEMENTS

I would like to express my sincere thanks to my thesis advisor, Professor Tawatchai Charinpanitkul, D.Eng. and my thesis co-advisor, Dr, Kritapas Laohhasurayotin, PhD from Chulalongkorn University, and the National Nanotechnology Center (NANOTEC), NSTDA, respectively, for practical suggestions, helpful support, and belief in me to continue the whole course of this work.

I am grateful to Dr. Giang T. T. Le for her kind and valuable assistance. Additionally, I would like to thank all members of Prof. Tawatchai's research group for their helpful contributions I also thank all members of CEPT for their warm collaborations and teaching characterization instruments in our lab.

I also would like to thank Professor Sarawut Rimdusit, PhD. as the chairman, Assistance Professor Chalida Klaysom, PhD, and Assistance Weerawut Chaiwat, PhD as the members of the thesis committee for their comments and suggestions.

I am also thankful to Pohnpawee Nontasorn from NANOTEC for your support of characterization and useful suggestions.

Furthermore, I would like to appreciate the financial support from the Center of Excellence in Particle Technology and Material Processing (CEPT), and Ratchadapisek Somphot fund, Chulalongkorn University.

Finally, I greatly acknowledge my family for their good wishes and encouragement. I also appreciate my aunt's family for their kind support.

Tanapat Rodruangnon

TABLE OF CONTENTS

	Page
.....	iii
ABSTRACT (THAI)	iii
.....	iv
ABSTRACT (ENGLISH)	iv
ACKNOWLEDGEMENTS	v
TABLE OF CONTENTS	vi
LIST OF TABLES	x
LIST OF FIGURES	xi
CHAPTER 1 INTRODUCTION	1
1.1 Motivation.....	1
1.2 Research objective	2
1.3 Scope of this research	2
CHAPTER 2 FUNDAMENTAL KNOWLEDGE AND LITERATURE REVIEW ...	3
2.1 Carbon nanotubes	3
2.2 Synthesis of carbon nanotubes via chemical vapor deposition	4
2.3. Magnetic property of materials.....	6
2.4. Classification of magnetic properties	7
2.4.1 Diamagnetism.....	7
2.4.2 Paramagnetism	7
2.4.3 Ferromagnetism.....	7
2.4.4 Antiferromagnetism.....	7
2.4.5 Ferrimagnetism.....	8
2.2.6 Superparamagnetism	9
2.5 Literature Review	10
2.5.1 Effect of catalyst on property of resultant CNTs	10

2.5.1.1 Using of ferrocene as catalyst	10
2.5.1.2 Using of nickel nitrate as catalyst.....	12
2.5.1.3 Effect of Ni to Fe molar ratio of catalyst.....	13
2.5.1.3.1 Yield of CNTs product	14
2.5.1.3.2 Thermal stability of CNTs.....	14
2.5.1.3.3 Crystallinity of CNTs	15
2.5.2 Effect of synthesis temperature on property of resultant CNTs.....	15
2.5.2.1 Yield of CNTs product	17
2.5.2.2 Morphology of CNTs	17
2.5.2.3 Thermal stability of CNTs.....	19
2.5.2.4 Crystallinity of CNTs	21
2.5.3 Effect of carbon precursor to catalyst molar ratio on property of resultant CNTs	23
2.5.3.1 Yield of CNT product.....	24
2.5.3.2 Morphology of CNTs	24
2.5.3.3 Crystallinity of CNTs	25
2.5.4 Magnetic properties	25
2.5.4.1 Effect of synthesis temperature	25
2.5.4.2 Effect of Ni to Fe molar ratio	26
2.5.4.3 Effect of ratio of carbon precursor to catalyst	28
CHAPTER 3 EXPERIMENTAL.....	29
3.1 Material and chemicals	29
3.2 Procedure	29
3.2.1 Catalyst preparation.....	29
3.2.2 Magnetic carbon nanotube synthesis.....	29
3.3 Characterization	30
3.4 Computational fluid dynamics modeling.....	35
CHAPTER 4 RESULTS AND DISCUSSION.....	37
4.1 Physical properties of catalysts.....	37

4.1.1 Catalyst characterization	38
4.2 Effect of catalyst on resultant MCNTs	40
4.2.1 Morphology of CNTs synthesized from eucalyptus oil and different catalyst.....	40
4.2.2 Thermal stability of MCNTs synthesized from eucalyptus oil and different catalyst	43
4.2.3 Crystallinity of MCNTs synthesized from eucalyptus oil and different catalyst.....	45
4.2.4 Total mass yield of MCNTs synthesized from eucalyptus oil and different catalyst.....	46
4.2.5 Magnetic properties of MCNTs synthesized from eucalyptus oil.....	49
4.3 Effect of synthesis temperature on property of CNTs synthesized from eucalyptus oil and 1:1 ferrocene impregnated with nickel nitrate.....	52
4.3.1. Morphology of MCNTs synthesized from eucalyptus oil and 1:1 ferrocene impregnated with nickel nitrate.....	53
4.3.2 Thermal stability of MCNTs synthesized from eucalyptus oil and 1:1 ferrocene impregnated with nickel nitrate.....	55
4.3.3 Crystallinity of MCNTs synthesized from eucalyptus oil and 1:1 ferrocene impregnated with nickel nitrate.....	57
4.3.4 Total mass yield of MCNTs synthesized from eucalyptus oil and 1:1 ferrocene impregnated with nickel nitrate.....	58
4.3.5 Magnetic properties of MCNTs synthesized from eucalyptus oil and 1:1 ferrocene impregnated with nickel nitrate.....	60
4.4 Effect of eucalyptus oil to catalyst molar ratio on resultant MCNTs	63
4.4.1 Morphology of MCNTs synthesized from different molar ratio of eucalyptus oil to 4:1 ferrocene impregnated nickel nitrate	63
4.4.2 Thermal stability of MCNTs synthesized from different molar ratio of eucalyptus oil to 4:1 ferrocene impregnated with nickel nitrate	67
4.4.3 Crystallinity of MCNTs synthesized from different molar ratio of eucalyptus oil to 4:1 ferrocene impregnated with nickel nitrate	69
4.4.4 Total mass yield of MCNTs synthesized from different molar ratio of eucalyptol to 4:1 ferrocene impregnated with nickel nitrate.....	70

4.4.5 Magnetic properties of MCNTs synthesized from different molar ratio of eucalyptus oil to 4:1 ferrocene impregnated with nickel nitrate	76
CHAPTER 5 CONCLUSIONS AND RECOMMENDATIONS	79
5.1 Conclusions.....	79
5.1.1 Effect of catalyst.....	79
5.1.2 Effect of synthesis temperature	80
5.1.3 Effect of molar ratio of eucalyptus oil to catalyst	80
5.2 Recommendations.....	81
REFERENCES	82
APPENDICES	88
APPENDIX A Eucalyptus Oil Specification.....	89
APPENDIX B Preparation of Ferrocene Impregnated with Nickel Nitrate	90
APPENDIX C Total Mass Yield of Synthesized CNTs	93
APPENDIX D CNT Diameter Distribution.....	99
APPENDIX E Calculation of Outlet Gas Flowrate from Reactor	107
APPENDIX F Effect of Fe to Ni Molar Ratio on Resultant CNTs	110
APPENDIX G Inlet Gas Volumetric Flowrate Calculation	118
VITA.....	120

LIST OF TABLES

	Page
Table 1 Properties of CNTs [18, 20].....	4
Table 2 A summary of the different types of magnetic properties [33].....	9
Table 3 Composition of Fe, Ni, and C, and saturation magnetization of the Ni-Fe-Carbon nanocapsules [49].....	28
Table 4 Element content of eucalyptus oil.....	29
Table 5 Space time of different molar ratio of eucalyptus oil to catalyst	72



LIST OF FIGURES

	Page
Fig. 1 Single-walled carbon nanotube and Multi-walled carbon nanotube [19].....	3
Fig. 2 Schematic diagram of a CVD setup in its simplest form	5
Fig. 3 CNT growth mechanism models: a) tip growth model and b) base growth model [23].....	5
Fig. 4 Example of hysteresis loop [25]	6
Fig. 5 Size-dependent magnetic domain structures from superparamagnetism to single-domain and multidomain ferromagnetism [35]	10
Fig. 6 FESEM images of as-synthesized CNTs from a) pyrolysis of ferrocene and b) co-pyrolysis of ferrocene and cyclohexane [36].....	11
Fig. 7 Morphology of CNTs synthesized from a) only ferrocene and b) ferrocene and camphor [37].....	12
Fig. 8 FESEM images of morphology of a) CNTs_1 and b) CNTs_2 [38].....	13
Fig. 9 TGA and DTG plots of CNTs which were synthesized by use of different molar ratio of Ni to Fe catalyst [41].....	15
Fig. 10 Raman analysis of the CNTs from 1:3, 1:2, 1:1, 2:1, and 3:1 Ni to Fe molar ratio of catalyst [39]	15
Fig. 11 Morphology of CNTs at various synthesis temperature a) 700 °C, b) 800 °C, and 900 °C [19].....	17
Fig. 12 SEM images of CNTs which was synthesized at a) 750 °C, b) 850 °C, and c) 950 °C [43].....	18
Fig. 13 FESEM images of CNTs which was synthesized at a) 700 °C, b) 800 °C, and c) 900 °C [36]	19
Fig. 14 DTG plots of as-synthesized CNTs at various synthesis temperature [19].....	20
Fig. 15 TGA curves of CNTs which were synthesized from different synthesis temperature [43].....	20
Fig. 16 Raman spectra of CNTs which were synthesized at synthesis temperature of a) 700 °C, b) 800 °C, and c) 900 °C [19].....	21
Fig. 17 Raman spectra of CNTs which were synthesized in synthesis temperature range of 700 °C to 900 °C [44].....	22

Fig. 18 Raman spectra of CNTs which were synthesized from synthesis temperature of 700 °C, 800 °C, and 900 °C [36]	23
Fig. 19 FESEM images of CNTs synthesized by different molar ratio of C ₂ H ₂ to catalyst a) 1.3:1, b) 1.9:1, and c) 3.2:1 [45]	24
Fig. 20 FESEM images of CNTs synthesized by different molar ratio of C ₂ H ₂ to catalyst a) 3.5:1, b) 4.9:1, and c) 6.3:1 [46]	25
Fig. 21 Raman spectra of CNTs which were synthesized by different molar ratio of C ₂ H ₂ to catalyst [45]	25
Fig. 22 Magnetization vs magnetic field curves of Ni and Ni-Fe alloy nanoparticles for different composition at 27 °C a) in a whole range and b) magnified range -75 -75 Oe [13]	27
Fig. 23 Magnetization vs temperature curves of Ni and Ni-Fe alloy nanoparticles for different composition [13]	27
Fig. 24 The experimental set up for synthesizing MCNTs	30
Fig. 25 X-ray diffractometer	31
Fig. 26 Fourier transform infrared spectroscopy	31
Fig. 27 Energy-dispersive spectroscopy	32
Fig. 28 X-ray fluorescence	32
Fig. 29 Scanning electron microscope	33
Fig. 30 Raman spectroscopy	33
Fig. 31 Thermogravimetric analyzer	34
Fig. 32 Vibrating sample magnetometer	35
Fig. 33 2-D simulation domain and its boundary condition: a) nitrogen gas inlet, b) eucalyptus oil inlet, and c) outlet	36
Fig. 34 a) Overall and b) inset of meshed geometry	36
Fig. 35 Camera images of catalysts a) ferrocene, b) nickel nitrate, and c) 1:1 ferrocene impregnated with nickel nitrate	38
Fig. 36 XRD spectra of ferrocene, nickel nitrate, 1:1 ferrocene impregnated with nickel nitrate	39
Fig. 37 FTIR spectra of ferrocene, nickel nitrate, 1:1 ferrocene impregnated with nickel nitrate	40

Fig. 38 SEM images of morphology of as-synthesized CNTs from co-pyrolysis of eucalyptus oil with different catalyst: a) CNT_F1N0, b) CNT_F1N1, and c) CNT_F0N1	41
Fig. 39 CNT diameter distribution of a) CNT_F1N0, b) CNT_F1N1, and c) CNT_F0N1	43
Fig. 40 a) TGA and b) DTG curves of as-synthesized CNTs from co-pyrolysis with eucalyptus oil and different catalyst	44
Fig. 41 Raman spectra of CNTs synthesized by use of different catalyst	46
Fig. 42 Total mass yield of as-synthesized CNTs from different catalyst.....	47
Fig. 43 XRD patterns of synthesized CNTs from different catalyst.....	49
Fig. 44 Photograph of resultant product responding to magnetic field.....	50
Fig. 45 Magnetic hysteresis loops of as-synthesized CNTs from different catalyst at room temperature in a) a whole range and b) magnified range of -300 G to 300 G....	51
Fig. 46 The temperature profiles of quartz tube reactor at each synthesis temperature	52
Fig. 47 SEM images of as-synthesized MCNTs at synthesis temperature of a) 700 °C, b) 800 °C, and c) 900 °C.....	53
Fig. 48 CNT diameter distribution of as-synthesized MCNTs at synthesis temperature of a) 700 °C, b) 800 °C, and c) 900 °C	55
Fig. 49 a) TGA curves and b) DTG curves of as-synthesized MCNTs from different synthesis temperature.....	57
Fig. 50 Raman spectra of as-synthesized MCNTs at different synthesis temperature	58
Fig. 51 Relationship of total mass yield and outlet gas flowrate on synthesis temperature	59
Fig. 52 XRD patterns of as-synthesized MCNTs from different synthesis temperature	60
Fig. 53 Magnetic hysteresis loops of as-synthesized MCNTs from different synthesis temperature at room temperature in a) a whole range and b) magnified range of -200 G to 200 G.....	62
Fig. 54 SEM images of morphology of carbon products synthesized from different molar ratio of eucalyptus oil to catalyst: a) 2:1, b) 5:1, and c) 10:1	64
Fig. 55 CNT diameter distributions of as-synthesized products by use of different eucalyptus oil to catalyst molar ratio of a) 5:1 and b) 10:1	65

Fig. 56 Outlet gas flowrate from the reactor at different molar ratio of eucalyptus oil to catalyst	66
Fig. 57 a) TGA curves and b) DTG curves of as-synthesized carbon from different molar ratio of eucalyptus oil to catalyst.....	68
Fig. 58 Raman spectra of as-synthesized carbon from different molar ratio of eucalyptus oil to catalyst.....	70
Fig. 59 Total mass yield of as-synthesized carbon products from different eucalyptus oil to catalyst molar ratio	71
Fig. 60 Contour of velocity magnitude (10^{-2} m/s) at eucalyptus oil to catalyst molar ratio of a)-b) 5:1 and c)-d) 10:1	73
Fig. 61 Contour of eucalyptus oil volume fraction at eucalyptus oil to catalyst molar ratio of a)-b) 5:1 and c)-d) 10:1	74
Fig. 62 Magnetic hysteresis loops of as-synthesized carbon from different molar ratio of eucalyptus oil to catalyst at room temperature in a) a whole range and b) magnified range of -300 G to 300 G	77

CHAPTER 1

INTRODUCTION

1.1 Motivation

Recently, there has been much interest in magnetic nanoparticles in nanotechnology. Different magnetic properties have been employed in various applications such as analytical chemistry, bio-sensing, and nanomedicine. For instance, ferromagnetism and superparamagnetism were conducted. Ferromagnetism is the strongest type and is responsible for the common phenomenon of magnetism in magnets encountered in everyday life. The materials can be magnetized by an external magnetic field and remain magnetized after the external field is removed. Ferromagnetism is crucial in industry, modern technology, many electrical and electromechanical devices such as electromagnets, electric motors, generators, transformers, magnetic storage, and so on [1].

On the other hand, superparamagnetic materials have high magnetic susceptibility in a magnetic field and then lose their magnetization completely after the magnetic field is removed. These properties have attracted biomedical applications such as magnetic resonance imaging, drug delivery, protein separation, and others [2]. Therefore, the preparation and functionalization of magnetic nanomaterials to obtain either ferromagnetism or superparamagnetism for different specific applications have attracted intensive studies.

However, magnetic nanoparticles have some disadvantages. They are easy to agglomerate due to their small size and unstable because of the active surface [3]. Surface coating is an efficient strategy to improve the stability and expand the application of magnetic materials. During the past years, numerous materials have been developed as the protective layer such as chitosan [4], silica [5], or carbon [6].

Among various shell layer materials, carbon shell has attracted significant interest in recent years due to its easy functionalization and acid-base stability. Magnetic carbon nanoparticles (MCNPs) are either embedded in an amorphous carbon matrix or encapsulated by crystalline carbon such as carbon nanotubes (CNTs). The carbon layer provides oxidation resistance to bare metal nanoparticles and isolates the magnetic particles from each other, thus avoiding problems resulting from interactions among closely compacted magnetic particles [7, 8]. In particular, the carbon-encapsulated magnetic nanoparticles with the core-shell structure are of great technological importance because the encapsulated species can be immunized against environmental degradation effects [9] and because the structure offers an opportunity to study the dimensionally confined systems.

Several methods from many researchers have been provided to synthesize efficient CNTs. For reducing many steps and complex synthesis, the one-step process is one of the interesting alternative methods to synthesize CNTs. A simple technique to synthesize CNTs is chemical vapor deposition or co-pyrolysis with carbon precursors and metal catalysts. This method provides easy operation and the possibility of mass

production [10]. The properties of CNTs depend on the raw materials and catalysts used in the synthesis.

Among various catalysts, Ni-Fe bimetallic be used as a good performance catalyst for CNT synthesis and obtained good quality of CNTs [11, 12]. They also possess extremely high magnetic permeability, low coercivity, and nominal core losses with low remanence [13-15]. Therefore, it has been widely applied in electronic devices and industry, for example, shielding of electromagnetic interference, sensor, thin-film applications, and so on. This work prepared a new catalyst by wet impregnating nickel nitrate solution onto pure ferrocene.

Eucalyptus oil is one of the attractive carbon sources for the CNT production because it comes from a natural source that is bio-circular, low toxicity, and renewable. Next, there is high carbon content because eucalyptus oil consists of eucalyptol, the main component, and various other hydrocarbon compounds [16].

In this work, magnetic carbon nanotubes (MCNTs) were synthesized by co-pyrolysis of eucalyptus oil and ferrocene impregnated with nickel nitrate was used as new catalyst, and easily synthesized from ferrocene and nickel nitrate hexahydrate in ethanol solution. The as-synthesized MCNTs also possesses magnetic property due to the presence of Ni and Fe in the catalyst. The effects of synthesis temperature, catalyst, and molar ratio of eucalyptus oil to catalyst on characterization of all MCNT samples were investigated and discussed.

1.2 Research objective

This research aims to investigate the quality of carbon products and magnetic properties of MCNTs synthesized via co-pyrolysis of eucalyptus oil and ferrocene impregnated with nickel nitrate under designated synthesizing conditions which are synthesis temperature, catalyst, and eucalyptus oil to catalyst molar ratio.

1.3 Scope of this research

The scope of this research was designed to cover 3 main parts: the synthesis of MCNTs via co-pyrolysis of eucalyptus oil and catalyst. The effect of synthesis temperature, catalyst, and molar ratio of eucalyptus oil to catalyst on CNT synthesis and its magnetic property.

1.3.1. Study effect of catalyst: Ferrocene, Nickel nitrate, Ferrocene impregnated with nickel nitrate which were 4:1 and 1:1 molar ratio of Fe to Ni

1.3.2. Study effect of synthesis temperature: 700 °C, 800 °C, and 900 °C

1.3.3. Study effect of molar ratio of eucalyptus oil to catalyst: 2:1, 5:1, and 10:1

CHAPTER 2

FUNDAMENTAL KNOWLEDGE AND LITERATURE REVIEW

2.1 Carbon nanotubes

CNTs are cylindrical large molecules consisting of a hexagonal arrangement of sp^2 hybridized carbon atoms, which may be formed by rolling up a single sheet of graphene (single-walled carbon nanotubes, SWCNTs) or by rolling up multiple sheets of graphene (multi-walled carbon nanotubes, MWCNTs) [17, 18]. Both are shown in **Fig. 3** and their properties are illustrated in **Table 1**.

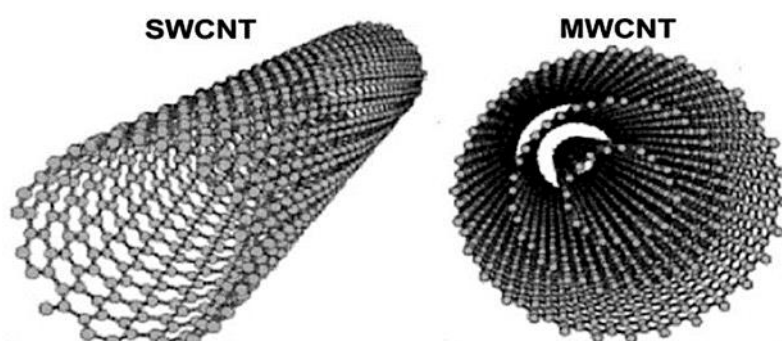


Fig. 1 Single-walled carbon nanotube and Multi-walled carbon nanotube [19]

CNTs are recognized as a promising material because they exhibit several properties. They are promising materials for mechanical applications due to their superior mechanical properties. In theory, they are the most resistant fibers with a Young modulus of 2.8–3.6 TPa and 1.7–2.4 TPa for SWCNTs and MWCNTs, respectively, and can be bent several times at 90° without undergoing structural changes, and their structure is not easily changed even high pressure (over 1.5 GPa) [18, 20].

The nano-tubular carbon has low heat capacity and high thermal conductivity. Indeed, experimental measurements on single CNTs indicate a thermal conductivity higher than that of diamonds, in the range between 3,000 and 3,500 W/mK. This property is useful in electrical applications since it reduces thermal dissipation and may be exploited to produce thermally conductive composites [21].

CNTs are also interesting as microporous materials. The presence of a pore decreases the density of CNTs and increases their surface area, making them useful as electrodes in energy storage for portable electronic devices. CNTs are good sorbents for gases and therefore they have been proposed for hydrogen storage [21], and also as catalyst supports have been observed due to their properties which turn out CNT attractive and competitive. The tubular morphology of CNTs allows combining the low electrical resistivity and high porosity. CNTs allow high accessibility of the active phase and the absence of any micro-porosity diminish the mass transfer limitations due to the hindrance of the accessibility of the reactants to the active phase [22].

Table 1 Properties of CNTs [18, 20]

Properties	SWCNT	MWCNT
Density (g/cm ³)	0.8	1.8
Electrical conductivity (S/cm)	10 ² -10 ⁶	10 ³ -10 ⁵
Thermal conductivity (W/mK)	3,000-3,500	3,000-3,500
Strength (GPa)	50-500	10-60
Elastic Modulus (TPa)	2.8-3.6	1.7-2.4
Thermal stability (°C in air)	400-600	400-600
Surface area (m ² /g)	400-900	200-400

2.2 Synthesis of carbon nanotubes via chemical vapor deposition

There are many methods of carbon nanotube synthesis. Laser ablation, arc-discharge, and chemical vapor deposition (CVD) are common. The major advantage of the two first methods is that it is possible to produce nanotubes with a high degree of crystallinity, which leads to superior electrical and mechanical properties. This is due to the high temperature at which the process operates (above 2,000 K), the major drawback is that the nanotubes have to be separated from other carbon products and catalyst residue [22].

CVD or co-pyrolysis process is a more popular method for the synthesis of CNTs because it offers a promising route to bulk production of high-purity nanotubes. This is a simple technique, controllable growth parameters, several carbon sources, and mild conditions (low temperature and ambient pressure). Therefore, co-pyrolysis is the most popular method of CNTs at present [23].

Many hydrocarbon, oil, and organic compounds can be used as carbon sources for the method, and many transition-metal compounds are also frequently used as catalysts. The reactants were decomposed with an inert gas that was purged through the reactor. A tubular reactor was heated by an energy source to decompose the precursor for the CNTs' nucleation and growth on the internal tubular tube as shown in **Fig. 4**. The product was coated substrates in the hot zone of the reactor to catalyze the growth. Finally, the hybrid is collected at room temperature [22, 23].

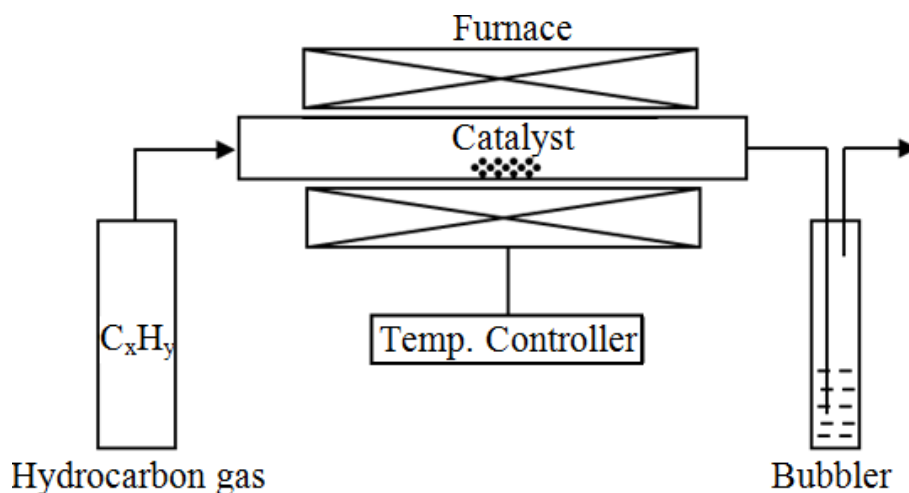


Fig. 2 Schematic diagram of a CVD setup in its simplest form

In mechanism of CNT synthesis, Vapor-solid-solid model is the widely accepted CNT formation model proposed by Persson et al. [24] CNT growth mechanism is shown in **Fig 3** [23]. The growth model can be described in 4 steps. First, the decomposition gas of carbon sources or hydrocarbon gas is transferred to catalyst surface by precipitation of decomposed gas or carrier gas. Next, hydrocarbon gases decompose into carbon atom on catalyst surface and diffuse into the catalyst. Following step is CNTs elevated the edge of catalyst with 2 main types of models: tip growth model and base growth model. For tip growth model, CNTs grow under catalyst due to the weak interaction between catalyst and substrate. In contrary, base growth model demonstrates the growth of CNTs above catalyst due to strong interaction of catalyst and substrate. Finally, CNT growth will terminate when metal catalysts is deactivated from full of carbon.

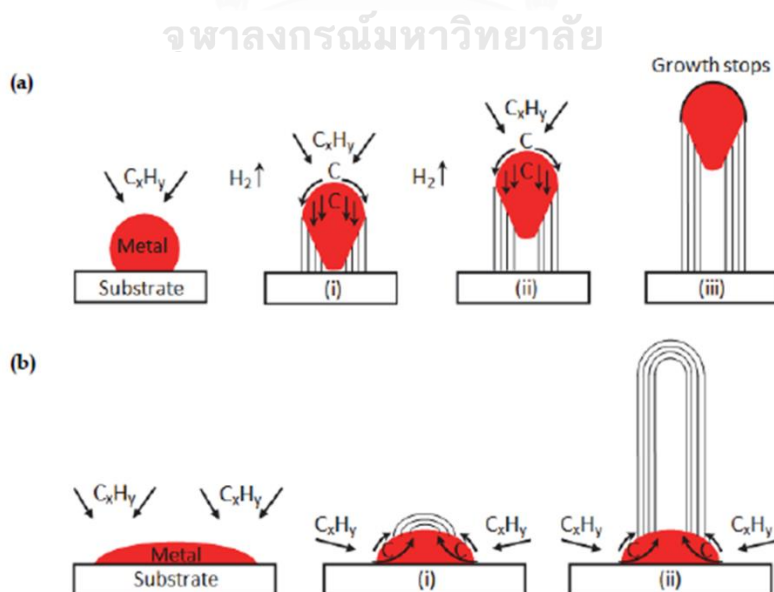


Fig. 3 CNT growth mechanism models: a) tip growth model and b) base growth model [23]

2.3. Magnetic property of materials

A great deal of information can be learned about the magnetic properties by studying its hysteresis loop, as shown in **Fig. 4**. It is a plot of magnetization M (or flux density B) as a function of magnetic field H . For example, when a material is magnetized in one direction, it will not back to zero magnetization when the magnetic field is removed. This hysteresis is related to the existence of magnetic domains in the material. Once the magnetic domains are reoriented, it takes some energy to return them to their initial magnetization.

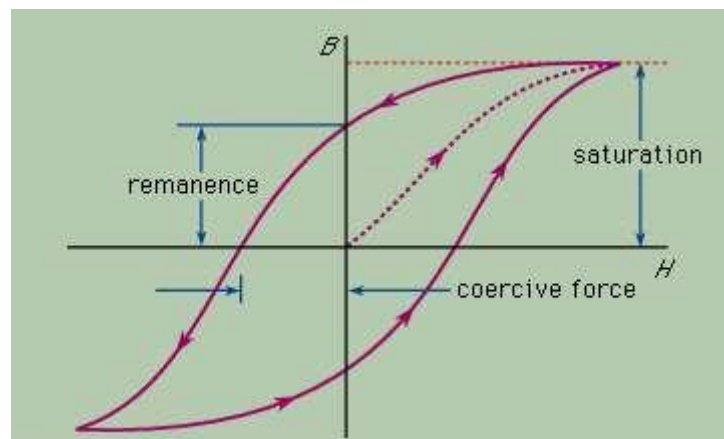


Fig. 4 Example of hysteresis loop [25]

The critical parameters of the loop are the remanence (M_r), the coercive force or coercivity (H_c), and the saturation magnetization (M_s). The saturation magnetization is the maximum value of magnetization. It only depends on the number of spin moments within the sample. The M_r is the magnitude of the magnetization after an applied field is reduced to zero. M_r is an extrinsic quantity that depends on microstructure and shape. The H_c is the field required to return the sample's magnetization from saturation to zero. Squareness is also a measure of the degree to which the shape of a hysteresis loop is approximated by a rectangle, and is a dimensionless quantity between 0 and 1, defined by the ratio M_r/M_s [26, 27].

Materials with a low M_r and H_c are referred to as soft magnetic materials, while opposite parameters occur in hard materials. There are considerable variations in the hysteresis of different magnetic materials. It is known that the area within the hysteresis loop is the energy dissipated in one cycle. Thus, a narrow hysteresis loop indicates a small amount of dissipated energy in repeatedly reversing the magnetization that is desired for systems such as motor cores to minimize the energy dissipation. A wide loop represents the situation where a large fraction of the saturation field retains when the driving field is removed. This is desirable for magnetic recording and memory devices [28].

2.4. Classification of magnetic properties

The magnetic properties depend on orbital and spin motions of electrons, and how the electrons interact with each other. An excellent way to introduce the different types of magnetism is to describe how materials respond to the magnetic field. The main difference is that there is no collective interaction of atomic magnetic moments in some materials. In contrast, there is a strong interaction between atomic moments in other materials. There are six major groups based on a magnetic behavior of a material as follows:

2.4.1 Diamagnetism

Diamagnets have a negative magnetic susceptibility, or the magnetization and magnetic field are opposite. The electrons in the atoms of diamagnetic materials are all paired, and there is no spin magnetic moment. When a material is placed into a magnetic field, its atoms acquire an induced magnetic moment pointing in a direction opposite to the external field and the material becomes magnetic. Even though it is composed of atoms that have no net magnetic moment, it reacts in a particular way to an applied field [29].

2.4.2 Paramagnetism

Paramagnets have a weak positive magnetic susceptibility, and their atoms usually have unpaired electrons of the same spin. All the magnetic moments of the electrons in their atoms do not demagnetize, and each atom has a magnetic moment. The materials have a permanent magnetic moment and can interact with a magnetic field. An external magnetic field tends to align the magnetic moments in the direction of the applied field. However, thermal motion tends to randomize the directions [29].

2.4.3 Ferromagnetism

Ferromagnetism is the basic property by which certain materials form permanent magnets. In ferromagnetic materials, electrons of atoms are grouped into “magnetic domains” in which each domain has the same charge. These domains line up so that charges are parallel throughout the compound when placed in an external magnetic field. Although the field is removed, the materials still show permanent magnetic properties. Whether a compound can be ferromagnetic or not depends on its number of unpaired electrons and its atomic size [30].

2.4.4 Antiferromagnetism

In an antiferromagnet, there is a tendency for the spin magnetic moments of neighboring valence electrons to point in opposite directions, unlike a ferromagnet. When all atoms are arranged in a substance, each neighbor is anti-parallel. Antiferromagnets have a zero net magnetic moment, meaning that no field is produced. They are less common compared to the other types of properties and mostly observed at low temperatures [31].


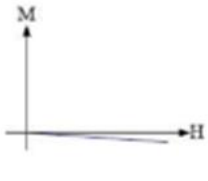
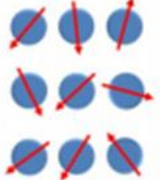
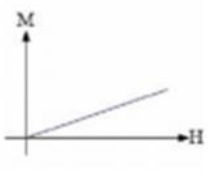
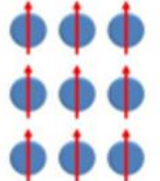
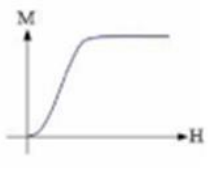
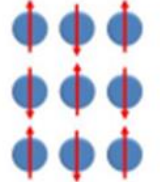
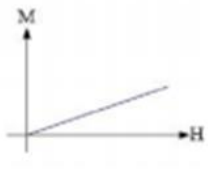
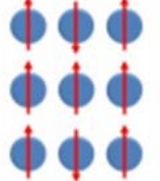
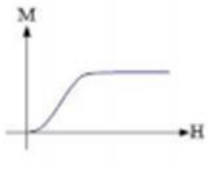
2.4.5 Ferrimagnetism

Ferrimagnets retain their magnetization in the absence of a field. However, like antiferromagnets, neighboring pairs of electron spins tend to point in opposite directions. These two properties are not in contrast because there is more magnetic moment from the sub-lattice of electrons that point in one direction, than from the sub-lattice that points in the opposite direction [32].

The summary of the previous magnetic properties shows in **Table 2**.



Table 2 A summary of the different types of magnetic properties [33]

Type	Example	Atomic / Magnetic behavior		
Diamagnetism	Inert gases; many metals Au, Cu, Hg; non-metallic elements B, Si, P, S; ions Na ⁺ , Cl ⁻ ; molecules H ₂ , N ₂ ; H ₂ O	Atoms have no magnetic moment. Susceptibility is small and negative, -10^{-6} to -10^{-5}		
Paramagnetism	Some metals Al, some diatomic gases O ₂ , NO; ions of transition metals and rare earth metals; rare earth oxides	Atoms have randomly oriented magnetic moments. Susceptibility is small and positive, 10^{-5} to 10^{-3}		
Ferromagnetism	Transitions metals Fe, H, Co, Ni, alloys of ferromagnetic elements; some alloys of Mn, MnBi, Cu ₂ MnAl	Atoms have parallel aligned magnetic moments. Susceptibility is large (below T_c)		
Anti-ferromagnetism	Transition metals Mn, Cr and many of their compounds, MnO, CoO, NiO, Cr ₂ O ₃ , MnS, MnSe	Atoms have antiparallel aligned magnetic moments. Susceptibility is small and positive 10^{-5} to 10^{-3}		
Ferrimagnetism	Fe ₃ O ₄ (magnetite); mixed oxides of iron and other elements such as Sr ferrite	Atoms have mixed parallel and antiparallel aligned magnetic moments. Susceptibility is large (below T_c)		

2.2.6 Superparamagnetism

Superparamagnet is a form of magnetism that appears in small ferromagnetic or ferrimagnetic nanoparticles. They display a strong paramagnetic nature for sufficiently small nanoparticles with high M_s and magnetic susceptibility under the influence of an externally applied magnetic field. Moreover, these nanoparticles might lose their magnetization completely when the magnetic field is removed, which results in zero H_c and remanence magnetization. The relationship between H_c and magnetic material size is shown in **Fig. 5**.

It is well established that bulk ferromagnetic and ferrimagnetic materials are composed of small magnetic domains. These magnetic domains resulted from a balance

of energy terms. The 2 main terms are external magnetostatic energy that tries to eliminate the magnetization and domain wall energy that tries to orient the magnetization in the same direction. In each domain, the magnetic moments of atoms are aligned in one direction giving a net magnetization of each domain. The magnetization directions of the domains are different [34, 35].

If the material sizes have a critical diameter (d_s) below which the materials cannot further into domains and are called “single domain particles”. They have no domain walls, so the magnetization will be reserved through spin rotation rather than through the motion of domain walls. This results in large H_c and maximum at d_s . However, the H_c will be decreased, and the H_c becomes zero at superparamagnetic diameter (d_{spm}). The magnetic moments in single-domain particles with very small volumes are prone to directional changes [34, 35].

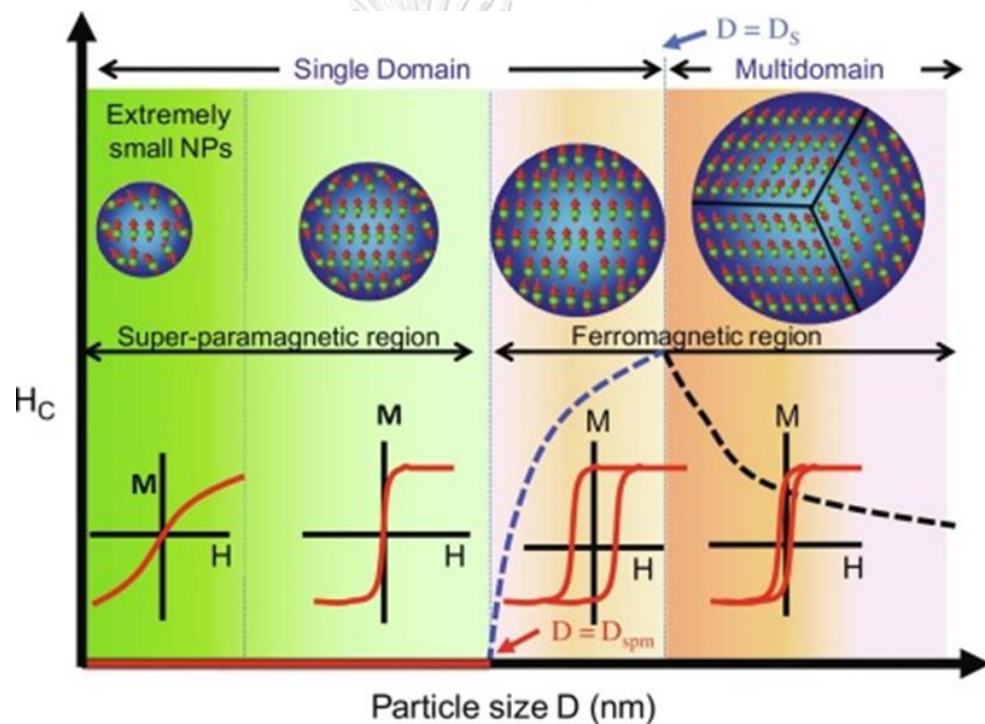


Fig. 5 Size-dependent magnetic domain structures from superparamagnetism to single-domain and multidomain ferromagnetism [35]

2.5 Literature Review

2.5.1 Effect of catalyst on property of resultant CNTs

2.5.1.1 Using of ferrocene as catalyst

Srisrattha et al. was synthesized CNTs by CVD method by use of a quartz tube reactor with outer diameter of 2.6 cm and 120 cm length. Ferrocene was used as carbon precursor and catalyst. Cyclohexane was injected as carbon precursor. N_2 was used as carrier gas with a flowrate of $21 \text{ cm}^3/\text{min}$. In their experiment, they fixed 1 g of ferrocene in CNT production at $800 \text{ }^\circ\text{C}$ synthesis temperature. Molar ratio of

cyclohexane to ferrocene was 10:1. The process time was 30 min. FESEM image of CNTs which were synthesized from ferrocene only is shown in **Fig. 6a**. The CNTs were short tubular structure. When cyclohexane was used to co-pyrolysis with ferrocene for CNT synthesis, their morphology was well-align nanotubes as FESEM images in **Fig. 6b**. The additional carbon source could help production of well-align and long CNTs.

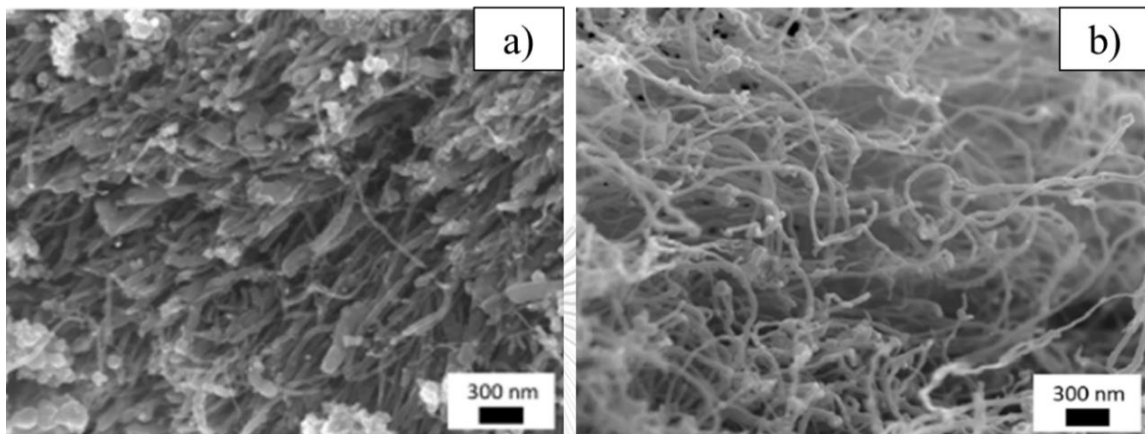


Fig. 6 FESEM images of as-synthesized CNTs from a) pyrolysis of ferrocene and b) co-pyrolysis of ferrocene and cyclohexane [36]

Wulan and Setiawati [37] synthesized CNTs by CVD method by use of vertical stainless-steel type 316 reactor. Ferrocene was used as carbon precursor and catalyst. Camphor was used as carbon precursor. In their experiment, they were fixed total weight of ferrocene and camphor. CNTs were synthesized from ferrocene only. SEM image of morphology of CNTs was unclear of tubular structure with irregular shape particles as shown in **Fig. 7a**. However, morphology of CNTs from co-pyrolysis of ferrocene and camphor was clear growth of CNT structure as shown in **Fig. 7b**. The cause of unclear structure was larger Fe clusters from high amount of ferrocene decomposition which then aggregated and grew into larger clusters with weaker catalytic effect than the smaller clusters.

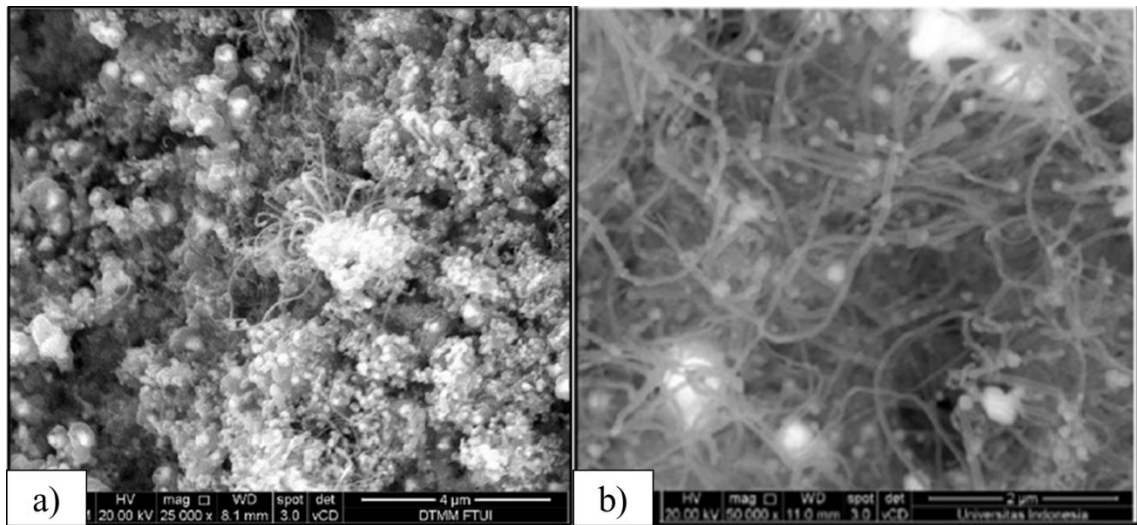


Fig. 7 Morphology of CNTs synthesized from a) only ferrocene and b) ferrocene and camphor [37]

2.5.1.2 Using of nickel nitrate as catalyst

Mitina et al. [38] was synthesized CNTs by CVD method using quartz tube reactor. Ethanol was used as carbon precursor. Nickel nitrate hexahydrate was used as Ni catalyst precursor. In their experiment, the researchers used catalyst which were prepared differently. First, crushed nickel nitrate hexahydrate in quartz boat, which Ni weight was 40 mg, was heated in air to synthesis temperature of 600 °C with a heating rate 30 °C/min, and then ethanol would inject into reactor for CNT synthesis with flowrate of 0.17 cm³/min for 30 min. CNTs synthesized with crushed nickel nitrate hexahydrate were labeled CNTs_1. In the second case, 1 cm³ of ethanol was added to catalyst precursor at room temperature before heating up to the synthesis temperature, and then the experiment was carried out as the first case. CNTs which were synthesized from the catalyst were labeled CNTs_2. CNT yield was increased when ethanol was added to catalyst precursor from 17.5% to 25.0%. Due to hydrogen in ethanol precursor, the hydrogen gas from decomposed added ethanol could help reduction of nickel nitrate to the metal. Therefore, catalyst from the second case was more active.

The morphology of CNTs is shown as **Fig. 8**. **Fig. 8a** shows CNTs_1 was thick tube structure with uneven surface formed when used catalyst. **Fig. 8b** shows CNTs_2 was smaller diameter and smoother. CNT diameter ranges of CNTs_1 and CNTs_2 were 300-500 nm and 20-70 nm, respectively. The decomposition of nickel nitrate in ethanol vapor could lead to the formation of smaller catalytic particles. Additionally, this result consistent to the yield results because the smaller catalytic particles were more active catalyst.

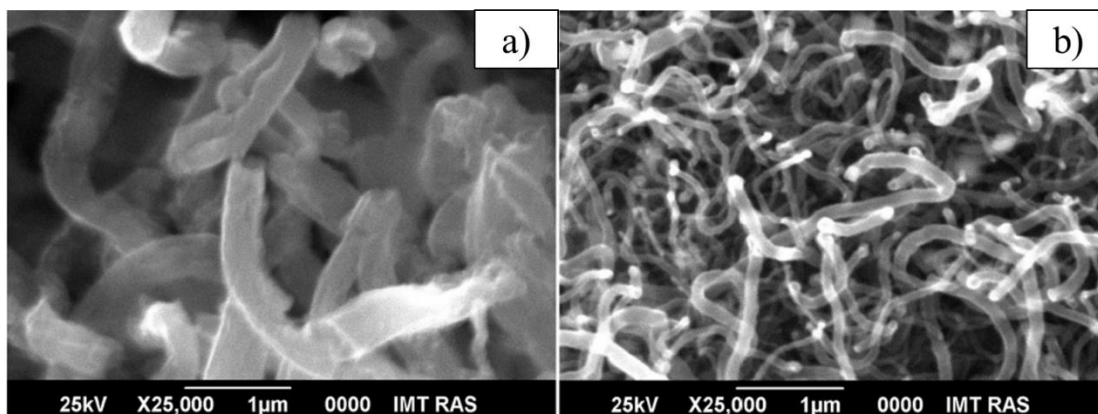


Fig. 8 FESEM images of morphology of a) CNTs_1 and b) CNTs_2 [38]

2.5.1.3 Effect of Ni to Fe molar ratio of catalyst

Li et al. [11] synthesized CNTs by CVD method using alumina tube reactor. Argon (Ar) was used as shielding gas. In their experiment, a cup which filled with powdery polyethylene waste (97 wt% of polyethylene) with Ni-Fe catalyst from $\text{Ni}(\text{NO}_3)_2 \cdot 6\text{H}_2\text{O}$ and $\text{Fe}(\text{NO}_3)_3 \cdot 9\text{H}_2\text{O}$ was placed in the reactor. The catalyst content was 0.50 wt% of the polyethylene weight. The Ni to Fe molar ratio of catalyst was varied as follow: 10:0, 2:8, 4:6, 5:5, 6:4, 8:2, and 0:10. Then, the reactor was heated to synthesis temperature of 700 °C with a heating rate of 5 °C/min for 120 min of process time.

Yao et al. [39] prepared CNTs by CVD method. Waste plastic was the mixture of 40 wt.% sample bottles (mainly made of high-density polyethylene), 35 wt.% plastic bags (specifically low-density polyethylene), 20 wt.% preservative boxes (mainly polypropylene) and 5 wt.% lunch boxes (mainly polystyrene) was used as carbon precursor. Ni-Fe supported on alumina was used as catalyst. CNTs were synthesized in a two-stage fixed bed reactor. The reaction system consists of a quartz tube reactor with 4 cm of inner diameter equipped with furnace. The furnace was divided 2 temperature zone. The upper zone was pyrolysis zone in range of 31 cm height, and under zone was catalysis zone in range of 31 cm height. In their experiment, different Ni to Fe molar ratios of catalyst were 1:3, 1:2, 1:1, 2:1, and 3:1. 0.5 g of each catalyst was placed in the middle of catalysis zone, and the zone was heated to 800 °C. Argon was introduced as a carrier gas with a 110 cm³/min flow rate. After temperature of catalysis zone reached to set point, waste plastic in quartz basket was introduced into the center of pyrolysis zone. The range was heated up to 500 °C with a heating rate of 10 °C/min and held at the temperature for 15 min.

Fazle Kibria et al. [40] synthesized CNTs by CVD method by use of quartz tube reactor. Ethylene (C_2H_2) was used as carbon precursor. Fe catalyst, Ni catalyst, and Fe-Ni catalyst supported on alumina were used as catalysts whose weight ratio of metal to alumina was 40:60. For bimetallic catalyst, Fe to Ni molar ratio of catalyst were varied from 3.2:1, 1.1:1, and 0.4:1 (calculated from weight ratio of Fe to Ni were 30:10, 20:20, and 10:30, respectively). In their experiment, after 40 mg of each catalyst at the middle

of the reactor was activated. The C_2H_2/H_2 gases were fed to the reactor at 600 °C with a flowrate of 10/100 sccm for 60 min.

2.5.1.3.1 Yield of CNTs product

From Li et al. [11], yields by weight of CNTs were calculated from weight of product minus weight of Fe-Ni catalyst which were theoretically added divided by initial weight of polyethylene waste mixed with catalyst minus weight of Fe-Ni catalyst which were theoretically added. Their results found that carbon yield was only about 7% and 8% when using single Fe and Ni metal. However, when Fe-Ni bimetallic catalyst was used, the yield increased significantly. Moreover, with the Fe to Ni molar ratio in the catalyst increasing from 2:8 to 8:2, the yield increased from 18% to 22%. These results suggested a higher amount of metal-assisted carbon growth with more Fe loading.

From Fazle Kibria et al. [40], yields by weight of CNTs were calculated from weight of catalyst after CNT synthesis minus weight of catalyst before the synthesis divided by the catalyst weight before CNT synthesis. The results reveal that yields for the Fe catalyst, Ni catalyst, 3.2:1, 1.1:1, and 0.4:1 molar ratio of Fe to Ni in catalysts were 16.1%, 11.3%, 94.1%, 60.3%, and 39.4%. The yields for the bimetallic catalysts are remarkably higher than those for the single metal catalysts. Moreover, Fe content in the catalyst was increased, the yield also increased.

2.5.1.3.2 Thermal stability of CNTs

From Yao et al. [39], thermal stability of CNTs was characterized by a thermogravimetric analyzer, TGA and DTG were used heating rate of 10 °C/min in air. TGA and DTG curves of CNTs by use of different Ni-Fe catalyst are shown in **Fig. 9**. All TGA plots revealed that synthesized CNTs started decomposed at temperature 500 °C approximately. These results shown that most of carbon form in their study were CNTs. However, peak from DTG curves demonstrate when the molar ratio of Ni to Fe of catalyst increased from 1:3 (NiFe13) to 3:1 (NiFe31), weights of CNT samples were lost at 500-600 °C and 550-650 °C, respectively. The results indicated that Ni composition in the catalyst enhanced the thermal stability.

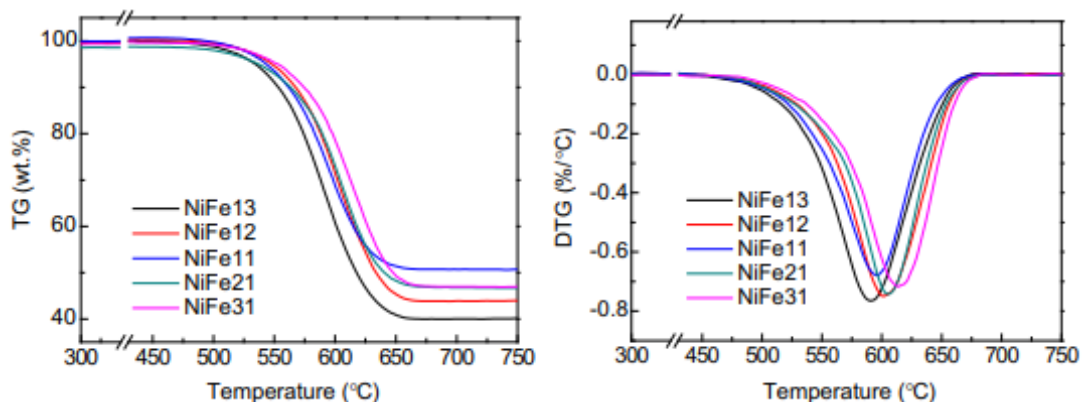


Fig. 9 TGA and DTG plots of CNTs which were synthesized by use of different molar ratio of Ni to Fe catalyst [41]

2.5.1.3.3 Crystallinity of CNTs

From Yao et al. [39], Raman spectroscopy from **Fig. 10**, the peak at $1,350\text{ cm}^{-1}$ was attributed to D-band which represented the presence of amorphous carbon. The peak at $1,580\text{ cm}^{-1}$ was attributed to G-band which represented the presence of CNT structure. From their experiment, I_D/I_G ratio of CNTs were 1.03, 1.07, 0.71, 0.64, and 0.68 when synthesized by use of catalyst which were 1:3, 1:2, 1:1, 2:1, and 3:1 molar ratio of Ni to Fe (NiFe13, NiFe12, NiFe11, NiFe21, and NiFe31, respectively). I_D/I_G decreased at higher ratios of the Ni to Fe catalysts. Therefore, Ni can be improved crystallinity of carbon.

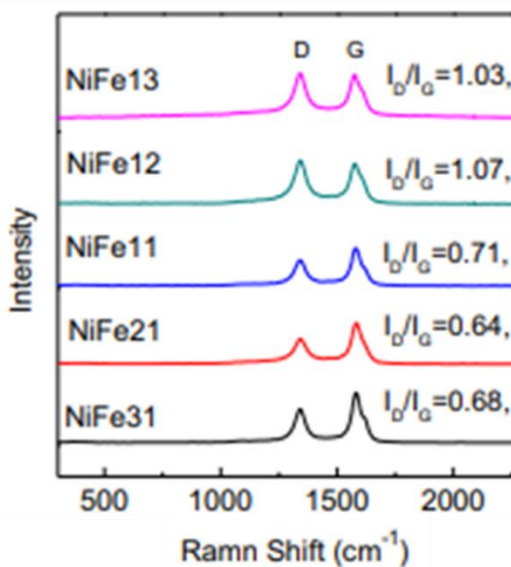


Fig. 10 Raman analysis of the CNTs from 1:3, 1:2, 1:1, 2:1, and 3:1 Ni to Fe molar ratio of catalyst [39]

2.5.2 Effect of synthesis temperature on property of resultant CNTs

Acomb et al. [19] synthesized CNTs by CVD method using two-stage pyrolysis reactor. The reactor was made of stainless steel and had a total length of 32 cm and an

internal diameter of 2.2 cm. N₂ was used as the carrier gas with a flow rate of 80 cm³/min. Low density polyethylene (LDPE) was used as a carbon precursor. Fe/ γ -Al₂O₃ was used as catalyst. In their experiment, sample boat which was filled with 1 g of LDPE was placed in the first stage and the 0.5 g of catalyst was placed in the second stage. The second stage of reactor was heated to different synthesis temperature of 700 °C, 800 °C, or 900 °C. After the synthesis temperature was reached, the first stage was heated to 600 °C at a heating rate of 50 °C/min for total process time of 30 min.

Mongkolsamai et al. [42] synthesized CNTs by CVD method using a quartz tube reactor with inner diameter of 4.2 cm and length of 60 cm. N₂ was used as a carrier gas. Ethanol (C₂H₅OH) was used as a carbon precursor. Ferrocene (C₁₀H₁₀Fe) was used as catalyst. In their experiment, ferrocene which was contained in ceramic boat was placed in the middle of reactor. The reactor was heated to synthesis temperature. The temperature was varied from 700 °C, 800 °C, and 900 °C. After synthesis temperature was reached, ethanol was sprayed from an ultrasonic nebulizer by lead of N₂ gas with flowrate of 2,000 cm³/min into the quartz tube reactor. Molar ratio of ethanol to ferrocene was 58:1 (calculated from ethanol-to-ferrocene weight ratio of 93:7). The synthesis time was hold at 45 min.

Lee et al. [43] synthesized CNTs by CVD method in quartz tube reactor which diameter of tube was 55 cm. C₂H₂ was used as carbon precursor. A thin film of Fe of 30 nm on p-type Si substrate was used as catalyst. The substrate has 2 cm x 3 cm sized and 300 nm thickness. Argon was used as carrier gas with 1,000 sccm (standard cubic centimeters per minute). The reactor was heated to synthesis temperature which was varied from 750 °C, 850 °C, and 950 °C. After synthesis temperature was achieved, NH₃ was used for catalyst pretreatment with flow rate of 100 sccm for 20 min. After that, C₂H₂ was fed into the reactor with a flowrate of 30 sccm for 10 min for the CNT growth.

Shamsudin et al. [44] was synthesized CNTs by CVD method using quartz tube reactor equipped with a furnace with two temperature stages. Champor oil was used as a carbon precursor. Ferrocene (C₁₀H₁₀Fe) was used as catalyst. In their experiment, ferrocene and camphor oil were placed in different alumina boats was placed at the center of the first furnace. Then, the quartz tube was heated under N₂ ambient with flow rate of 10 sccm as a carrier gas. The first stage was heated to 180 °C to evaporate camphor oil and ferrocene. The second stage was heated to synthesis temperature which was varied from 700 °C to 900 °C. Synthesis time was fixed at 60 min.

Srisrattha et al. [36] was synthesized CNTs by CVD method by use of a quartz tube reactor with outer diameter of 2.6 cm and 120 cm length. 1 g of ferrocene was used as carbon precursor and catalyst. Cyclohexane was used as carbon precursor. Molar ratio of cyclohexane to ferrocene was 10:1. N₂ was used as carrier gas with a flowrate of 21 cm³/min. In their experiment, they fixed 1 g of ferrocene in CNT production at different synthesis temperature which were 700 °C, 800 °C, and 900 °C. The process time was 30 min.

2.5.2.1 Yield of CNTs product

From Acomb et al. [19], yields by weight of CNTs were calculated from weight of CNTs divided by initial weight of LDPE. Their results found that an increase in synthesis temperature from 700 °C to 800 °C and 900 °C raised CNT yields from 2.0% to 18.7% and 21.3% (calculated from amounts of CNTs which was synthesized at 700 °C, 800 °C, and 900 °C were 20 mg, 187 mg, and 213 mg respectively, and 1 g of initial weight of LDPE) due to the increase in the diffusion rate of carbon through the catalyst particle, an important step in the formation of carbon nanotubes.

From Mongkolsamai et al. [42], yields by weight of CNTs were calculated from weight of CNTs divided by total weight of ethanol and ferrocene. When synthesis temperature was increased from 700 °C to 800 °C and 900 °C, CNT yields increased from 3.13% to 6.61% and 6.68%. This result indicated that an increase in synthesis temperature increased CNT yields. The increasing synthesis temperature could lead to the decomposition rate and CNT formation rate which affected CNT yields.

From Srisrattha et al. [36], yields by weight of CNTs were calculated from weight of CNTs divided by total weight of cyclohexane and ferrocene. In their experiment, CNT yield was increased from 13% to 29% and 32% when raised synthesis temperature from 700 °C to 800 °C and 900 °C. The increasing synthesis temperature could lead to the decomposition rate of precursor.

2.5.2.2 Morphology of CNTs

From Acomb et al. [19], morphology of CNTs were characterized by SEM as shown in **Fig. 11**. There was large number of irregular-shape particles occurred in CNT products which was synthesized at 700°C. There were none of irregular-shape found at synthesis temperature 800 °C. At synthesis temperature of 900 °C, CNTs were found as rough tubes. Diameter ranges of CNTs were 20-30 nm, 20-30 nm, and 30-60 nm when the synthesis temperature was 700 °C, 800 °C, and 900 °C, respectively.

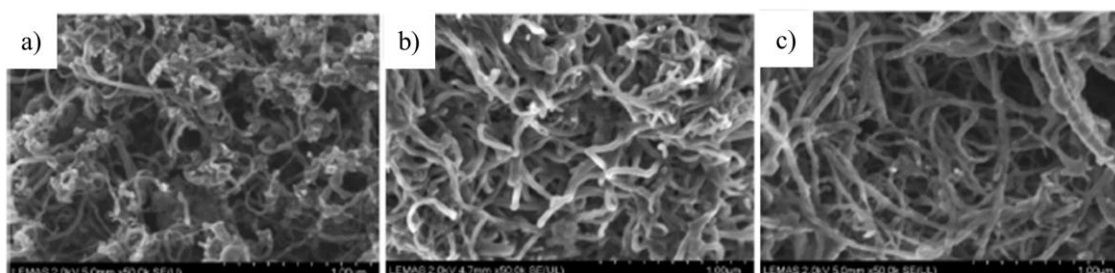


Fig. 11 Morphology of CNTs at various synthesis temperature a) 700 °C, b) 800 °C, and 900 °C [19]

From Lee et al. [43], morphology of CNTs were characterized by FESEM. **Fig. 12a** shows some carbonaceous particles on the CNT surface synthesized at 750 °C. CNT synthesized at 850° C and 950 °C; no carbonaceous particles were on the surface

as shown in **Fig. 12b-12c**. Diameters of synthesized CNTs were 30 ± 5 nm, 60 ± 10 nm, and 130 ± 20 nm when the synthesis temperature was 750 °C, 850 °C, and 950 °C, respectively. An increment of CNT diameters was due to the sintering of Fe particle on Si substrate. The size of Fe particles was 40 ± 10 nm, 90 ± 20 nm, and 150 ± 40 nm when the synthesis temperature was 750 °C, 850 °C, and 950 °C, respectively.

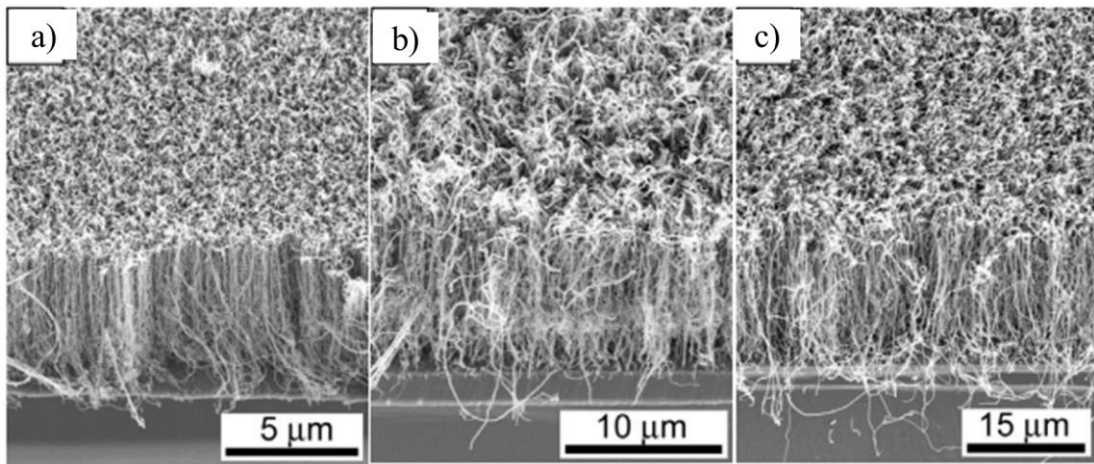


Fig. 12 SEM images of CNTs which was synthesized at a) 750 °C, b) 850 °C, and c) 950 °C [43]

From Srisrattha et al. [36], morphology of CNT in product was characterized by FESEM as shown in **Fig. 13**. There were some irregular shape particles with tubular structure in CNT product which was synthesized at 700 °C. There were no irregular shape particles in products produced at 800 °C and 900 °C. CNT diameter was 54 ± 20 nm, 51 ± 13 nm, and 93 ± 44 nm when synthesis temperature was 700 °C, 800 °C, and 900 °C, respectively. Increment in CNT diameter was due to an increasing wall of CNT. The result was from increasing decomposition of the precursors at high temperature.

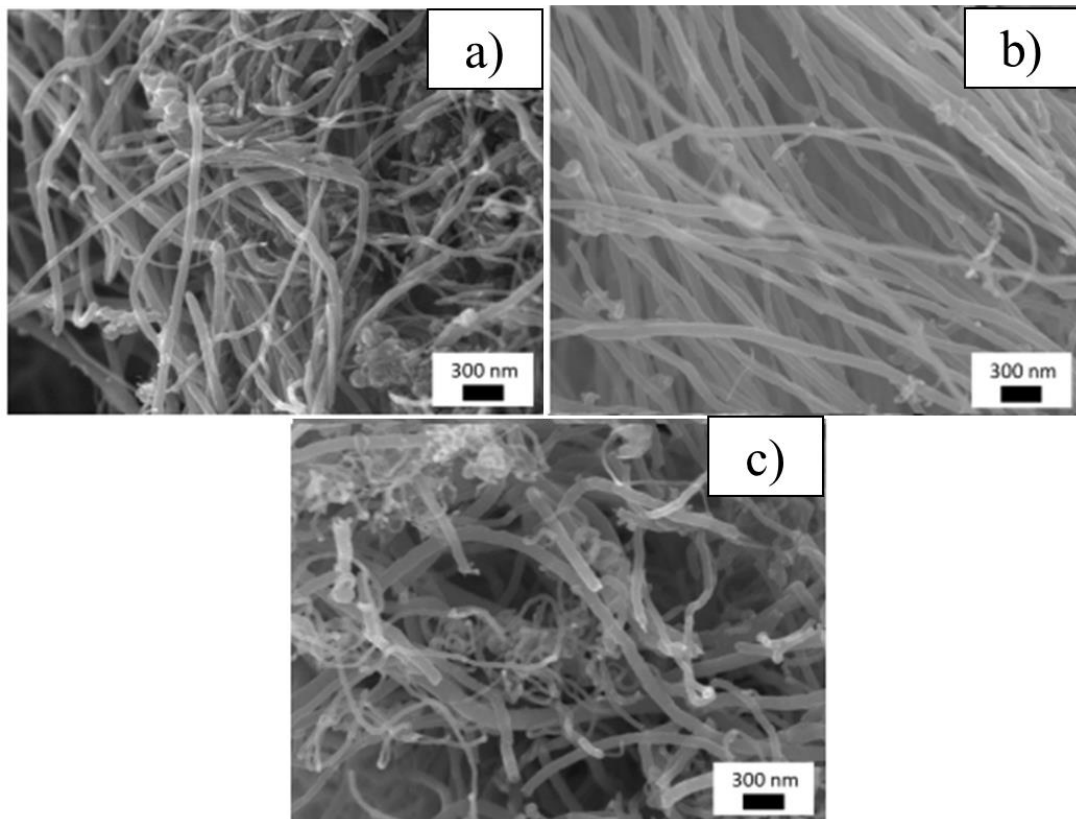


Fig. 13 FESEM images of CNTs which was synthesized at a) 700 °C, b) 800 °C, and c) 900 °C [36]

2.5.2.3 Thermal stability of CNTs

From Acomb et al. [19], thermal stability of CNTs was characterized by a thermogravimetric analyzer. DTG was used heating rate of 15 °C/min in air. DTG curves of CNTs at various synthesis temperature varied from 700 °C to 800 °C and 900 °C are shown in **Fig. 14**. The DTG plot of CNTs synthesized at 700 °C shows two distinct peaks at oxidized temperature of 400 °C and 500 °C. Meanwhile, the DTG plots of CNTs synthesized at 800 °C and 900 °C show a different peak at 600 °C and 650 °C, respectively. Therefore, it could indicate that CNTs had more thermal stability when the synthesis temperature increased.

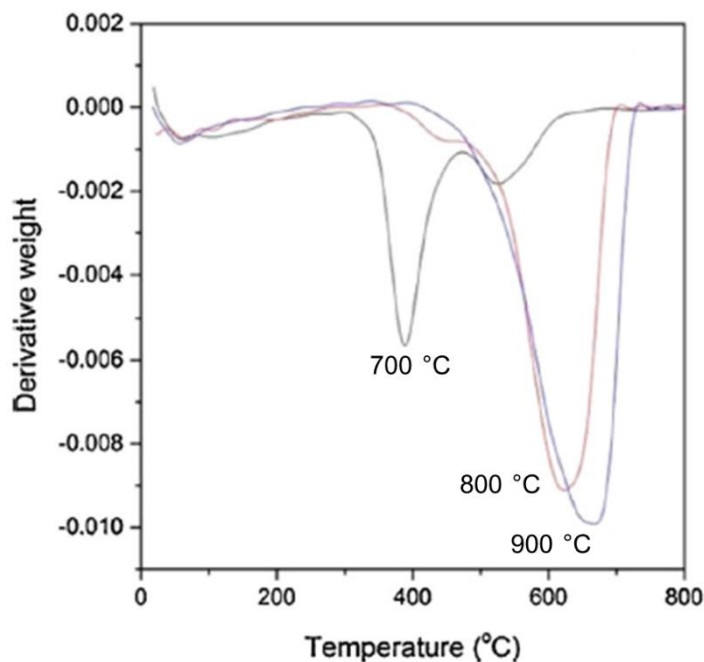


Fig. 14 DTG plots of as-synthesized CNTs at various synthesis temperature [19]

From Lee et al. [43], thermal stability of CNTs was characterized by a thermogravimetric analyzer. TGA was used a heating rate of 10 °C/min in air. TGA curves of CNTs synthesized at 750 °C, 850 °C, and 950 °C are shown in **Fig. 15**. This graph reveals that CNT sample weight was lost over the range of 300-600 °C, 450-650 °C, and 500-670 °C when synthesis temperature was increased from 750 °C to 850 °C and 950 °C, respectively. These results confirmed that CNTs had higher thermal stability when the synthesis temperature increased.

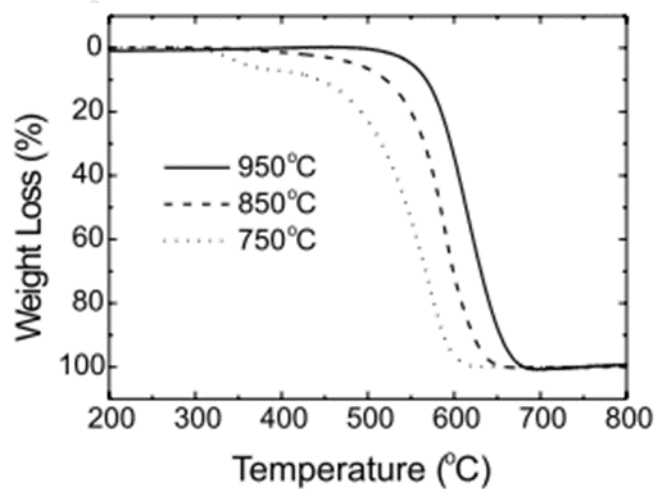


Fig. 15 TGA curves of CNTs which were synthesized from different synthesis temperature [43]

2.5.2.4 Crystallinity of CNTs

From Acomb et al. [19], Raman spectroscopy of CNTs synthesized at synthesis temperature of 700 °C, 800 °C, and 900 °C was shown in **Fig. 16a**, **Fig. 16b**, and **Fig. 16c**, respectively. The peak at 1,348 cm⁻¹ was attributed to D-band, which represented the present of amorphous carbon. The peak at 1,589 cm⁻¹ was attributed to G-band which represented the present of CNT structure. From their experiment, an increase in synthesis temperature from 700 °C to 800 °C decreased I_D/I_G from 0.60 to 0.51. This could be attributed to the rise in CNT structure in carbon product. Meanwhile, an increase in synthesis temperature from 800 °C to 900 °C decreased I_D/I_G from 0.51 to 0.52. The I_D/I_G ratio was increased because there is more carbon deposition which caused less ordered carbon walls. Therefore, the quality of the CNT was lower.

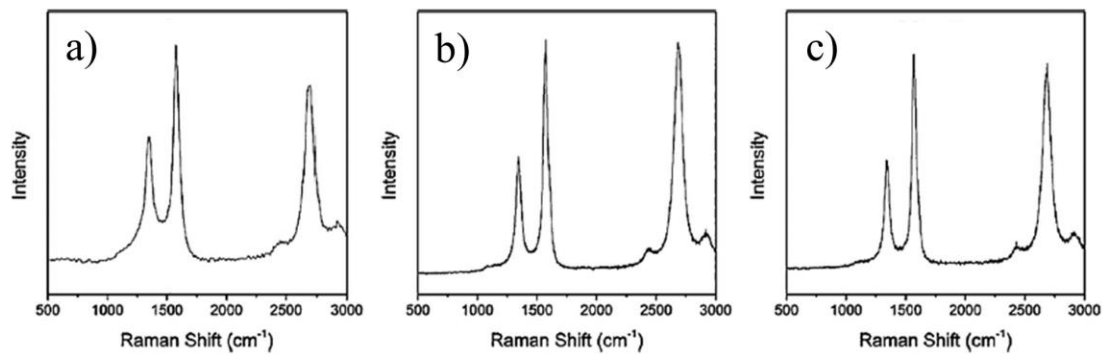


Fig. 16 Raman spectra of CNTs which were synthesized at synthesis temperature of a) 700 °C, b) 800 °C, and c) 900 °C [19]

From Shamsudin et al. [44], Raman spectroscopy from **Fig. 17**, the peak at 1,345 cm⁻¹ was attributed to D-band, which represented the presence of amorphous carbon. The peak at 1,573 cm⁻¹ was attributed to G-band, which illustrated the presence of CNT structure. From their experiment, an increase in synthesis temperature from 700 °C to 800 °C decreased I_D/I_G from 0.72 to 0.52. Nevertheless, an increase in synthesis temperature from 800 °C to 900 °C decreased I_D/I_G from 0.52 to 0.57. A decrease in I_D/I_G could be attributed to an increase in CNT structure in carbon products. However, an increase in I_D/I_G could be assigned to non-uniform nanotubes.

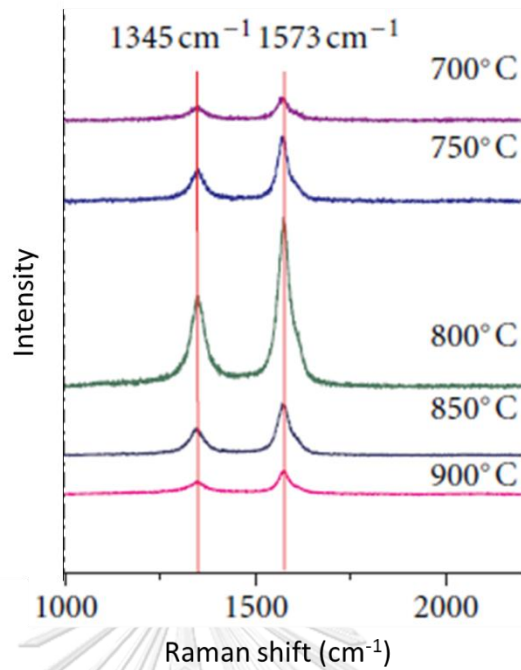


Fig. 17 Raman spectra of CNTs which were synthesized in synthesis temperature range of 700 °C to 900 °C [44]

From Srisrattha et al. [36], Raman spectra from **Fig. 18** indicated the G-band and D-band with different I_D/I_G ratio. The G-band is representative of amount of graphitic carbon or CNT structure in product. The D-band represents the amount of defect carbon or amorphous carbon. The ratio of produced carbon from synthesis temperature of 700 °C to 800 °C was increased from 1.60 to 0.61. This result indicated that the CNT product synthesized at 700 °C contains more amorphous carbon than the product produced at 800 °C. However, I_D/I_G ratio increased from 0.61 to 0.67 when increased in synthesis temperature from 800 °C and 900 °C because of non-uniform nanotubes in CNT product.

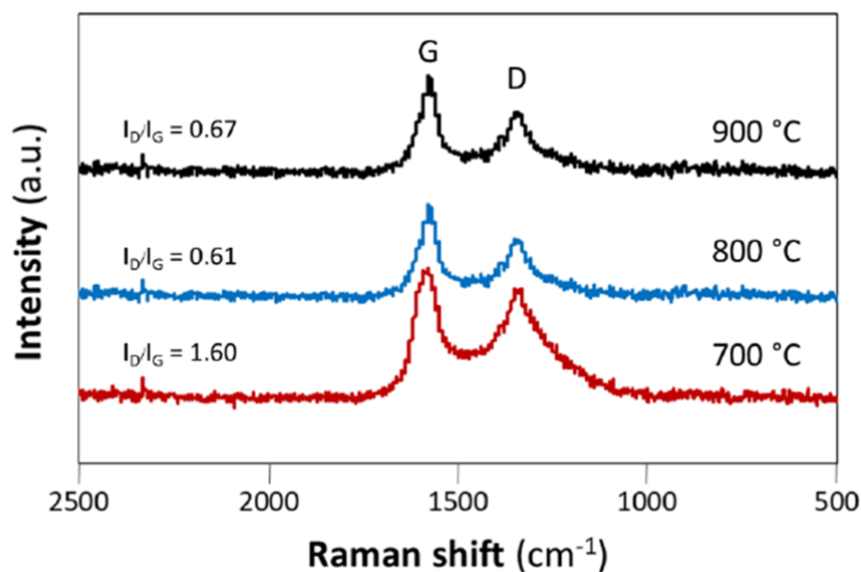


Fig. 18 Raman spectra of CNTs which were synthesized from synthesis temperature of 700 °C, 800 °C, and 900 °C [36]

2.5.3 Effect of carbon precursor to catalyst molar ratio on property of resultant CNTs

Tripathi et al. [45] synthesized CNTs via CVD method in quartz tube reactor with diameter 6.5 cm and length 65 cm. Acetylene (C_2H_2) was used as carbon precursor. A thin film of Fe of 2 nm thickness on 5 mm x 5 mm n-type Si substrate was used as catalyst. The catalyst was placed at the center of furnace. Argon was used as carrier gas with a flowrate 50 sccm. The reactor was heated to synthesis temperature of 800 °C. After that, C_2H_2 was fed to the reactor for 10 min. The C_2H_2 to catalyst molar ratio were varied from 0.6:1, 1.3:1, 1.9:1, 2.6:1 and 3.2:1 (calculated from C_2H_2 flowrate were 10 sccm, 20 sccm, 30 sccm, 40 sccm, and 50 sccm respectively and initial Fe weight in the catalyst was 0.394 g).

Venkatesan et al. [46] synthesized CNTs by CVD method in a quartz tube reactor with 7 cm of diameter and 30 cm of length. C_2H_2 was used as carbon precursor. Ni supported on alumina was used as catalyst. The initial weight percentage of Ni loading to alumina was 5 wt%. In their experiment, the 0.1 g of catalyst was loaded into the center of the hot zone reactor. Then, the reactor was heated from room temperature (assumed 25 °C) and argon gas was supplied with a flowrate 100 cm^3/min until temperature was reached to 900 °C. Then, argon was stopped and C_2H_2 was fed to the reactor for 25 min. The molar ratio of C_2H_2 to Ni was varied from 3.5:1, 4.9:1, and 6.3:1 (calculated from flowrate of C_2H_2 was varied from 100 cm^3/min , 140 cm^3/min , 180 cm^3/min respectively, and Ni weight from catalyst was 5 mg). Later carbon precursor feed was replaced with argon gas until the furnace reached room temperature.

2.5.3.1 Yield of CNT product

From Tripathi et al. [45], yields by weight of CNTs were calculated from weight of product minus weight of catalyst divided by weight of C_2H_2 feed. Their results found that an increase in molar ratio of C_2H_2 to Ni in catalyst from 0.6:1 to 1.3:1 raised CNT yields due to the increase in the diffusion rate of carbon through the catalyst particle to formation of CNTs. However, CNT yields when the molar ratio was increased from 1.3:1 to 3.2:1 decreased because decomposition rate of C_2H_2 became higher than diffusion rate of carbon to make CNTs. The remaining of carbon deposited on CNT surface in amorphous form and covered catalyst surface. Therefore, the catalyst activity started to decrease, and speed of CNT growth was reduced.

2.5.3.2 Morphology of CNTs

From Tripathi et al. [45], morphology of CNTs were characterized by FESEM from **Fig. 19**. CNT structures were the thinnest when used 1.3:1 molar ratio of C_2H_2 to Ni. Then, the structures became thicker when used the molar ratio of 1.9:1 and 3.2:1. The diameter ranges of CNTs were 12-38 nm, 45-60 nm, and 85-94 nm when the molar ratio of C_2H_2 to Ni catalyst was 1.3:1, 1.9:1, and 3.2:1, respectively. An increase in CNT diameters was obtained due to increasing in C_2H_2 to Ni catalyst molar ratio.

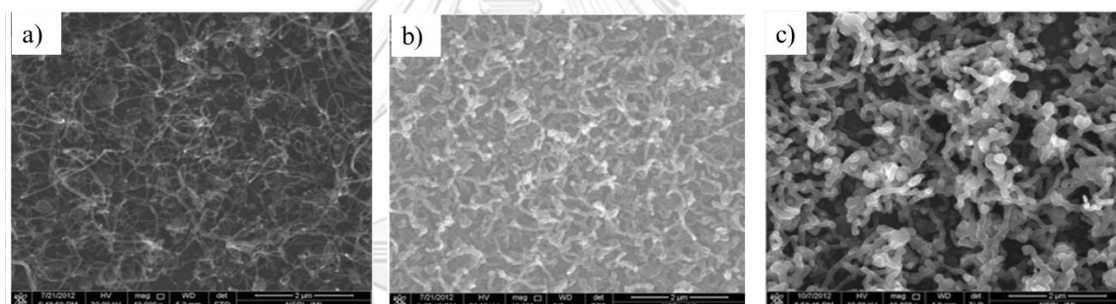


Fig. 19 FESEM images of CNTs synthesized by different molar ratio of C_2H_2 to catalyst a) 1.3:1, b) 1.9:1, and c) 3.2:1 [45]

From Venkatesan et al. [46], morphology of CNTs was characterized by FESEM. **Fig. 20a** indicates that there was longer tubular structure of CNTs which was synthesized using the 3.5:1 molar ratio. Shorter tubular structure of CNTs occurred in product which was synthesized by use of the 4.9:1 molar ratio, as shown in **Fig. 20b**. **Fig. 20c** illustrates rough carbon structure tubes in product synthesized using the 6.3:1 molar ratio. This figure indicated the deposition of amorphous carbon on the sidewalls of CNTs. The average diameters of CNTs were 20 nm, 32 nm, and 46 nm when the molar ratio of C_2H_2 to Ni was 3.5:1, 4.9:1, and 6.3:1 respectively. It could be inferred that the molar ratio increased average diameter of the CNTs.

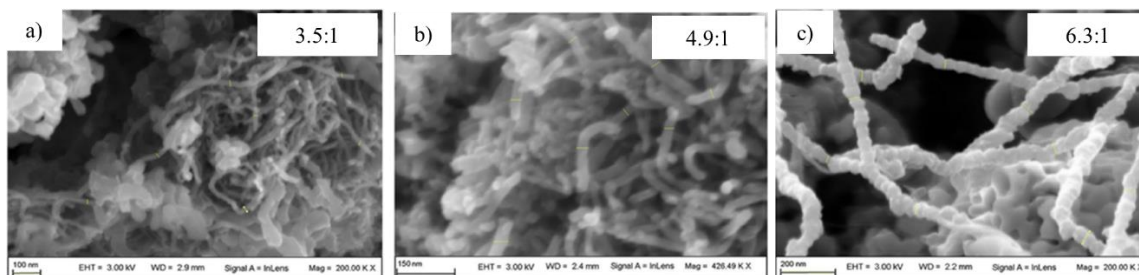


Fig. 20 FESEM images of CNTs synthesized by different molar ratio of C_2H_2 to catalyst a) 3.5:1, b) 4.9:1, and c) 6.3:1 [46]

2.5.3.3 Crystallinity of CNTs

From Tripathi et al. [45], Raman spectroscopy technique was used to characterize crystallinity of CNTs. From **Fig. 21**, the peak at $1,350\text{ cm}^{-1}$ was attributed to D-band which represented the presentation of amorphous carbon. The peak at $1,580\text{ cm}^{-1}$ was attributed to G-band which represented the given CNT structure. Their experiment showed a similarity of I_D/I_G from 0.808 to 0.807 when increased in C_2H_2 to Ni molar ratio from 0.6:1 to 1.3:1. Nevertheless, an increase in molar ratio from 1.3:1 to 3.2:1 increased I_D/I_G from 0.807 to 0.878. A decreased in I_D/I_G could be attributed to less amorphous carbon on CNT surface, but an increased in I_D/I_G could be assigned to deflect of CNT structure due to amorphous carbon deposition.

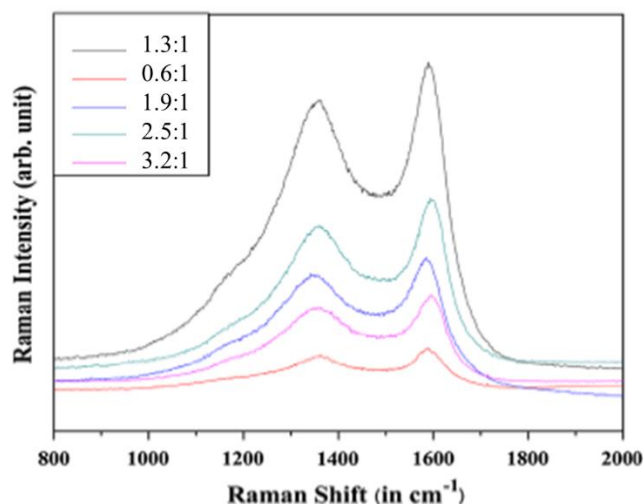


Fig. 21 Raman spectra of CNTs which were synthesized by different molar ratio of C_2H_2 to catalyst [45]

2.5.4 Magnetic properties

2.5.4.1 Effect of synthesis temperature

Xu et al. [47] studied the magnetic property of MCNPs at different benzene decomposition temperatures in the range of $430 - 600\text{ }^\circ\text{C}$. MCNPs were synthesized by the CVD method in quartz tube reactor in argon flow and using Ni-Fe nanoparticles as catalyst. The magnetic properties of the MCNPs were analyzed by SQUID

magnetometer. They observed increasing temperature result in a decreasing trend in saturated magnetization (M_s). However, the cause of the coercivity (H_c) trend was hard to identify because H_c is known to be sensitive to many structural parameters such as internal stress, orientation, defects, and shape.

Liu et al. [48] studied the magnetic property of different magnetic carbon nanostructures by the pyrolysis of ferrocene at different sublimation temperatures. Quartz tube in two temperature furnaces were used as a reactor. The first reactor was set up at various sublimation temperatures, and the second was set up at 1,100 °C. Argon was also flown to the reactor as carrier gas in 2,000 sccm. The researchers founded that temperature affects these nanostructures. At 110 °C, they obtain Fe nanoparticles have an enhanced H_c at room temperature when compared to the bulk Fe because Fe nanoparticles adhering to SWCNTs which is ascribed to the large surface anisotropy effect and the strong interactions between magnetic nanoparticles that can lead to ordering of magnetic moments. At 160-400 °C, higher Fe decorated on the outer surface of MWCNTs or filled in the inner channel of MWCNTs was arranged in a quasi-one-dimensional manner, that is a cause of H_c increasing.

2.5.4.2 Effect of Ni to Fe molar ratio

Dijith et al. [13] prepared Ni-Fe alloy nanoparticles from polyol method. They studied effect of iron to nickel molar ratio on magnetic property by VSM at 27 °C as shown in **Fig. 22a-22b**. They observed increasing Fe concentration in the alloys and decreasing particle size results in an increasing trend in saturated magnetization while coercivity decreases proportionally. Therefore, the increasing Fe and decreasing particle size can be changed from ferromagnetic state to paramagnetic state. As the temperature is increased towards the Curie temperature, the alignment (magnetization) within each domain decreases. Above the Curie temperature, the material is purely paramagnetic and there are no magnetized domains of aligned moments. For higher Fe content alloys, Curie temperature could not be estimated, since the ferromagnetic to paramagnetic transition is expected to occur above 1000 K (727 °C), which is beyond the measurable temperature range as shown in **Fig. 23**.

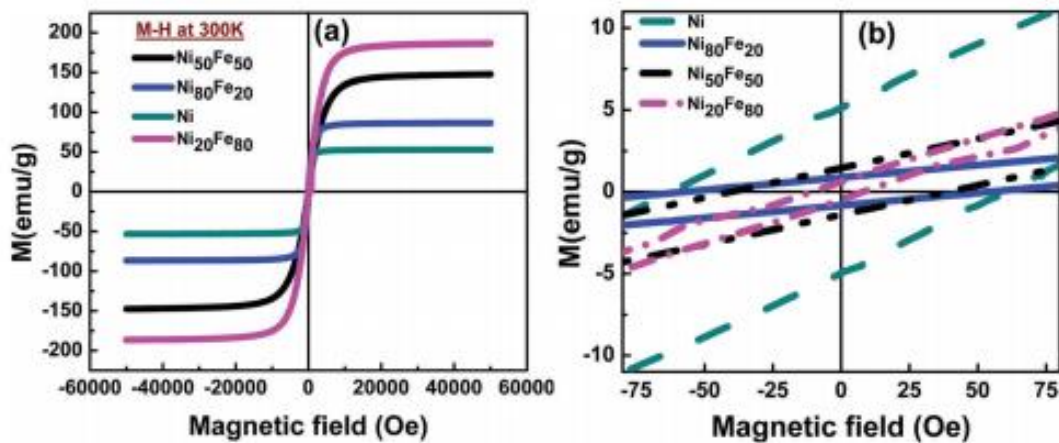


Fig. 22 Magnetization vs magnetic field curves of Ni and Ni-Fe alloy nanoparticles for different composition at 27 °C a) in a whole range and b) magnified range -75 -75 Oe [13]

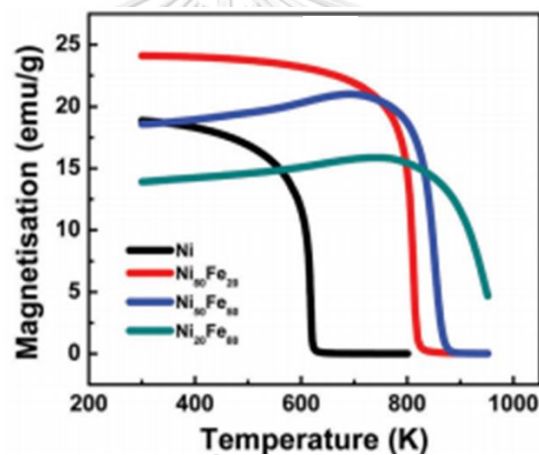


Fig. 23 Magnetization vs temperature curves of Ni and Ni-Fe alloy nanoparticles for different composition [13]

Dong et al. [49] synthesized MCNPs which are Ni-Fe-Carbon nanocapsules by arc-discharge. Effect of Ni to Fe weight ratio on the magnetic property was studied. This research reveals the saturation magnetization of MCNPs is mainly dependent upon Ni, Fe, and carbon composition and magnetic properties. The magnetic properties and composition directly determine the saturation magnetization. From samples A and B, carbon atoms indirectly affect the M_s by influencing the microstructure in Ni-Fe-Carbon nanocapsules as shown in **Table 2**.

Table 3 Composition of Fe, Ni, and C, and saturation magnetization of the Ni-Fe-Carbon nanocapsules [49]

Samples	Mother alloys (wt%)		Relative ratio (%) in Fe-Ni(C) nanocapsules		Composition (wt%)			Saturation magnetization (Am ² /kg)
	Fe	Ni	Fe	Ni	Fe	Ni	C	
(A)	85	15	84.80	15.20	~64.5	~11.5	23	34.3
(B)	70	30	72.29	27.71	49.8	19.1	20	55.6
(C)	55	45	57.31	42.69	50.8	37.8	11	109.1
(D)	40	60	42.47	57.53	33.2	45.0	~10	102.2
(E)	21.5	78.5	22.24	77.76	20.0	70.0	9.5	76.4
(F)	10	90	8.80	91.20	7.6	79.0	11	62.1

2.5.4.3 Effect of ratio of carbon precursor to catalyst

Kerdnawee et al. [50] synthesized MCNPs via glycerol and ferrocene copolyolysis with magnetic induction in quartz tube reactor at 800 °C. N₂ was used as carrier gas. They studied the effect of the molar ratio of glycerol to ferrocene and magnetic susceptibility. The magnetic susceptibility at 0 Hz, $X_{r,0}$, was estimated by extrapolating the real part of the complex number of the AC magnetic susceptibility. They observed $X_{r,0}$ values of high glycerol to ferrocene ratio was low due to the reducing proportion of Fe. This effect resulted in a lower proportion of the magnetic responsive MCNPs.

Sajitha et al. [51] prepared MCNPs via maleic anhydride and ferrocene copolyolysis. They were synthesized in a quartz tube reactor with one end closed, which heated at 8 °C/min heating rate taking about 2 h to reach the set temperature of 900 °C. Sajitha team studied the effect of molar ratio of maleic anhydride to ferrocene (2:1 to 20:1) to magnetic properties that were measured by SQUID magnetometer at 27 °C. This study reported the value of saturated magnetization of 2:1_MCNP and 20:1_MCNP were 20.2 emu/g and 9.9 emu/g. The values reduced due to a higher proportion of Fe. Coercivity of 2:1_MCNP and 20:1_MCNP were 338 Oe and 270 Oe, respectively. 20:1_MCNP has more superparamagnetic state than 2:1_MCNP because coercivity exhibits reciprocal of Fe particle diameter.

CHAPTER 3

EXPERIMENTAL

In this research, the experiment can be divided into 2 parts. The first part is the preparation of ferrocene impregnated with nickel nitrate. The second part is the synthesis of magnetic carbon nanotubes (MCNTs).

3.1 Material and chemicals

- 1) Ferrocene (Sigma-Aldrich, 98%)
- 2) Nickel (II) nitrate hexahydrate ($\text{Ni}(\text{NO}_3)_2 \cdot 6\text{H}_2\text{O}$, KEMUAS, AR Grade, 99%)
- 3) Ethanol (QRec, AR Grade, 99%)
- 4) Nitrogen gas (Linde (Thailand), 99.999% purity)
- 5) Eucalyptus oil (Chanjao Longevity, Thailand, 80.33% eucalyptol), the elemental composition is listed in **Table 4**, and its specification is shown in **Appendix A**.

Table 4 Element content of eucalyptus oil

Element	Percentage composition (wt%)
Carbon	47.62
Hydrogen	6.72
Nitrogen	1.12
Oxygen	44.54

3.2 Procedure

3.2.1 Catalyst preparation

Ferrocene impregnated with nickel nitrate catalysts were prepared by a simple method with the different molar ratio of Fe to Ni (4:1 and 1:1). $\text{Ni}(\text{NO}_3)_2 \cdot 6\text{H}_2\text{O}$ was solute in 7.5 ml ethanol solvent, and then this solution was dripped to 0.75 g of ferrocene. They were mixed at room temperature. Next, the mixture solvent was evaporated in a hot oven at 80 °C for 180 min. The resultant solid was grounded to reduce particle size of less than 300 μm and kept in a desiccator. These products were called '4:1 ferrocene impregnated with nickel nitrate' and '1:1 ferrocene impregnated with nickel nitrate'.

For nickel nitrate preparation, $\text{Ni}(\text{NO}_3)_2 \cdot 6\text{H}_2\text{O}$ flake was crushed in laboratory mortar. After that, it was dried in a hot oven at 80 °C for 180 min. The resultant solid was grinded and screened by using 300 μm - size sieves.

3.2.2 Magnetic carbon nanotube synthesis

MCNTs were prepared in a quartz tube reactor equipped with an electrical furnace (SL Heater, 220V, 9000W, Suan Luang Engineering, Thailand) as shown in

Fig. 24. The inner diameter and length of quartz tube are 4.2 cm and 110 cm, respectively. Different catalysts which contained 0.15 g of total metal were preloaded in a ceramic boat and placed at the left-handed and outer side in the quartz tube reactor. The designated weight of all catalysts was shown in **Table C1** in **Appendix C**. Nitrogen gas with a flow rate of 51 cm³/min was supplied into the reactor using a mass flow controller (CR-300, KOFLOC, Japan) while the reactor was heated to different synthesis temperatures (700 °C, 800 °C, and 900 °C). Then, the ceramic boat was moved to designated position in the electrical furnace. At the same time, eucalyptus oil with the different molar ratio of eucalyptus oil to catalyst (2:1, 5:1, and 10:1) was also fed into the reactor through a syringe pump (KDS-100-B, KdScientific, USA) The initial amount of eucalyptus oil and feed flowrate was shown in **Table C2** in **Appendix C**. After 30 minutes of process time, the reactor cooled down to the ambient temperature. The collected product from the surface of the tube which mainly contained MCNTs was kept in a desiccator.

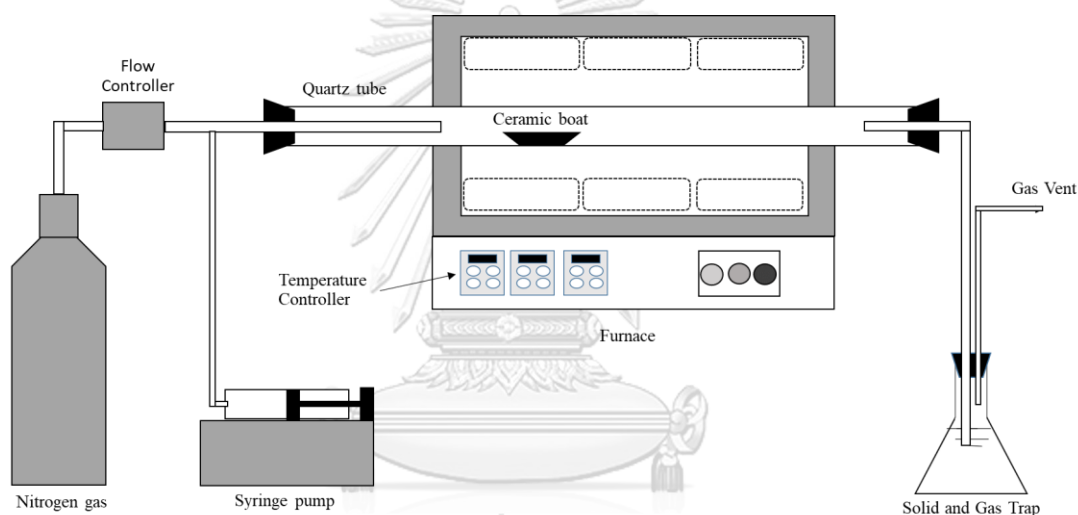


Fig. 24 The experimental set up for synthesizing MCNTs

3.3 Characterization

Ferrocene impregnated with nickel nitrate was characterized by the following techniques:

- X-ray diffractometer (XRD, D76181, Bruker AXS) as shown in **Fig. 25** was used to identify particle crystal structure using Cu/K α radiation ($\lambda = 0.154$ nm) at 40 kV and 300 mA in the 2θ range from 5° to 80° with scanning speed of 10°/min.



Fig. 25 X-ray diffractometer

- Fourier transform infrared (FTIR, Nicolet 6700, Thermo Scientific) spectroscopy as shown in **Fig. 26** was used to observe the functional group of the catalyst with a nominal resolution of 4 cm^{-1} in the range of $500\text{-}4000\text{ cm}^{-1}$.



Fig. 26 Fourier transform infrared spectroscope

- Energy-dispersive spectroscopy (EDS, Oxford EDS XMax) as shown in **Fig. 27** was used for elemental analysis.



Fig. 27 Energy-dispersive spectroscopy

- X-ray fluorescence (XRF, Bruker S8 TIGER) as shown in **Fig. 28** was used to determine metal composition.



Fig. 28 X-ray fluorescence

The magnetic CNT samples would be characterized by various techniques as follow:

- Scanning electron microscope (SEM, FEI QUANTA 450) as shown in **Fig. 29** was used to the microstructure and morphology of all CNT samples.



Fig. 29 Scanning electron microscope

- Raman spectroscopy (NT-MDT, model NTEGRA Spectra, Russia) as shown in **Fig. 30** was used to measure the crystallinity of CNTs under red laser with a wavelength of 632.8 nm. Raman shift was studied in the range $1,000\text{ cm}^{-1}$ to $2,000\text{ cm}^{-1}$. For CNT characterization, intensity of D band could be assigned to the vibration of non- sp^2 bonded carbon atom or applied to identify amorphous carbon. Intensity of G band could be represented to the vibration of sp^2 bonded carbon atom or applied to identify CNTs. The intensity of D-band to G-band ratio (I_D/I_G) was used to determine the crystallinity of carbon products from each sample.

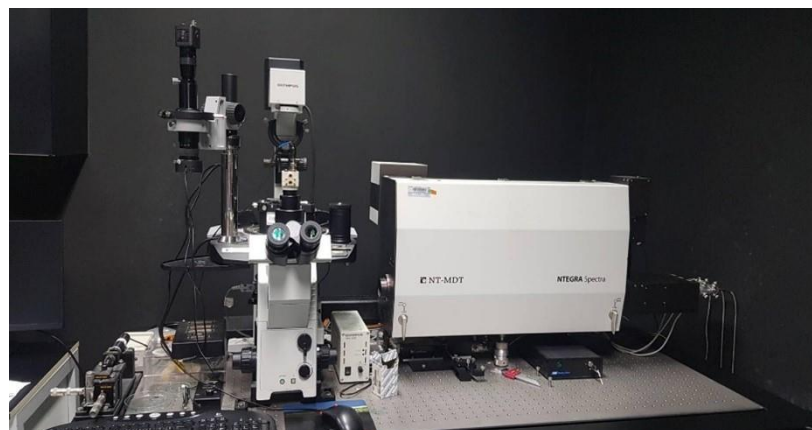


Fig. 30 Raman spectroscopy

- Thermogravimetric analyzer (TGA, Mettler-Toledo TGA/DSC1, STAR System), as shown in **Fig. 31**, was used to analyze thermal stability and residue. 4 mg of each carbon sample was examined under pure oxygen atmosphere with an oxygen flow rate of 50 cm³/min, a heating rate of 10 °C/min, and temperature range of 100–900 °C.



Fig. 31 Thermogravimetric analyzer

- X-ray diffractometer (XRD) as shown in **Fig. 24** was used to identify particle crystal structure. The average crystalline size (d) of metal was evaluated using the Scherrer equation as shown in **Eq 1**.

$$d = \frac{k\lambda}{\beta \cos \theta} \quad \text{Equation 1}$$

where the Scherrer constant (k) was taken to be 0.9, λ was the X-ray wavelength, β is the line width at half maximum height of the peak in radians, and θ is the position of the peak in radians.

- Vibrating sample magnetometer (VSM, model 7404, Lakeshore, USA) as shown in **Fig. 32** was used to measured magnetic hysteresis loops of all carbon samples at room temperature with a magnetic field cycled between –6000 G and +6000 G.

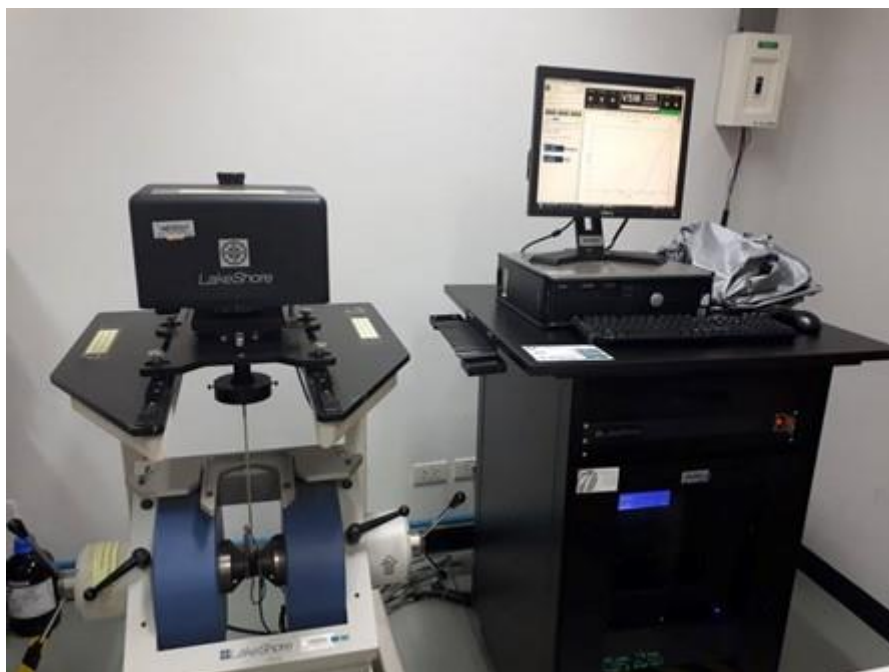


Fig. 32 Vibrating sample magnetometer

3.4 Computational fluid dynamics modeling

Computational fluid dynamics (CFD) modeling using software ANSYS FLUENT (ANSYS Inc., USA) was simulated to explain the flowing of eucalyptus oil in CNT synthesis system at room temperature with different molar ratio of eucalyptus oil to catalyst. A drawing of the computational physical domain considered to 2-dimensional as shown in **Fig 33**. The first step was generating the grid of eucalyptus oil and nitrogen gas feed line equipped with a quartz tube reactor, as shown in **Fig 34a**. The detail of meshed geometry from the red frame is illustrated in **Fig. 34b**. This was used for simulation. The element size was 0.038 cm. The 2-D configuration required about 65,929 cells.

The flow in the reactor was assumed to be incompressible fluid. For the modeling process, the multiphase model of volume of fluid was used to stimulate eucalyptus oil feed. The inlet velocity of nitrogen gas was 4.34×10^{-2} m/s, so the Reynold number was about 137. This indicated that the flow in the reactor is laminar. Laminar viscous model was used to stimulate the magnitude velocity of eucalyptus oil and its volume fraction along the reactor. The SIMPLE algorithm solved the coupling of pressure and velocity in solution methods. Second order upwind scheme was used to calculate momentum and volume fraction.

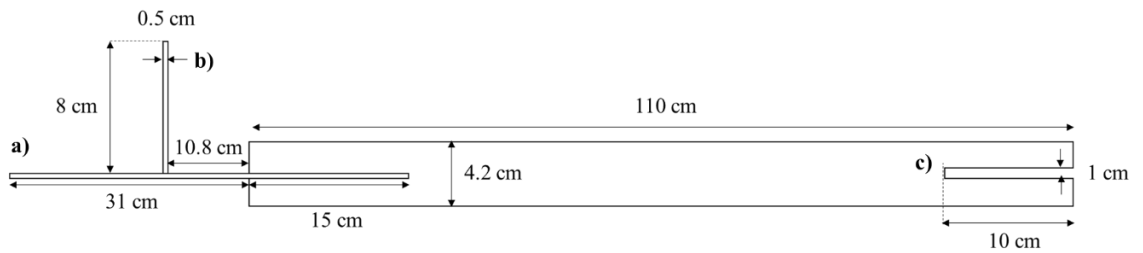


Fig. 33 2-D simulation domain and its boundary condition: a) nitrogen gas inlet, b) eucalyptus oil inlet, and c) outlet

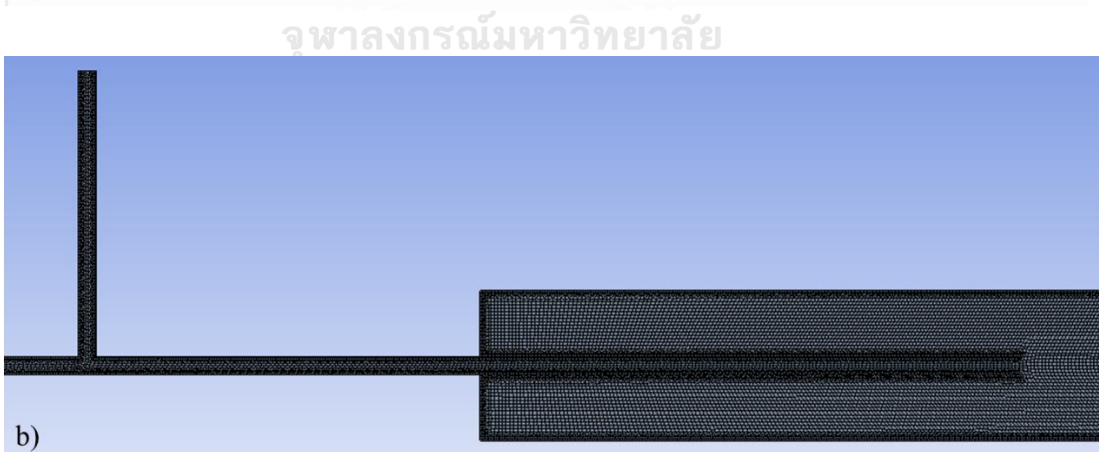
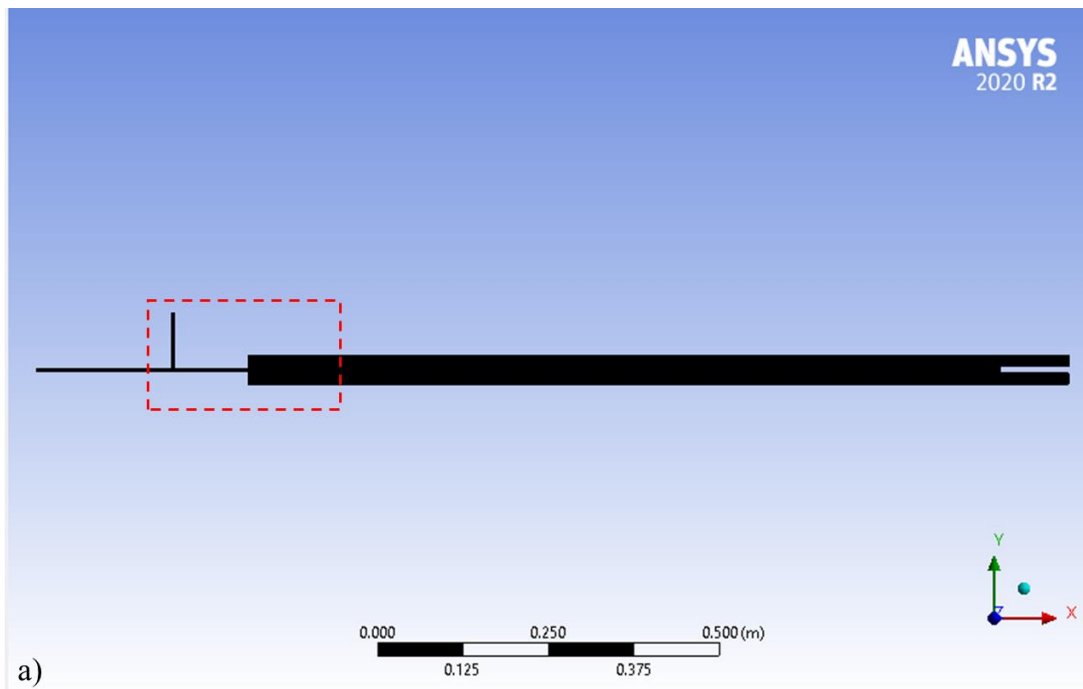


Fig. 34 a) Overall and b) inset of meshed geometry

CHAPTER 4

RESULTS AND DISCUSSION

This research focused on synthesizing magnetic carbon nanotubes (MCNTs) by using co-pyrolysis of eucalyptus oil and different catalysts. Ferrocene, nickel nitrate, 4:1 ferrocene impregnated with nickel nitrate, and 1:1 ferrocene impregnated with nickel nitrate were catalysts. The effects of synthesis temperature in the range of 700 °C, 800 °C, and 900 °C and eucalyptus oil to catalyst molar ratio range of 2:1, 5:1, and 10:1 on characteristics of CNT products were also investigated. CNT properties were characterized by SEM, TGA, Raman spectroscopy, XRD, and VSM. An appropriate condition for synthesizing high quality and yield of MCNTs was examined.

4.1 Physical properties of catalysts

Appearance of all catalysts are demonstrated in **Fig 35**. All catalysts were grinded in laboratory mortar and then screened by use of 300 μm -size sieves. **Fig 35a** shows ferrocene powder. Nickel nitrate powder is illustrated in **Fig 35b**. 1:1 ferrocene impregnated with nickel nitrate is shown in **Fig 35c**. Bulk density of ferrocene, nickel nitrate, and 1:1 ferrocene impregnated with nickel nitrate was 0.673 g/cm^3 , 0.975 g/cm^3 , and 0.690 g/cm^3 , respectively. Bulk density of nickel nitrate was significantly higher than the density of ferrocene and 1:1 ferrocene impregnated with nickel nitrate. Generally, nickel nitrate density (2.05 g/cm^3) is higher than density of ferrocene (1.10 g/cm^3). Porosity of ferrocene, nickel nitrate, and 1:1 ferrocene impregnated with nickel nitrate were 0.42, 0.50, and 0.47, respectively. Similarity of physical property could confirm that there was not effect of particle size on catalyst vaporization.

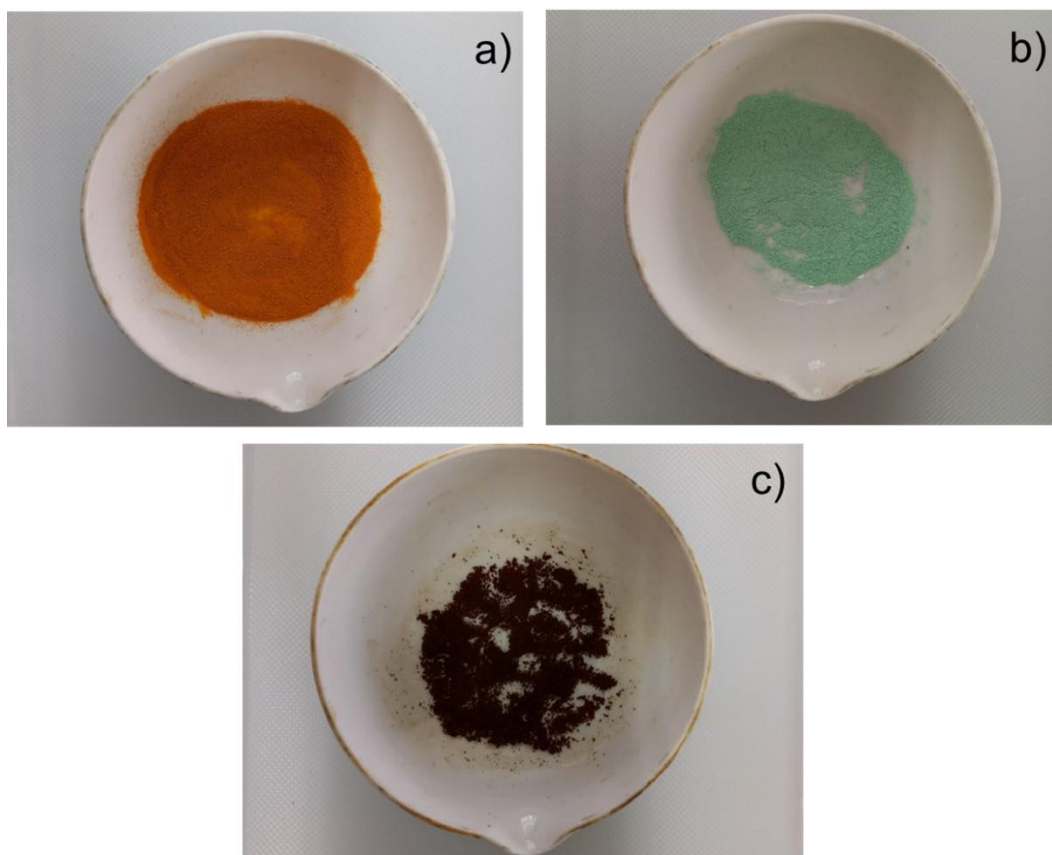


Fig. 35 Camera images of catalysts a) ferrocene, b) nickel nitrate, and c) 1:1 ferrocene impregnated with nickel nitrate

4.1.1 Catalyst characterization

All catalyst powder was characterized to confirm their element. XRD patterns of ferrocene, nickel nitrate, and 1:1 ferrocene impregnated with nickel nitrate were used to demonstrate that these catalysts as shown in **Fig. 36**. Diffraction peaks at 15.6° , 17.6° , 18.7° , 19.3° , 20.0° , 21.9° , 23.2° , 25.6° , 27.3° , and 29.8° confirm ferrocene (PDF 00-029-1711). The diffraction peaks at 21.0° , 24.2° , 27.5° , 29.9° , 34.7° , 36.9° , 44.6° , 46.5° , 49.9° , 54.5° , and 56.0° correspond to nickel nitrate (PDF 00-014-0593). The other peaks were noise because nickel nitrate is sensitive to moisture. XRD pattern of 1:1 ferrocene impregnated with nickel nitrate is clearly shown diffraction peaks of ferrocene. These results did not show bimetallic in ferrocene impregnated with nickel nitrate because they were prepared at 80°C . The preparation temperature is lower than decomposition temperature of ferrocene (500°C [52]) and decomposition temperature of nickel nitrate hexahydrate (300°C [53]). Therefore, bimetallic Ni-Fe could not produce in catalyst preparation.

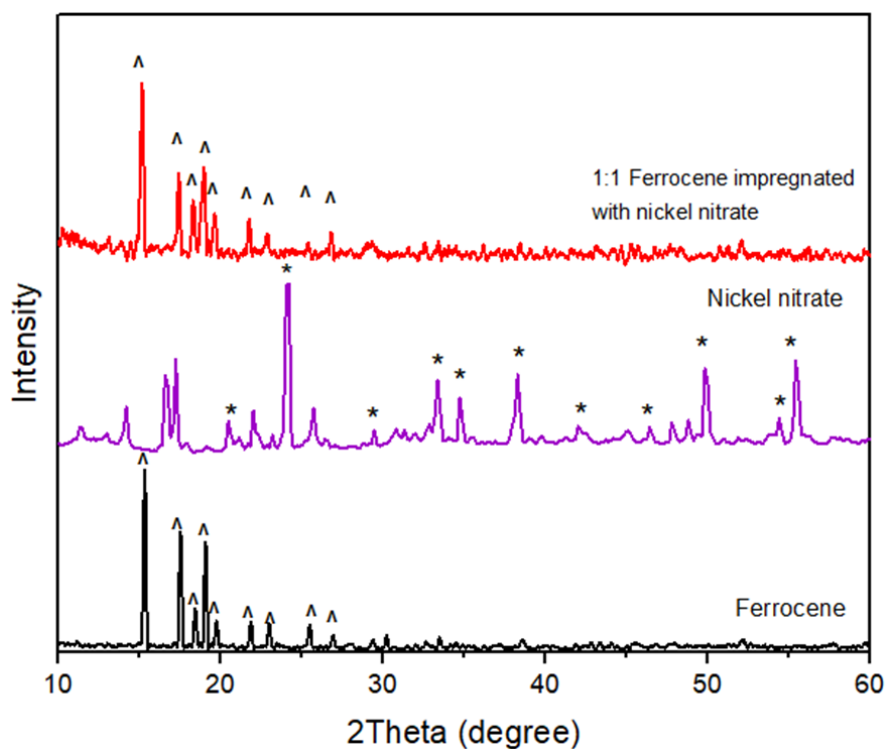


Fig. 36 XRD spectra of ferrocene, nickel nitrate, 1:1 ferrocene impregnated with nickel nitrate

To confirm nickel nitrate, FTIR spectra were evidence of production of 1:1 ferrocene impregnated with nickel nitrate. This was used to demonstrate these catalysts as shown in **Fig. 37**. Both catalysts reveal the characteristic of -OH stretching at $3,462\text{ cm}^{-1}$. The band at $1,653\text{ cm}^{-1}$ and $1,408\text{ cm}^{-1}$ are ascribed to asymmetric and symmetric vibrations of N-O, respectively. These peaks are characteristic of nickel nitrate. The peaks at $1,107\text{ cm}^{-1}$, 997 cm^{-1} , and 813 cm^{-1} contribute to vibration of C=C bending. The 488 cm^{-1} peak is due to the out-of-plane bending of C-H bond. These are characteristic peaks of ferrocene. The results confirmed attaching of ferrocene and nickel nitrate to the catalyst. The atomic composition of 1:1 ferrocene impregnated with nickel nitrate could be confirmed by EDS spectrum and XRF which shows in **Appendix B**.

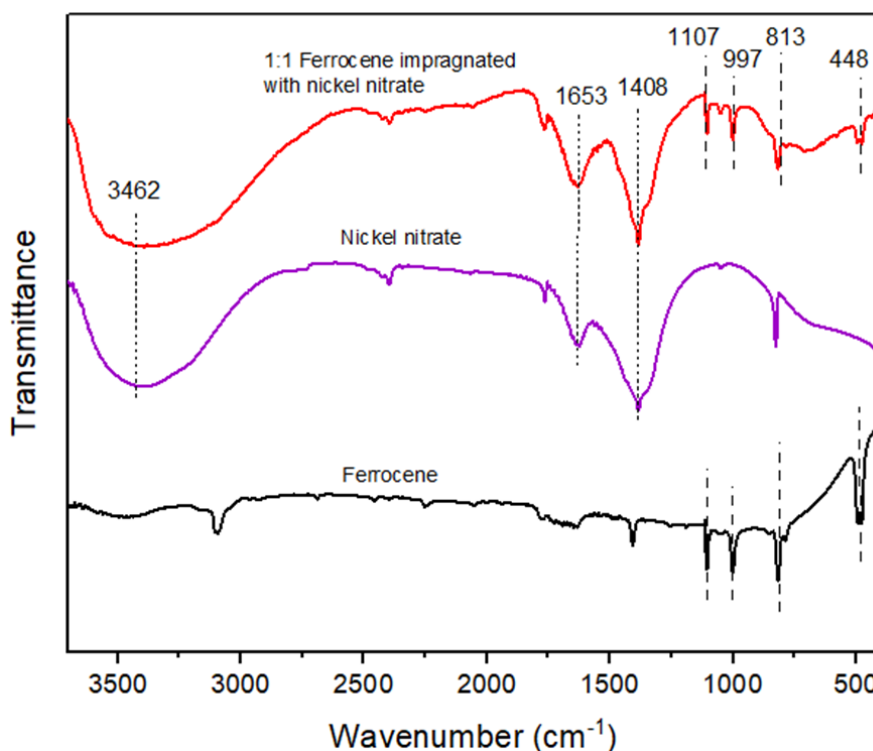


Fig. 37 FTIR spectra of ferrocene, nickel nitrate, 1:1 ferrocene impregnated with nickel nitrate

4.2 Effect of catalyst on resultant MCNTs

For the synthesis of MCNTs in this part, eucalyptus oil and different catalysts were decomposed within the quartz tubular reactor. Synthesis temperature of 800 °C was selected because the condition could be obtained high quality of CNTs [36, 42]. Ferrocene, nickel nitrate, and 1:1 ferrocene impregnated with nickel nitrate were used as catalysts. Molar ratio of eucalyptus oil to catalyst was 5:1. The objective of this section is to examine effect of different types of catalysts. Repeated experimental and analytical results could confirm its effect on improved quality and yield of MCNTs.

4.2.1 Morphology of CNTs synthesized from eucalyptus oil and different catalyst

Fig. 38a-38c show the morphology of synthesized CNTs by use of different catalyst: ferrocene, nickel nitrate, and 1:1 ferrocene impregnated with nickel nitrate, observed from Scanning Electron Microscope (SEM). CNTs synthesized from eucalyptus oil and different catalyst were labeled as CNT_F1N0, CNT_F1N1, and CNT_F0N1, respectively. All SEM images indicated CNT structure in all carbon samples. However, there was high amount of irregular shape carbon in CNT_F1N0 sample as seen in **Fig. 38a**. There was flake shape carbon in CNT_F0N1 sample as illustrated in **Fig. 38b**.

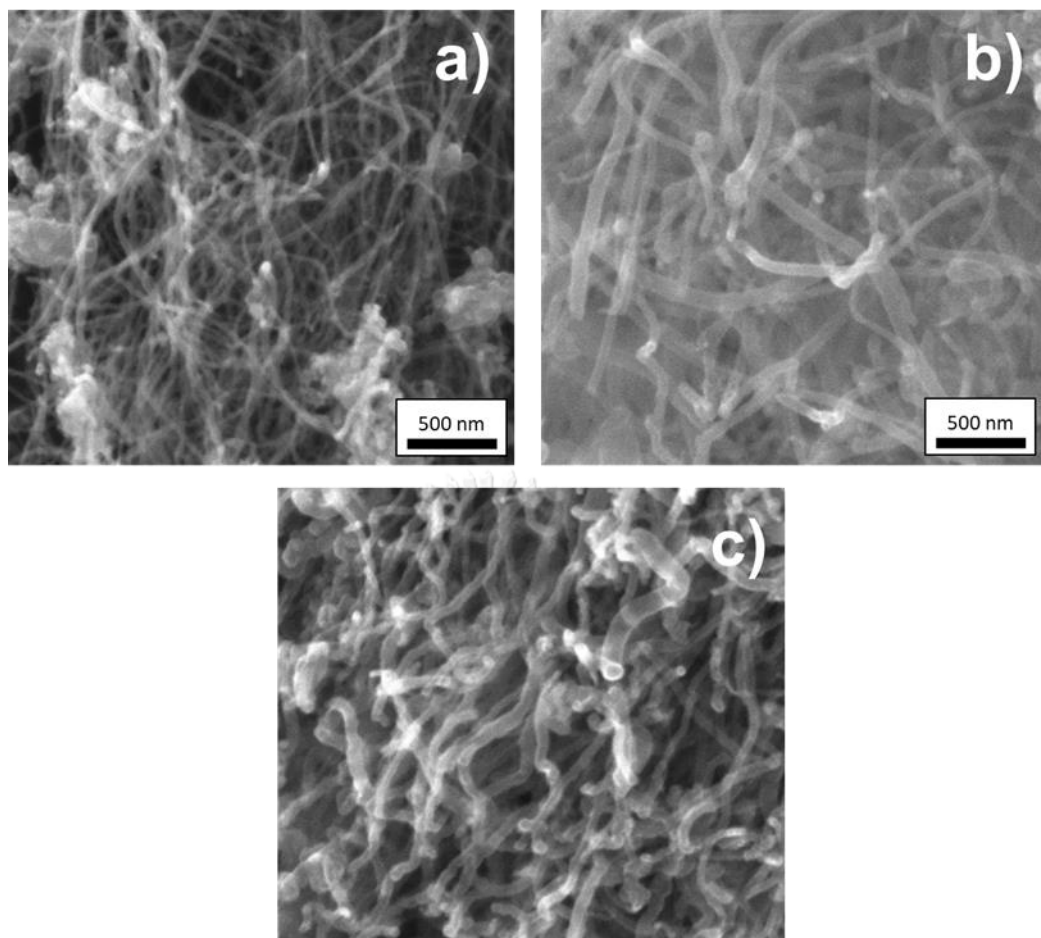
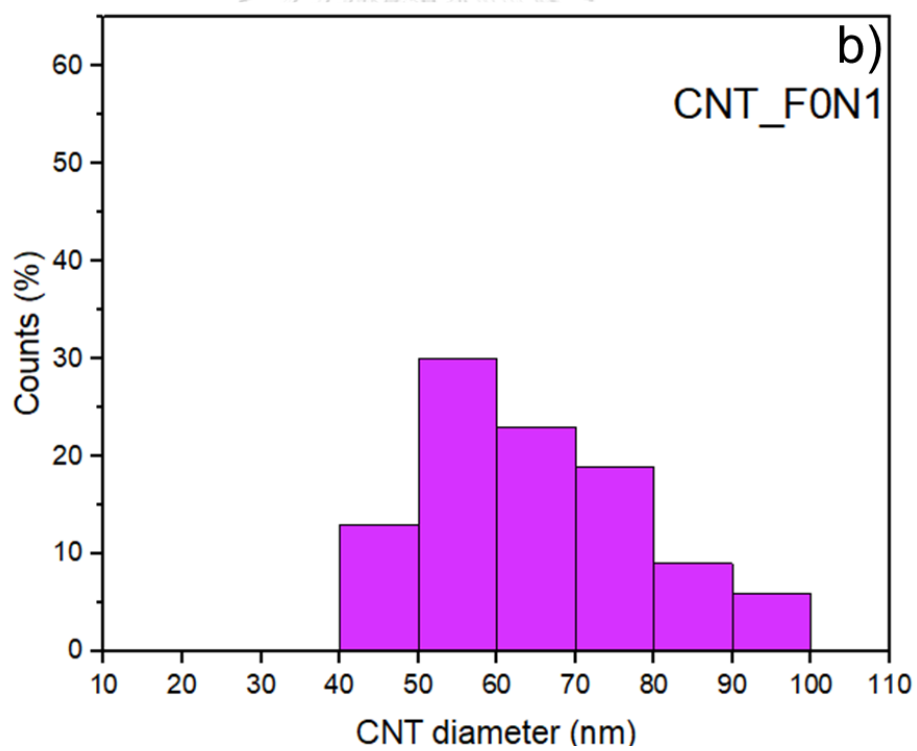
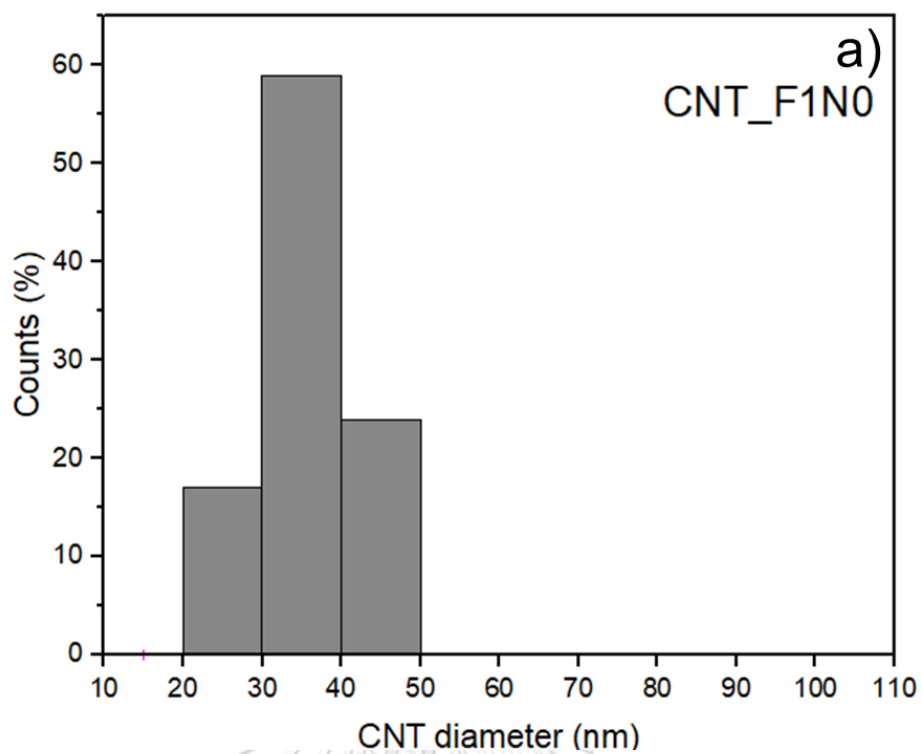


Fig. 38 SEM images of morphology of as-synthesized CNTs from co-pyrolysis of eucalyptus oil with different catalyst: a) CNT_F1N0, b) CNT_F1N1, and c) CNT_F0N1

Average diameter of synthesized CNTs was determined by employing ImageJ. All data sheets of CNT diameter are exhibited in **Appendix D**. The average diameter of synthesized CNT was in the range of 30-60 nm which is defined as MWCNTs [54]. Diameter distributions of CNTs from different catalyst are shown in **Fig. 39a-39c**. Average diameter of CNT_F1N0, CNT_F0N1, and CNT_F1N1 were 36 ± 5 nm, 65 ± 14 nm, and 47 ± 13 nm, respectively. These results suggested that increasing of nickel nitrate proportion caused the increment of average CNT diameter.



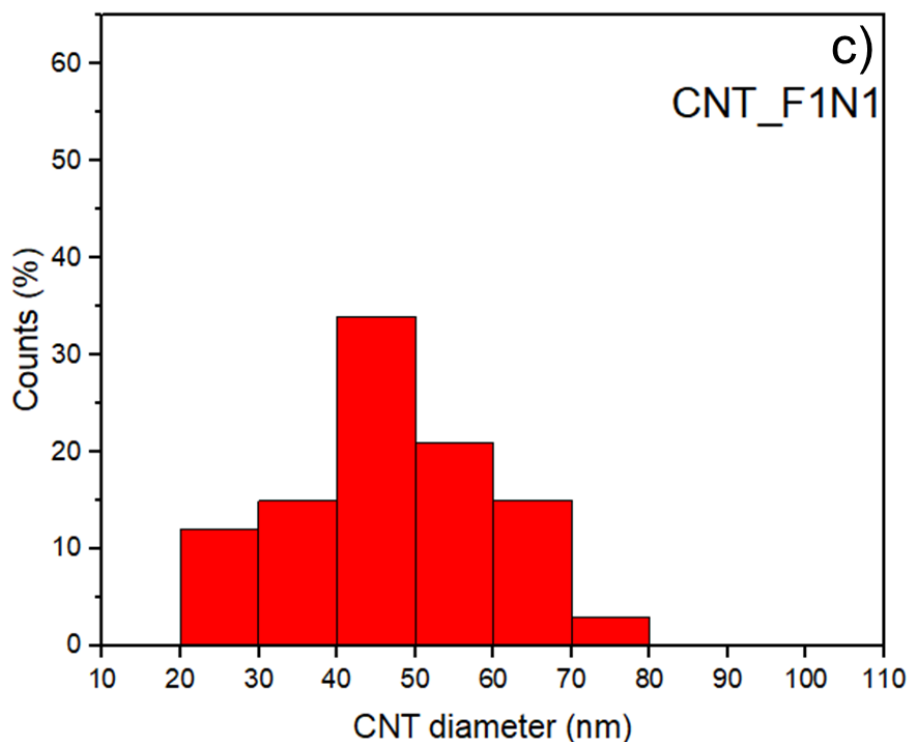


Fig. 39 CNT diameter distribution of a) CNT_F1N0, b) CNT_F1N1, and c) CNT_F0N1

4.2.2 Thermal stability of MCNTs synthesized from eucalyptus oil and different catalyst

The thermal stability of synthesized CNTs could be observed by Thermogravimetric analyzer (TGA) under O₂ atmosphere. **Fig. 40a-40b** illustrate TGA and DTG curves of CNTs synthesized from different catalyst. TGA curves were plotted between the weight percentage of carbon samples against oxidation temperature. DTG curves were plotted between the derivative sample weight percentage against oxidation temperature. Significant weight loss at 430-600 °C would be attributed to the decomposition of synthesized CNTs [43]. **Fig. 40a** reveals that CNT_F1N0, CNT_F0N1, and CNT_F1N1 were started to decompose at temperature of 447 °C, 610 °C, and 473 °C, respectively. Additionally, DTG analysis was employed to figure out a peak temperature with maximum weight loss rate as shown in **Fig. 40b**. DTG curves of CNT_F1N0, CNT_F0N1, and CNT_F1N1 indicated the peaks at oxidation temperature of 515 °C, 665 °C, and 579 °C. These results suggested that a high proportion of nickel nitrate in catalyst could be increased thermal stability of CNTs. The thermal stability had been reported by Yao et al. [39], when molar ratio of Ni to Fe in catalyst was increased from 1:3 to 3:1, oxidation temperature increased from 500-600 °C to 550-650 °C. It can be concluded that more Ni content in catalyst could improve thermal stability of CNTs. Moreover, the TGA curve of CNT_F0N1 also present the started decomposition temperature at 610 °C. Its DTG curve also illustrate the peak at 665 °C. The results could be confirmed a present of graphite in carbon sample due to the graphite is higher thermal stability than CNTs [55].

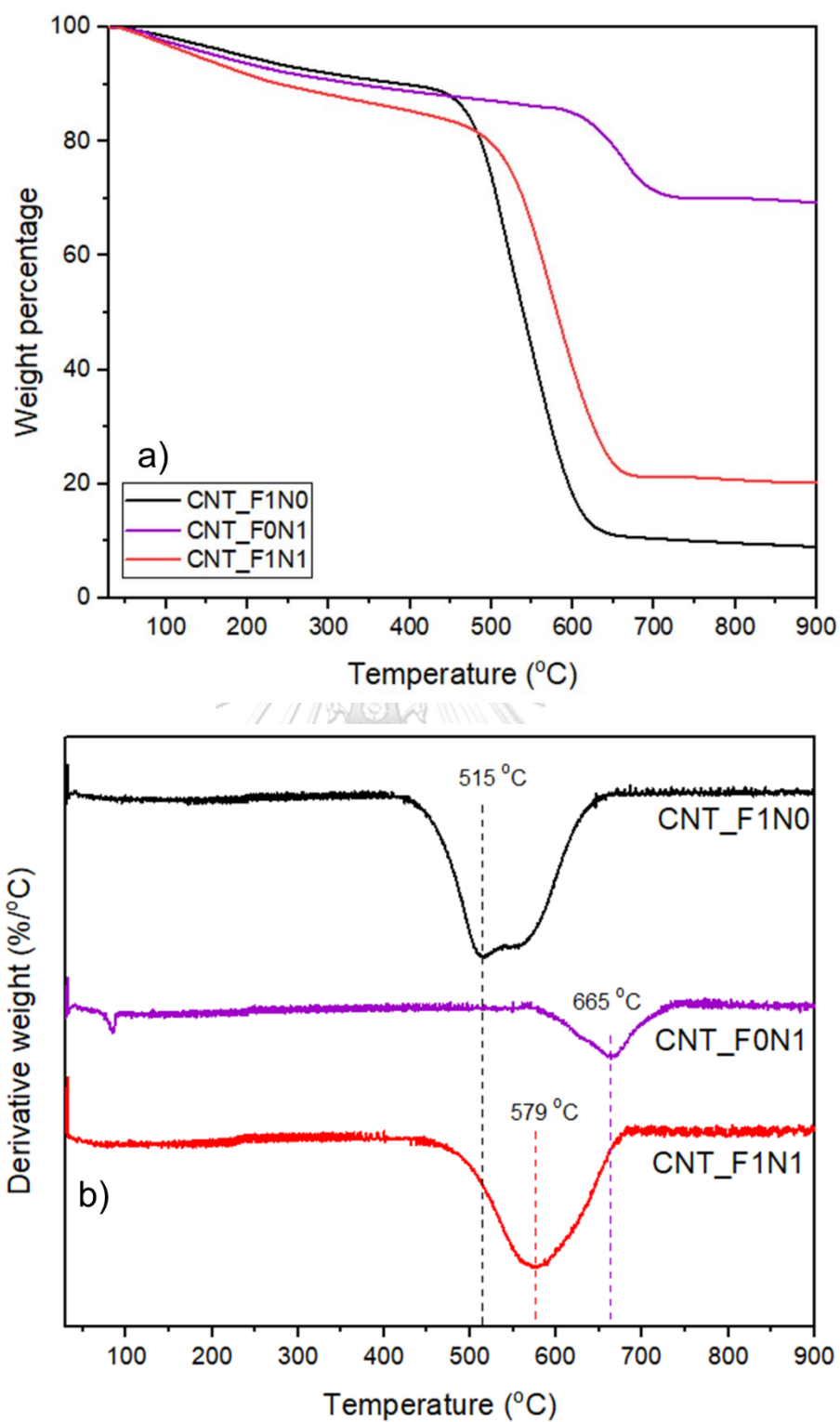


Fig. 40 a) TGA and b) DTG curves of as-synthesized CNTs from co-pyrolysis with eucalyptus oil and different catalyst

4.2.3 Crystallinity of MCNTs synthesized from eucalyptus oil and different catalyst

The crystallinity of synthesized CNTs using different catalysts could be observed from Raman spectra, as shown in **Fig. 41**. D-band at Raman shift $1,323\text{ cm}^{-1}$ represents the vibration of non- sp^2 bonded carbon atom. The band is applied to identify amorphous carbon or defect structure. G-band at Raman shift $1,588\text{ cm}^{-1}$ assigns to the vibration of sp^2 bonded carbon atom. The band is used to identify CNT structure [56]. The ratio of intensity of D-band to G-band ($I_{\text{D}}/I_{\text{G}}$) could determine the crystallinity of carbon product. The higher crystallinity of carbon product was obtained at lower $I_{\text{D}}/I_{\text{G}}$. From this experiment, $I_{\text{D}}/I_{\text{G}}$ ratio of CNT_F1N0, CNT_F0N1, and CNT_F1N1 was 1.19, 0.87, and 1.05, respectively. The results suggested the addition nickel nitrate of catalyst could decrease in $I_{\text{D}}/I_{\text{G}}$ ratio.

The ratio decreased when the use of ferrocene was replaced by using 1:1 impregnated with nickel nitrate catalyst was increased. The addition of Fe in Ni catalyst suppressed the formation of amorphous carbon while promoting the growth of CNTs [57]. It mainly attributed to the oxidization of amorphous carbon because CNTs as the type of graphitic carbon were more difficult to be oxidized than the amorphous carbon. The low amount of amorphous carbon was supported by SEM and TGA results. Moreover, Fe-Ni synergistic effect played dominant role in CNT synthesis. Generally, Fe catalyst can induce carbon dissolution. Meanwhile, Ni catalyst can promote graphene layer nucleation [58]. The superior performance of the catalyst was derived from the integrated Fe and Ni. Therefore, ferrocene impregnated with nickel nitrate catalyst could improve the crystallinity of CNTs.

However, the crystallinity degree of CNT_F1N0 was highest due to graphite in carbon sample as characterization from SEM and TGA. Graphite has more crystallinity degree than CNTs in general [59].

There were some reports of effect of molar ratio of Ni to Fe in catalyst on crystallinity of CNTs. Yao et al. [39] reported that the $I_{\text{D}}/I_{\text{G}}$ ratio of as-synthesized CNTs was 1.03, 1.07, 0.71, 0.64, and 0.68 when synthesized using catalyst which had 1:3, 1:2, 1:1, 2:1, and 3:1 molar ratio of Ni to Fe. The results suggested that more nickel proportion of Ni-Fe catalyst could improve the crystallinity of CNTs.

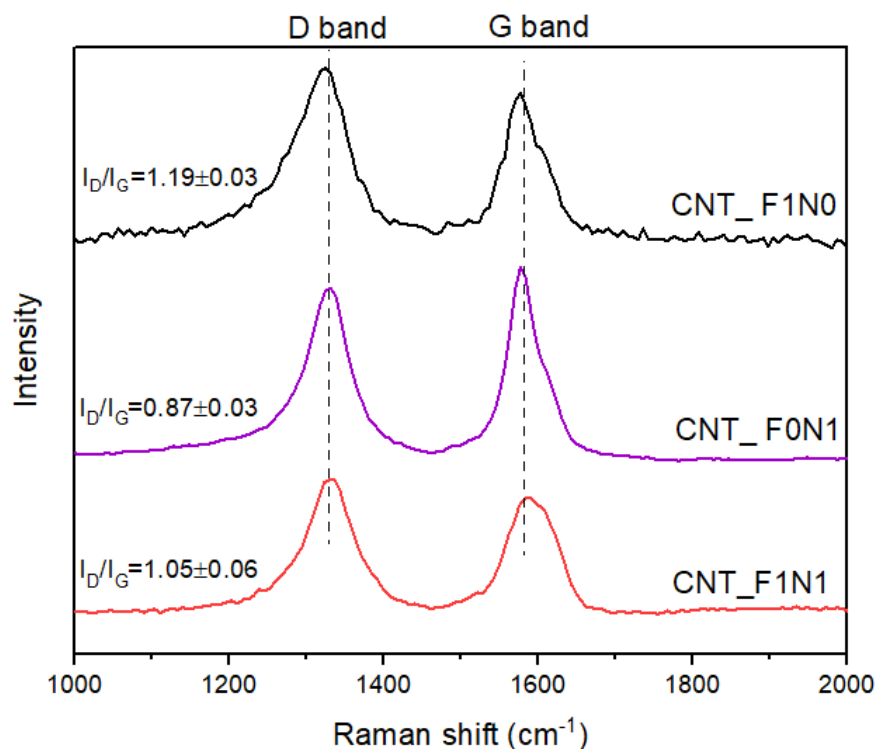


Fig. 41 Raman spectra of CNTs synthesized by use of different catalyst

4.2.4 Total mass yield of MCNTs synthesized from eucalyptus oil and different catalyst

Total mass yields by weight of synthesized products could be calculated by **Eq 2**. The weight of eucalyptus oil and catalyst was calculated from **Eq C1** and **Eq C2** in **Appendix C**, respectively.

$$Total\ mass\ yield(\%) = \frac{W_p}{W_{oil} + W_{cat}} \times 100 \quad \text{Equation 2}$$

Where W_p represented weight of synthesized product

W_{oil} represented weight of eucalyptus oil

W_{cat} represented weight of catalyst

Total mass yield of each condition is shown in **Fig. 42**. When ferrocene, 1:1 ferrocene impregnated with nickel nitrate, and nickel nitrate were used as catalyst in CNT synthesis, total mass yield was $15.6 \pm 1.4\%$, $7.7 \pm 1.5\%$, and $13.9 \pm 1.2\%$ respectively. It was lower than the yield from use of ferrocene because of lower H_2 supply for metal catalyst reduction.

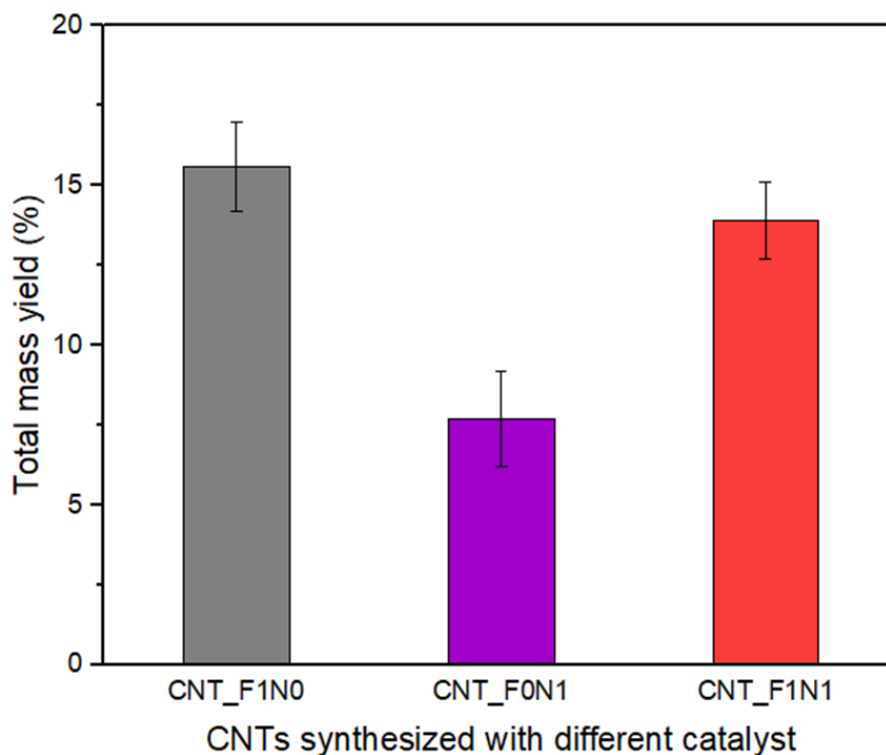


Fig. 42 Total mass yield of as-synthesized CNTs from different catalyst

At the beginning, pyrolysis of eucalyptus oil without using any catalysts was conducted. The process could not provide any product because eucalyptus oil was thermally vaporized and decomposed before flowing out from the quartz tube reactor. There were no detectable solid products within in the reactor. Therefore, CNT synthesis yield without catalyst was null. As a strategy of this work, different catalysts including ferrocene, nickel nitrate, and 1:1 ferrocene impregnated with nickel nitrate were employed for the synthesis of CNTs.

Pyrolysis of ferrocene provided solid product depositing on the inner surface of the quartz tube reactor. This could be attributed to the fact that ferrocene could provide hydrogen gas, carbon clusters, and Fe atom after its decomposition at as shown in **Eq 3** [52]. Such carbon clusters would undergo self-assembly induced by the presence of catalytic Fe nanoparticles. Srisrattha et al. [36] and Wulan and Setiawati [37] also reported that pyrolysis of ferrocene under nitrogen atmosphere could provide CNTs.



With co-pyrolysis of eucalyptus oil and ferrocene, **Fig. 38a** suggested that a substantial amount of CNTs could be synthesized from co-pyrolysis of eucalyptus oil and ferrocene. These results would be ascribed that decomposition of eucalyptus oil could contribute to an increase in carbon clusters which would be essential for the self-assembly of CNTs.

For CNT synthesis from co-pyrolyzed eucalyptus oil with nickel nitrate, there are certain thermal decomposition steps of nickel nitrate, including melting, dehydration, and decomposition to NiO [53]. Reduction of solid-phase NiO by H₂ would lead to the formation of metallic nickel with a developed crystalline size with high catalytic activity [60].

Because eucalyptus oil, which eucalyptol contains hydrogen within its molecule, decomposition of eucalyptus oil would contribute to the activation of metallic Ni catalyst and self-assembly of CNTs. As confirmed by the SEM analyses, CNTs with 65-nm diameter would be preferable under this condition. These results would suggest that Ni catalyst would also provide positive effect on the formation of CNTs.

The co-pyrolysis of eucalyptus oil with 1:1 ferrocene impregnated with nickel nitrate could provide the higher total mass yield. The good performance of the catalyst may be due to the interaction between bimetallic Fe and Ni, which promoted the dissociation of C-H bond for more hydrogen and carbon [41, 61]. Additionally, it is noteworthy that ferrocene, which also contained H₂ within its molecule, would contribute to additional supply of H₂. The presence of H₂ from eucalyptus oil and ferrocene would attribute to the enhanced reduction of Fe and Ni nanoparticles. As a result, using eucalyptus oil with ferrocene impregnated with nickel nitrate could provide much improved production yield and characteristics of the resultant products compared to other previous conditions as SEM, TGA, and Raman results.

Fig. 43 shows crystallography of the CNT_F1N0, CNT_F0N1, CNT_F1N0.25, and CNT_F1N1. All XRD patterns show diffraction peak of graphite at $2\theta = 26.5^\circ$ which can be assigned to (002) planes of CNTs (PDF 03-065-6212). For metal indication, the XRD patterns of CNT_F1N0 exhibited diffraction peak at $2\theta = 44.7^\circ$ represented (110) plan of Fe (PDF 03-065-4899). Also, they indicated diffraction peaks of $2\theta = 37.7^\circ, 39.9^\circ, 40.7^\circ, 42.9^\circ, 43.8^\circ, 45.9^\circ, 49.2^\circ, 51.8^\circ, 54.5^\circ$ and 58.1° reflected Fe₃C phase (121), (210), (201), (211), (102), (112), (221), (122), (301) (PDF 03-065-2411). At the same time, crystallography of CNT_F0N1 shows diffraction peaks of and Ni at $2\theta = 44.5^\circ, 51.9^\circ,$ and 76.4° , which indicated to (111), (200), and (220) planes (PDF 00-004-0850), respectively. The results could confirm the H₂ from decomposed eucalyptus oil reduced NiO. The crystallinity peaks of CNT_F1N1 at and FeNi₃ peaks at $2\theta = 44.3^\circ, 51.6^\circ,$ and 75.7° which match with (111), (200) and (222) planes of the bimetal (PDF 00-038-0419). These peaks of FeNi₃ could confirm interaction between Fe and Ni.

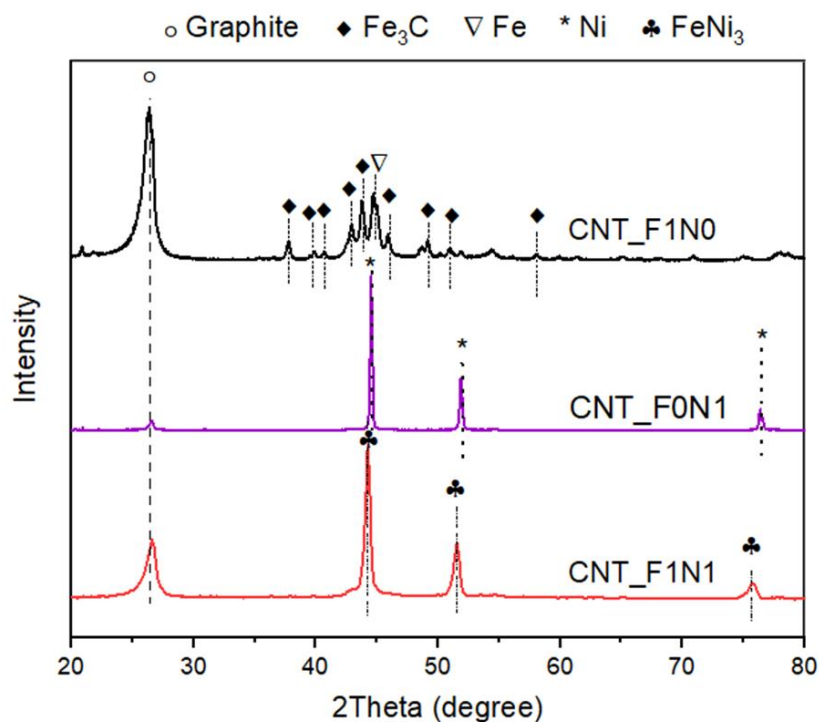


Fig. 43 XRD patterns of synthesized CNTs from different catalyst

There were some studies of effect of molar ratio of Fe to Ni in catalyst on product yield. Li et al. [11] found that carbon yield was only about 7% and 8% when using single Fe and Ni metal. However, Fe-Ni bimetallic catalyst was used, the yield increased significantly. Moreover, with the Fe to Ni molar ratio of catalyst increasing from 2:8 to 8:2, the yield increased from 18% to 22%. From Fazle Kibria et al. [40], their results revealed that yields of CNTs by use of Fe catalyst and Ni catalyst were 16.1% and 11.3%, respectively. For use of bimetallic catalysts, which were 3.2:1, 1.1:1, and 0.4:1 molar ratio of Fe to Ni in catalyst, yields were 94.1%, 60.3%, and 39.4%, respectively. These results confirmed that the yields of CNTs from Fe-Ni bimetallic catalysts were remarkably higher than those for the single metal catalysts. Furthermore, the yield also increased due to addition of Fe catalyst. However, 1:1 ferrocene impregnated with nickel nitrate could provide slight fewer total mass yield than using ferrocene because of lower H_2 resource for catalyst reduction.

4.2.5 Magnetic properties of MCNTs synthesized from eucalyptus oil

As a preliminary investigation of magnetic property of all resultant products, a simple test using a magnetic bar was conducted. As shown in **Fig. 44**, it would be observed that particulate products could be responsive to the magnetic bar. After moving the magnetic bar far away from the product container, the resultant product would return to its particulate form due to gravity.



Fig. 44 Photograph of resultant product responding to magnetic field

To investigate the magnetic properties of MCNTs that synthesized different catalysts, VSM was used to measure the hysteresis loops of the samples at room temperature. **Fig. 45a-45b** show all hysteresis loops for the MCNTs. The all shapes of the hysteresis loop indicated ferromagnetic properties at room temperature. Hysteresis loop results indicated the saturation (M_s) and coercivity (H_c) values of all products. M_s values of CNT_F1N0, CNT_F0N1, and CNT_F1N1 were 20.2 emu/g and 84.2 emu/g, and 33.0 emu/g, respectively. The results suggested that addition of nickel nitrate could increase in M_s . The addition of Ni content to the Fe-rich region enhances electron distribution because the number of positive-spin electrons was raised and hence a decline of magnetic moment [62].

Additionally, CNT_F1N0 had M_s less than the M_s of bulk Fe (212 emu/g) and bulk Fe_3C (140 emu/g) [63] because of the small dimensions of Fe in carbon sample and diamagnetic effect from carbon [48]. However, in case of CNT_F0N1, the M_s was higher than the value of Bulk Ni which was 54.4 emu/g [64]. For Ni nanoparticles, CNT structure where strong diamagnetic tube for nickel that could enhance the extrinsic magnetic moment of a magnet embedded inside it. It could help magnetic moment extended further apart to the length of the tubes without changing its strength, thus giving an extrinsic enhancement to the magnetic moment [65]. CNT structure would help to raise M_s of Ni nanoparticles, M_s value of CNT_F1N1 was higher than M_s of CNT_F1N0. However, it was less than M_s of bulk $FeNi_3$ (125 emu/g [66]) due to influence of carbon.

The H_c of all samples were determined from magnetic hysteresis curves. H_c of CNT_F1N0, CNT_F0N1, and CNT_F1N1 were 211.0 G, 23.2 G, and 118.0 G, respectively. The results suggested the addition of nickel nitrate could be reduced H_c . The reduction of H_c was caused by increment of magnetic particle diameter. Its enhancement could result in multi-domain properties of particles [34, 35]. The phenomena could be supported by diameter of CNT_F0N1, CNT_F1N1, CNT_F0N1 increase from 36 nm to 47 nm and 65 nm. The size of metallic particle related to CNT

diameter. Moreover, all H_c were higher than H_c of bulk Fe (1 G [67]), bulk $FeNi_3$ (66 G [68]) and bulk Ni (0.7 G [69]) because metal particles were arranged in a quasi-one-dimensional manner in CNT structure [48]. The CNT anisotropies are assisted to stabilize magnetic order against thermal fluctuations in such reduced dimensions, thus they would attribute high H_c of MCNTs [70].

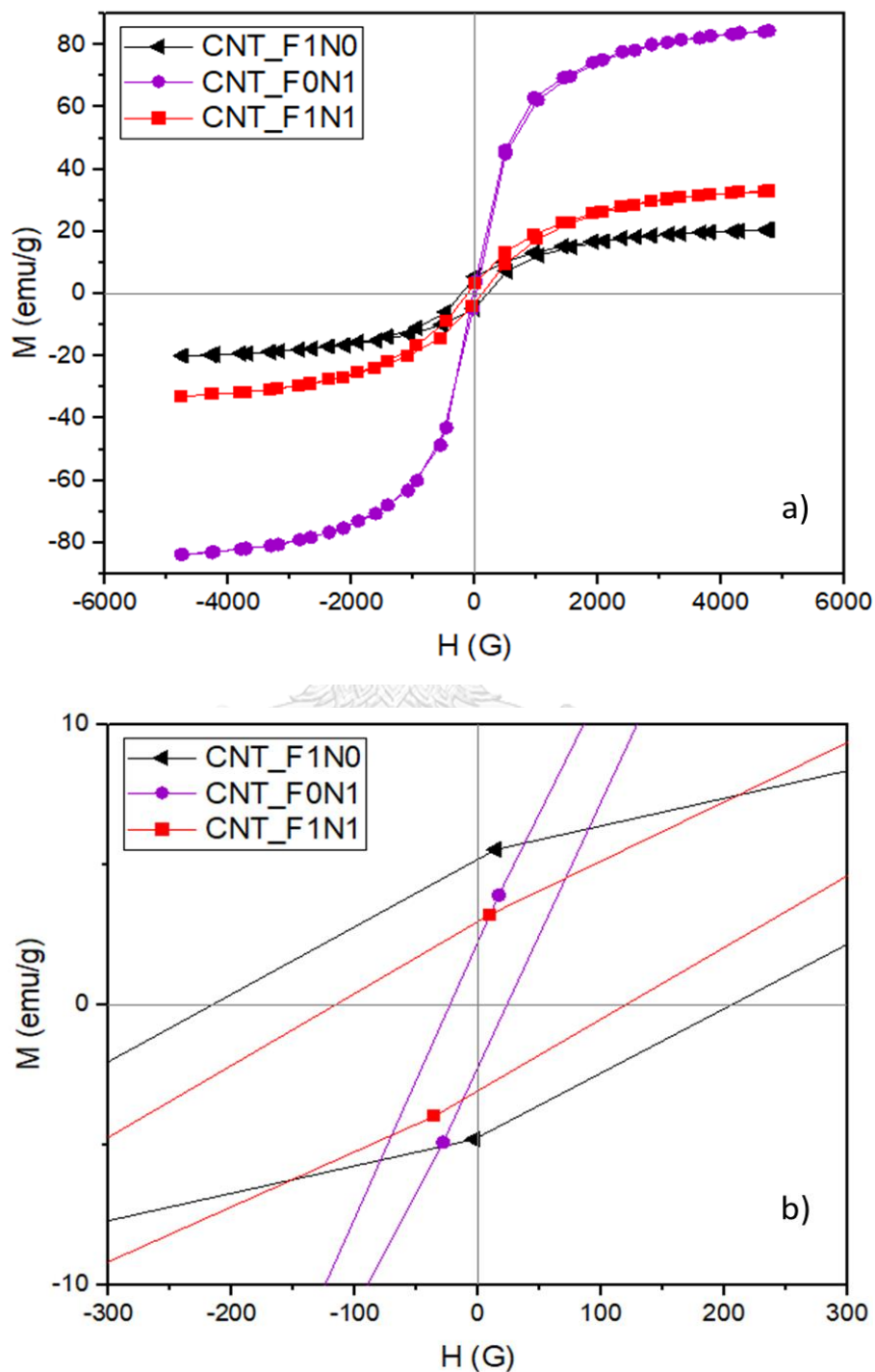


Fig. 45 Magnetic hysteresis loops of as-synthesized CNTs from different catalyst at room temperature in a) a whole range and b) magnified range of -300 G to 300 G

From the study effect of catalyst on MCNT properties, ferrocene, nickel nitrate, and 1:1 ferrocene impregnated with nickel nitrate were used in MCNT synthesis. The results revealed that 1:1 ferrocene impregnated with nickel nitrate provided good quality of CNTs with good diameter distribution, high thermal stability, and high crystallinity degree. Therefore, in study effect of synthesis temperature, 1:1 ferrocene impregnated with nickel nitrate was used as catalyst.

4.3 Effect of synthesis temperature on property of CNTs synthesized from eucalyptus oil and 1:1 ferrocene impregnated with nickel nitrate

For the synthesis of MCNTs, eucalyptus oil and 1:1 ferrocene impregnated with nickel nitrate were fed to a quartz tubular reactor situated in an electrical furnace equipped with a temperature controller. The temperature profile along the quartz tube is illustrated in **Fig. 46**. A ceramic boat containing a designated amount of catalyst was shifted into the heating zone of reactor at the position of 35 cm from the tube inlet. Then, the designated amount of eucalyptus oil was supplied by a syringe pump with a constant feed rate. With this setting, it could be confirmed that synthesis temperature could be controlled in the designated range (700 °C, 800 °C, and 900 °C).

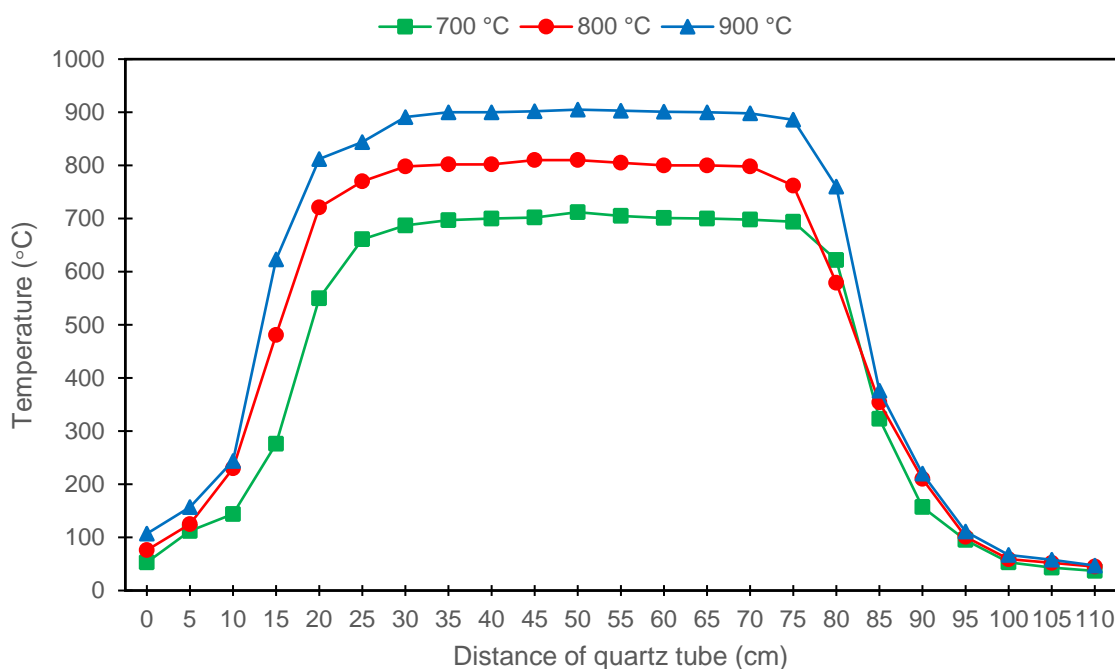


Fig. 46 The temperature profiles of quartz tube reactor at each synthesis temperature

4.3.1. Morphology of MCNTs synthesized from eucalyptus oil and 1:1 ferrocene impregnated with nickel nitrate

In **Fig. 47a-47c**, typical Scanning Electron Microscope (SEM) micrographs show morphology of synthesized MCNTs at different synthesis temperature. SEM images revealed that the product which was synthesized at 700 °C (**Fig. 46a**) consisted of irregular-shape carbon nanoparticles and as-grown MCNTs. When synthesis temperature was increased to 800 and 900 °C, it could be observed that synthesized product consisted of a large amount of CNTs with low amount of irregular-shape carbon nanoparticles (**Fig. 46b** and **Fig. 46c**, respectively). An increase in synthesis temperature accelerated decomposition and formation rate of MCNTs which showed the significant increase in CNT structure [19].

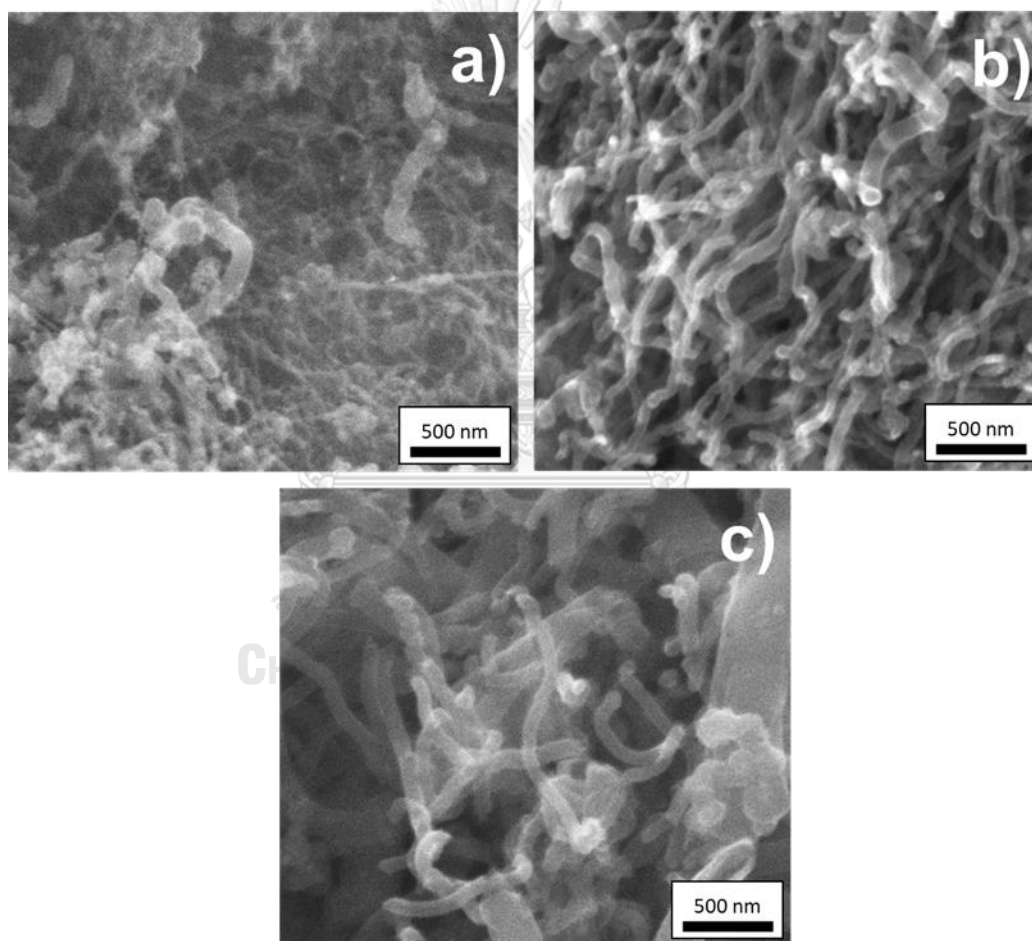
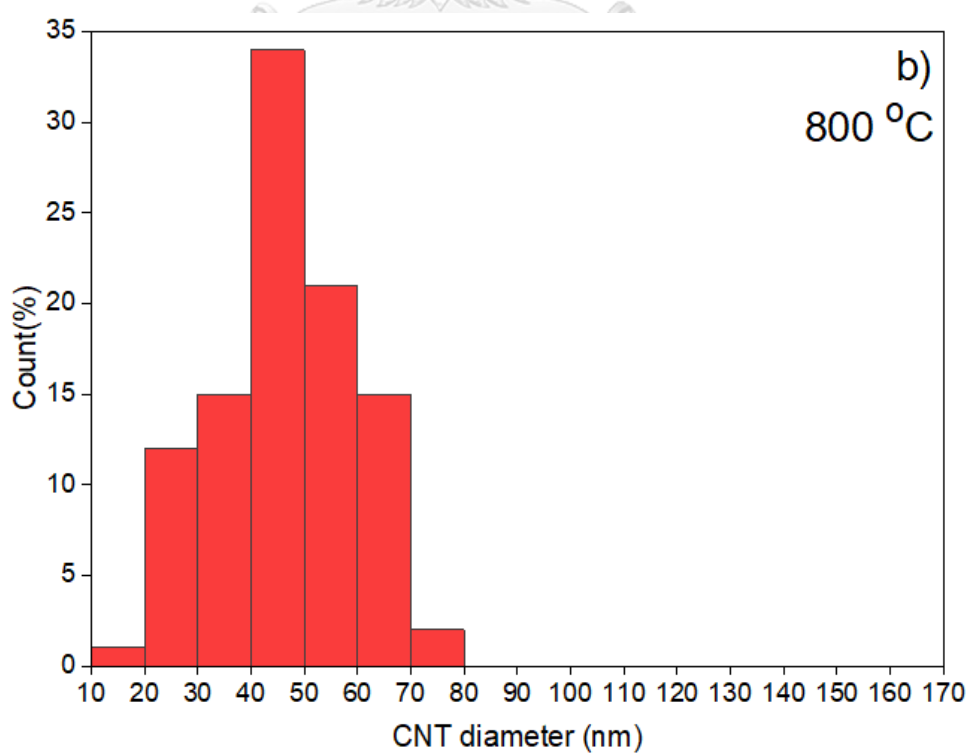
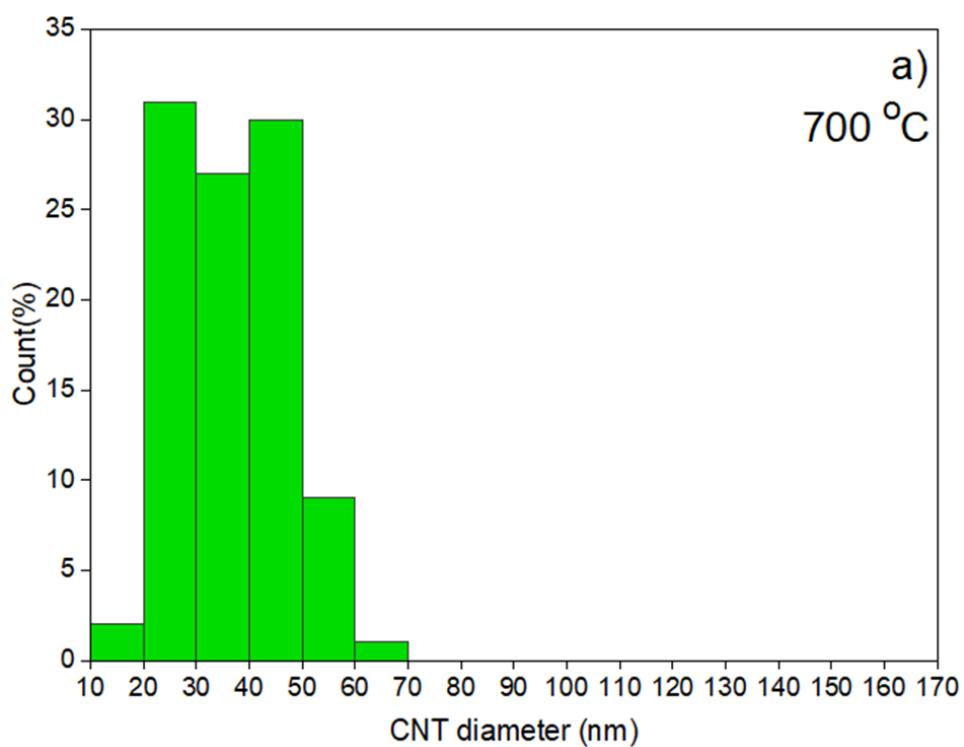


Fig. 47 SEM images of as-synthesized MCNTs at synthesis temperature of a) 700 °C, b) 800 °C, and c) 900 °C

Size distributions of CNTs at different temperature are shown in **Fig. 48a-48c**. When synthesis temperature was increased from 700 °C to 800 °C to 900 °C, an average diameter was increased from 37 ± 10 nm to 47 ± 13 nm to 101 ± 23 nm, respectively. These results would suggest that an increase in synthesis temperature would lead to a

higher decomposition of eucalyptus oil, resulting in an increase in carbon clusters which would undergo the self-assembly of CNTs with the presence of catalytic nanoparticles. It was also reported that the higher synthesis temperature could result in a higher agglomeration of catalytic nanoparticles [43].



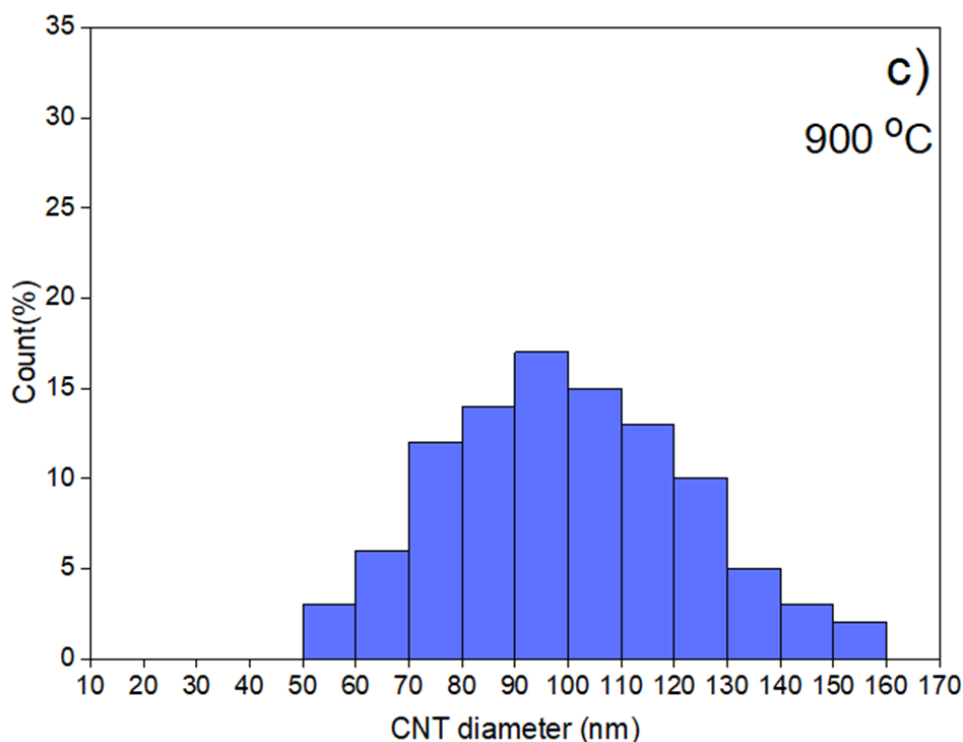


Fig. 48 CNT diameter distribution of as-synthesized MCNTs at synthesis temperature of a) 700 °C, b) 800 °C, and c) 900 °C

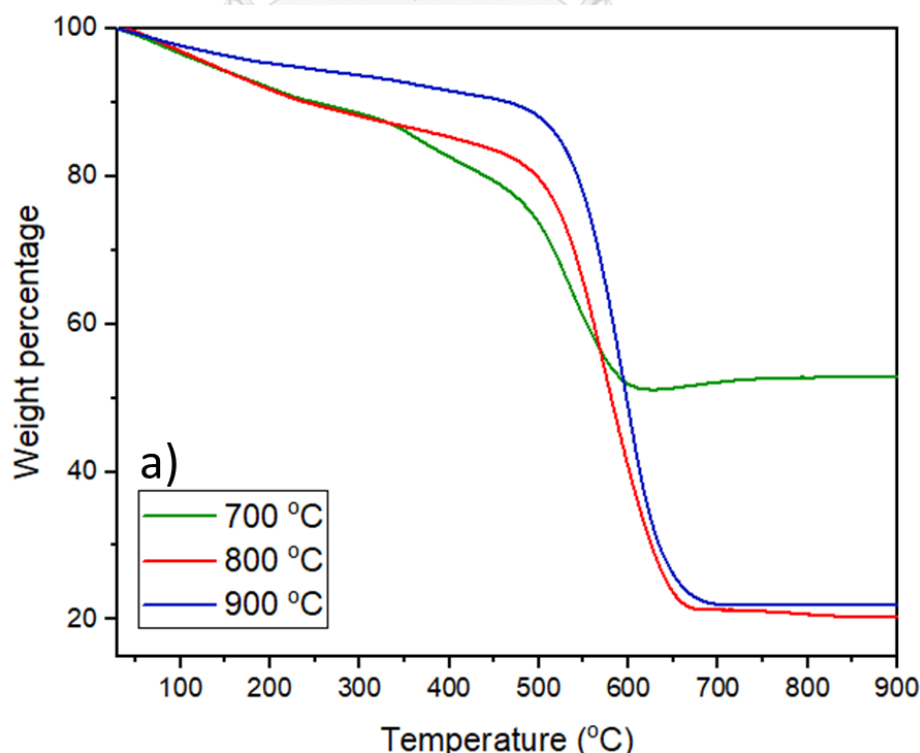
An increase in the average diameter of CNTs with an increase in synthesis temperature had been reported in some literatures. Lee et al. [43] reported that an increase in synthesis temperature from 750 °C to 850 °C and 950 °C could result in an increase in average CNT diameter from 30 ± 5 nm to 60 ± 10 nm and 130 ± 20 nm, respectively. Similarly, Srisrattha et al. [36] reported that an increase in synthesis temperature from 700 °C, 800 °C, to 900 °C could lead to an increase in the average diameters of CNTs from 54 ± 20 nm, 51 ± 13 nm, to 93 ± 44 nm, respectively. Lee et al. [43] proposed that an increment of CNT diameters was due to an increase in Fe particle size. When the synthesis temperature was 750 °C, 850 °C, and 950 °C, the size of Fe particles was 40 ± 10 nm, 90 ± 20 nm, and 150 ± 40 nm, respectively. Based on all results of this work, an increment of CNT diameter was resulted from an aggregation of catalyst particles.

4.3.2 Thermal stability of MCNTs synthesized from eucalyptus oil and 1:1 ferrocene impregnated with nickel nitrate

The thermal stability of synthesized MCNTs could be analyzed by Thermogravimetric analyzer (TGA) under O₂ atmosphere. **Fig. 49a-49b** exhibit TGA and DTG curves of CNTs synthesized at different synthesis temperature. TGA curves

were plotted between the weight percentage of sample against oxidation temperature. DTG curves were plotted between the derivative sample weight percentage against oxidation temperature. Significant weight loss at 430-600 °C would be attributed to decomposition of synthesized CNTs [43]. **Fig. 49a** reveals that synthesized MCNTs started to decompose at temperature of 350 °C to 466 °C and 498 °C when synthesis temperature was increased from 700 °C to 800 °C and 900 °C. Also, DTG analysis was employed to figure out a peak temperature with maximum weight loss rate as shown in **Fig. 49b**. For as-synthesized MCNTs produced at 700 °C, two peaks of DTG curve were detected at oxidation temperature of 350 °C and 532 °C. For MCNT products which were synthesized at 800 °C and 900 °C, similar peaks were detected at oxidation temperature of 574 °C, and 598 °C, respectively, indication greater thermal stability of MCNTs. Accordingly, an increase in synthesis temperature would result in formation of MCNTs with higher thermal stability. These results are in a good agreement with the apparent portion of amorphous carbon content in the MCNT samples as observed SEM images.

Thermal stability of CNTs had been reported by Acomb et al. [19] and Lee et al. [43]. Acomb et al. [19] reported that remaining weights of CNT samples was lower with an increase in synthesis temperature from 700 °C to 900 °C. Similar tendency reported by Lee et al. [43] reveals that the DTG peaks of CNT samples were shifted from 300-600 °C, 450-650 °C, to 500-670 °C when the synthesis temperature was increased from 750 °C, 850 °C, to 950 °C respectively. These results can support that CNTs with improved thermal stability could be synthesized with the higher synthesis temperature.



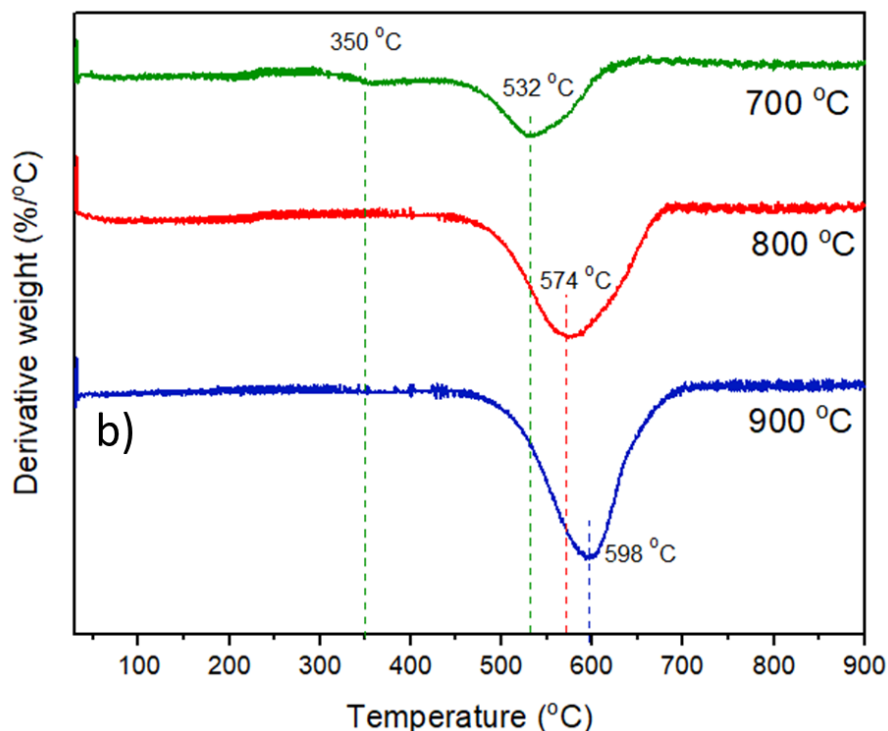


Fig. 49 a) TGA curves and b) DTG curves of as-synthesized MCNTs from different synthesis temperature

4.3.3 Crystallinity of MCNTs synthesized from eucalyptus oil and 1:1 ferrocene impregnated with nickel nitrate

The crystallinity of synthesized MCNTs at different synthesis temperature could be observed from Raman spectra as shown in **Fig. 50**. A peak at Raman shift of $1,323\text{ cm}^{-1}$ assigns to the vibration of non- sp^2 bonded carbon atom which is called D-band. Generally, D-band is applied to identify amorphous carbon. A peak at Raman shift of $1,588\text{ cm}^{-1}$ responds to the vibration of sp^2 bonded carbon atom which is called G-band. Generally, G-band was applied to identify CNTs [56]. The ratio of intensity of D-band to G-band (I_D/I_G) was used to identify the crystallinity of carbon product. The higher crystallinity of carbon product was obtained at lower I_D/I_G . From this experiment, I_D/I_G decreased from 1.56 to 1.05 when synthesis temperature was increased from $700\text{ }^\circ\text{C}$ to $800\text{ }^\circ\text{C}$. The crystallinity of the CNTs increased as synthesis temperature was raised. An increment of MCNT crystallinity was obtained from an increase of MCNT structure in synthesized product which was also supported by the characterization results from SEM and TGA. However, I_D/I_G increased from 1.05 to 1.12 when synthesis temperature was enhanced from $800\text{ }^\circ\text{C}$ to $900\text{ }^\circ\text{C}$ because of more carbon deposition. The quality of the MCNTs synthesized at $900\text{ }^\circ\text{C}$ was lower as characterization results of SEM.

The crystallinity of synthesized CNTs was previously reported in some literature. From Acomb et al. [19], an increase in synthesis temperature from 700 °C to 800 °C decreased I_D/I_G from 0.62 to 0.51. In contrast, I_D/I_G ratio of synthesized CNTs at synthesis temperature of 800 °C and 900 °C was increased from 0.51 to 0.52. From Shamsudin et al. [44], an increase in synthesis temperature from 700 °C to 800 °C decreased I_D/I_G from 0.72 to 0.52. However, I_D/I_G ratio of synthesized CNTs at synthesis temperature of 800 °C and 900 °C was enhanced from 0.52 to 0.57. Srisrattha et al. [36] reported that when synthesis temperature was increased from 700 °C to 800 °C, I_D/I_G ratio reduced from 1.60 to 0.61. Nevertheless, when synthesis temperature was increased from 800 °C to 900 °C, I_D/I_G ratio increased from 0.61 to 0.67. The decrease in I_D/I_G ratio was proportional to an increase in CNT structure in carbon product. However, the synthesis temperature was excessive, I_D/I_G ratio would increase because there was more carbon deposition on the CNT structure or low uniformity. Therefore, the quality of the CNTs was lower.

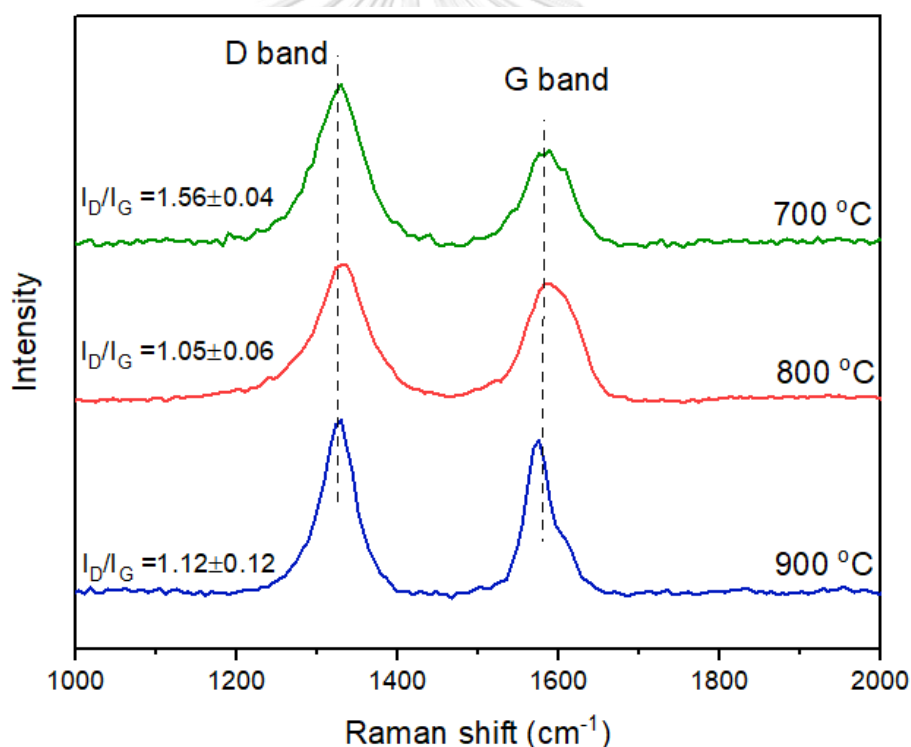


Fig. 50 Raman spectra of as-synthesized MCNTs at different synthesis temperature

4.3.4 Total mass yield of MCNTs synthesized from eucalyptus oil and 1:1 ferrocene impregnated with nickel nitrate

Total mass yields by weight of synthesized products could be calculated by **Eq 2**, in which weight of eucalyptus oil and catalyst were calculated from **Eq C1** and **Eq C2** in **Appendix C**, respectively.

Fig. 51 presents effect of synthesis temperature on total mass yields by weight of carbon product and outlet gas flowrate from the reactor at feeding time endpoint. Gas flowrate going out from the reactor at various synthesis temperature are shown in **Table E1** in **Appendix E**. Total mass yield at different synthesis temperature were $9.0\pm 1.5\%$, $13.9\pm 1.2\%$, and $17.5\pm 1.0\%$ for synthesis temperature of $700\text{ }^{\circ}\text{C}$, $800\text{ }^{\circ}\text{C}$, and $900\text{ }^{\circ}\text{C}$ respectively. The plot indicated that the elevation of synthesis temperature could increase both yield and gas flowrate going out from the reactor. An increase in gas flowrate going out from reactor was due to increment of decomposition rate of eucalyptus oil and 1:1 ferrocene impregnated with nickel nitrate. Thus, the higher total mass yield was obtained.

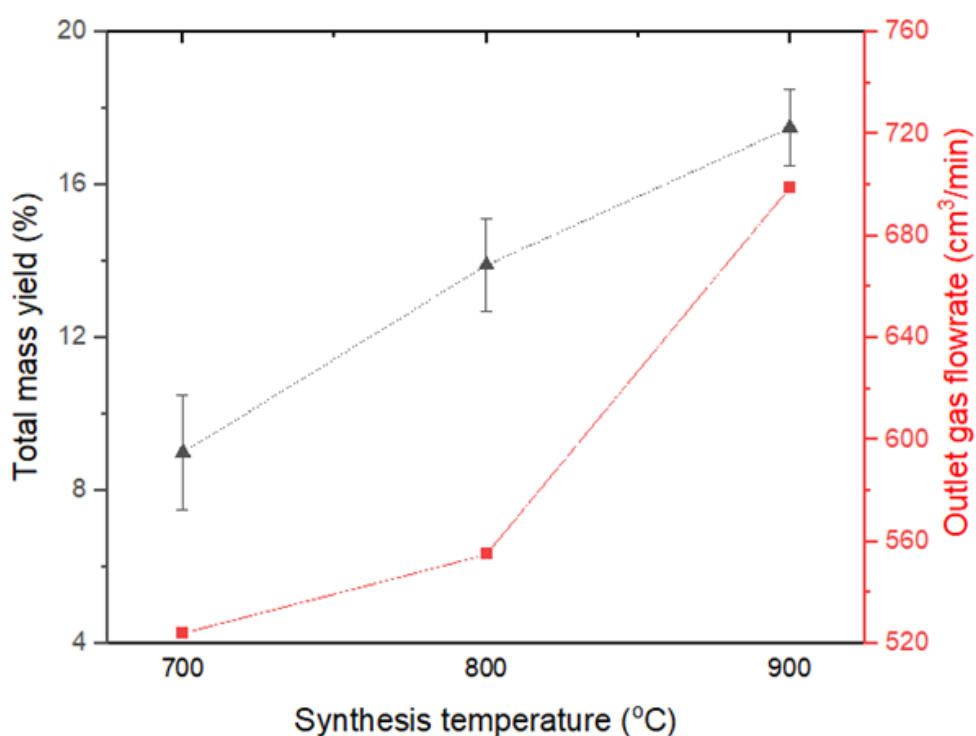


Fig. 51 Relationship of total mass yield and outlet gas flowrate on synthesis temperature

There were some studies reported about the yield of carbon products. From Acomb et al. [19], their results founded enhancement of product yields from 2.0% to 18.7% and 21.3% when increased in synthesis temperature from $700\text{ }^{\circ}\text{C}$ to $800\text{ }^{\circ}\text{C}$ and $900\text{ }^{\circ}\text{C}$. The increasing synthesis temperature could enhance the decomposition rate of carbon precursors, which is an important step in forming carbon nanotubes. Srisrattha et al. [36], the yield increased from 13% to 29% and 32% when the synthesis temperature was enhanced from $700\text{ }^{\circ}\text{C}$ to $800\text{ }^{\circ}\text{C}$ and $900\text{ }^{\circ}\text{C}$. From Mongkolsamai et al. [42], product yield increased from 3.13% to 6.61% and 6.68% when synthesis temperature was increased from $700\text{ }^{\circ}\text{C}$ to $800\text{ }^{\circ}\text{C}$ and $900\text{ }^{\circ}\text{C}$. From The increasing synthesis temperature could lead to the decomposition rate of carbon precursors. These results indicated that an increase in synthesis temperature increased CNT yields.

4.3.5 Magnetic properties of MCNTs synthesized from eucalyptus oil and 1:1 ferrocene impregnated with nickel nitrate

Fig. 52 demonstrates XRD patterns of MCNTs synthesized at different synthesis temperature. All patterns show diffraction peaks of graphite at $2\theta = 26.5^\circ$ assignable to (002) planes of CNTs (PDF 03-065-6212) and FeNi_3 peaks at $2\theta = 44.3^\circ$, 51.6° , and 75.7° which match the (111), (200) and (222) planes of the bimetal Ni-Fe (PDF 00-038-0419). These results confirmed no effect of synthesis temperature on magnetic phases. Also, they confirmed Ni-Fe bimetallic in CNT products.

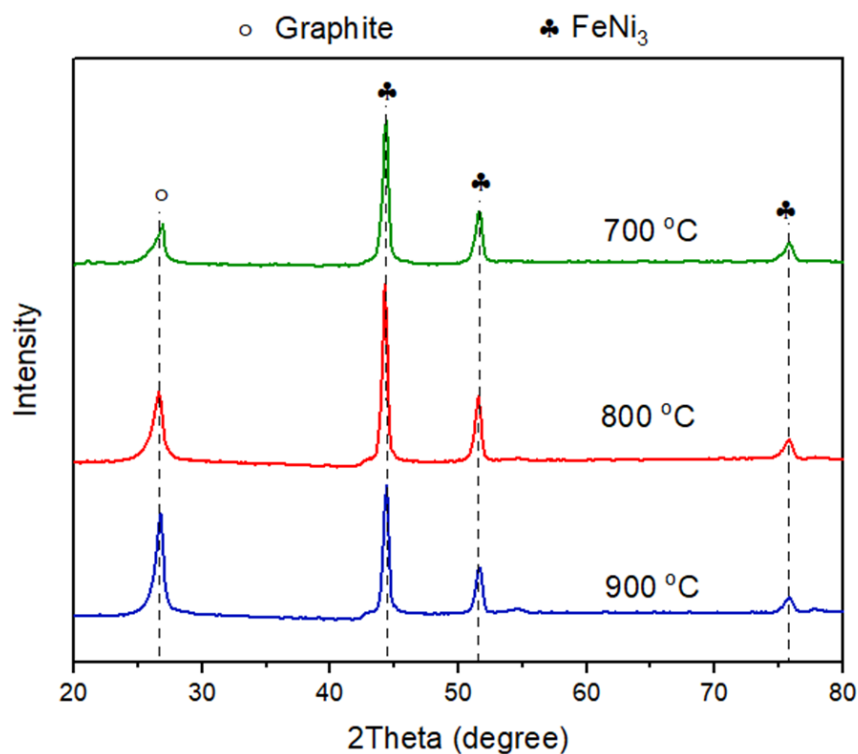
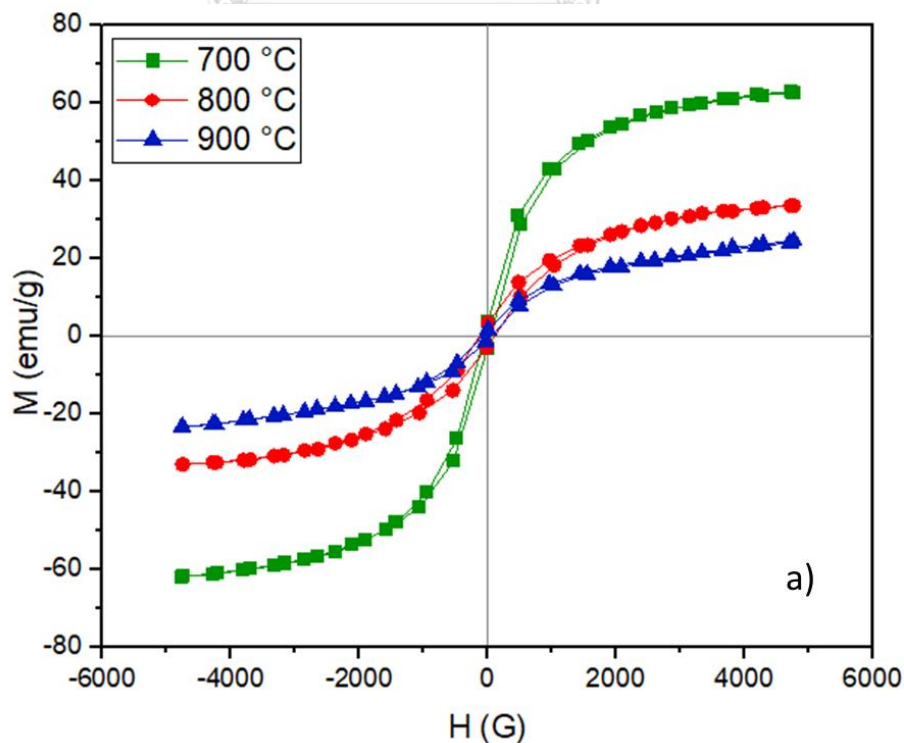


Fig. 52 XRD patterns of as-synthesized MCNTs from different synthesis temperature

To investigate the magnetic properties of MCNTs synthesized at different synthesis temperature, VSM was used to measure the hysteresis loops of the samples at room temperature. **Fig. 53a-53b** show all hysteresis loops for the MCNTs. All shapes of the hysteresis loop indicated that they were ferromagnetic at room temperature. The hysteresis loop results illustrated saturated magnetization (M_s) and coercivity (H_c) values. M_s values of MCNTs decreased from 62.5 emu/g to 33.3 emu/g and 24.0 emu/g when synthesis temperature was increased from 700 °C to 800 °C and 900 °C. One of possible causes was more carbon proportion coated FeNi_3 particles, it could lead to diamagnetic influence [71]. The obstruction between magnetic force and FeNi_3 particles was increased by carbon wall thickness. As Xu et al. results [47], M_s values of MCNTs decreased from 7.1 emu/g to 4.5 emu/g and 2.9 emu/g when synthesis

temperature was increased from 430 °C to 500 °C and 600 °C. The average size of MCNTs enhanced from 31 nm to 40 nm and 60 nm, respectively.

The H_c of all samples were determined from magnetic hysteresis curves. For increasing in synthesis temperature of 700 °C to 800 °C, H_c increased from 50 G to 118 G, respectively. Carbon product synthesized at 800 °C showed CNTs that could act on the metal encapsulation. It contributed to the large coercivity due to arrangement of $FeNi_3$ particles in a quasi-one-dimensional manner [48]. Large shape anisotropies of CNTs also contribute to the large coercivity, and the shape anisotropies are helpful to stabilize magnetic order against thermal fluctuations in such reduced dimensions [70]. However, when synthesis temperature was increased from 800 °C to 900 °C, H_c values reduced from 118 G to 68 G. Crystallinity size of $FeNi_3$ increased from 14.4 nm to 15.5 nm when synthesis temperature was increased from 800 °C to 900 °C. As the discussion in **section 4.3.1**, the increment could confirm that $FeNi_3$ particle size in MCNTs synthesized at 900 °C was larger than the metal particle size in MCNTs produced at 800 °C. The decrease in coercivity is derived from multi-domain properties of particles due to agglomeration of metal particles [34, 35]. The decrease in H_c had been reported by Sajitha et al [67]. They reported that H_c value reduced from 360 G to 330 G when synthesis temperature was enhanced from 900 °C to 980 °C. The crystalline size of Fe_3C in MCNTs increased from 11.2 nm to 12.0 nm, respectively. To compare with the H_c value of Bulk $FeNi_3$ is 66 G [68], the enhanced H_c value was obtained in the case of MCNTs synthesized at 800 °C and 900 °C. The high coercivity could be related to magnetic particle alignment in carbon nanotube structure [72].



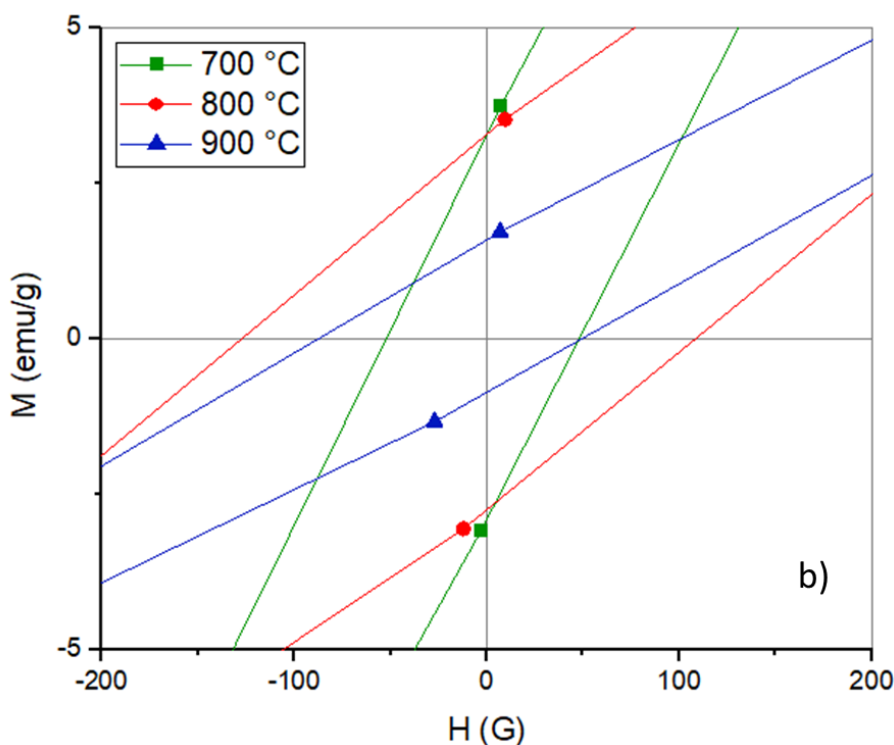


Fig. 53 Magnetic hysteresis loops of as-synthesized MCNTs from different synthesis temperature at room temperature in a) a whole range and b) magnified range of -200 G to 200 G

From these results in **section 4.3.1-4.3.4**, 1:1 ferrocene impregnated with nickel nitrate could insufficiently improve crystallinity degree of MCNTs (I_D/I_G ratio was higher than 1). Total mass yield was also lower than use of ferrocene as catalyst. Impregnation of nickel nitrate solution on pure ferrocene was adjusted. 4:1 molar ratio of Fe and Ni was used. 4:1 ferrocene impregnated with nickel nitrate would be copolyolyzed with eucalyptus oil for CNT synthesis. Then, effect of molar ratio of Fe to Ni molar ratio in the catalyst on CNT production was studied. The results and discussion are described in **Appendix F**. As these results, use of 4:1 ferrocene impregnated with nickel nitrate was better than using 1:1 ferrocene impregnated with nickel nitrate. 4:1 ferrocene impregnated with nickel nitrate could obtain higher total mass yield. CNTs synthesized from eucalyptus oil and 4:1 ferrocene impregnated with nickel nitrate were higher crystallinity degree and narrower CNT diameter distribution.

The section of research focused on the study effect of synthesis temperature on MCNT properties. 1:1 ferrocene impregnated with nickel nitrate was used as catalyst in each condition of MCNT synthesis. The results demonstrated synthesis temperature of 800 °C was the best condition because the temperature could provide high quality of MCNTs and high crystallinity. However, 1:1 ferrocene impregnated with nickel nitrate provided amount of defect or amorphous carbon are higher than amount of MCNTs. Preparation of ferrocene impregnated with nickel nitrate would be adjusted, and 4:1 ferrocene impregnated with nickel nitrate was obtained. From these results, the catalyst could provide more total mass yield and higher crystallinity than use of 1:1 ferrocene

impregnated with nickel nitrate. Thus, 4:1 ferrocene impregnated with nickel nitrate was used in study effect of eucalyptus oil to catalyst molar ratio on MCNT properties.

4.4 Effect of eucalyptus oil to catalyst molar ratio on resultant MCNTs

For the synthesis of MCNTs in this part, 4:1 ferrocene impregnated with nickel nitrate was selected as catalyst because the catalyst could obtain the best quality of MCNTs as the results in **Appendix F**. Eucalyptus oil was fed as carbon precursor at different flowrate for 15 minutes. Molar ratio of eucalyptus oil to catalyst was calculated from mole of eucalyptol in fed eucalyptus oil divided by mole of catalyst. Molar ratio of eucalyptus oil to catalyst in this study was 2:1, 5:1, and 10:1. As the objective of this part, eucalyptus oil proportion was raised to increase carbon cluster to engaging catalyst because eucalyptus oil cost is cheaper than the catalyst. The increment of eucalyptus oil might be reduced synthesizing cost.

4.4.1 Morphology of MCNTs synthesized from different molar ratio of eucalyptus oil to 4:1 ferrocene impregnated nickel nitrate

Fig. 54a-54c show the morphology of synthesized carbon product at different molar ratio of eucalyptus oil to catalyst observed from Scanning Electron Microscope (SEM). SEM image from **Fig. 53a** indicates the morphology of carbon product synthesized using the 2:1 molar ratio was irregular shape without tubular structure. In contrast, SEM images of carbon product were synthesized using the 5:1 molar ratio revealed mainly MCNTs, as shown in **Fig. 54b**. MCNT product produced using eucalyptus oil to catalyst molar ratio of 10:1 consisted irregular shape with tubular structure of MCNTs as seen in **Fig. 54c**. For CNT diameter distribution analysis, carbon product from the 2:1 molar ratio was cut off because of information from SEM. There was none of MCNT structure.

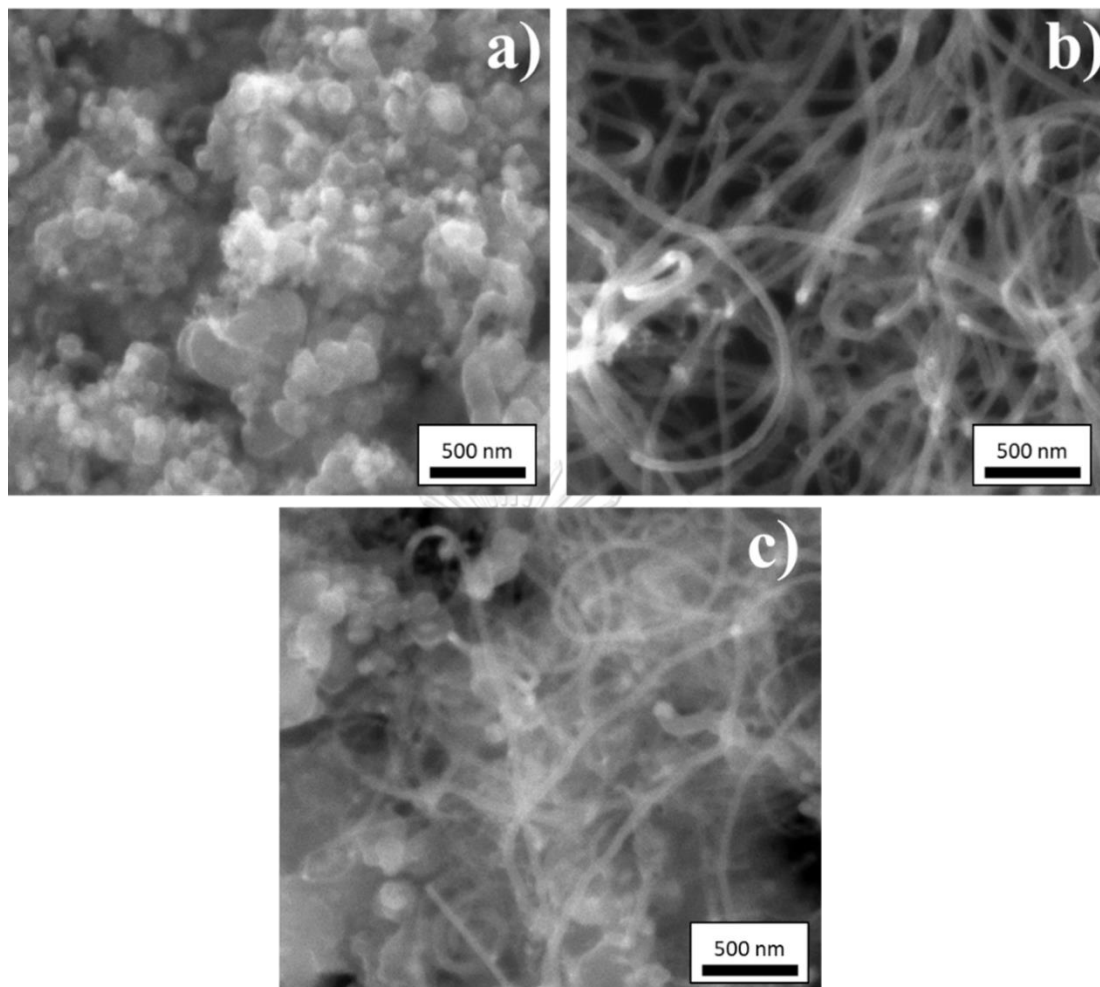


Fig. 54 SEM images of morphology of carbon products synthesized from different molar ratio of eucalyptus oil to catalyst: a) 2:1, b) 5:1, and c) 10:1

Distributions of diameter of CNTs at different molar ratio are shown in **Fig. 55a-55b**. An average diameter increased from 45 ± 7 nm to 55 ± 14 nm, when molar ratio of eucalyptus oil to catalyst was increased from 5:1 to 10:1, respectively. Because the increase decomposition of precursors results in larger diameters of CNTs. For explaining the reason for none of MCNT formation at 2:1 molar ratio and increment of CNT diameter when the molar ratio of eucalyptus oil was increased from 5:1 to 10:1, they would be described by mechanism of CNT formation.

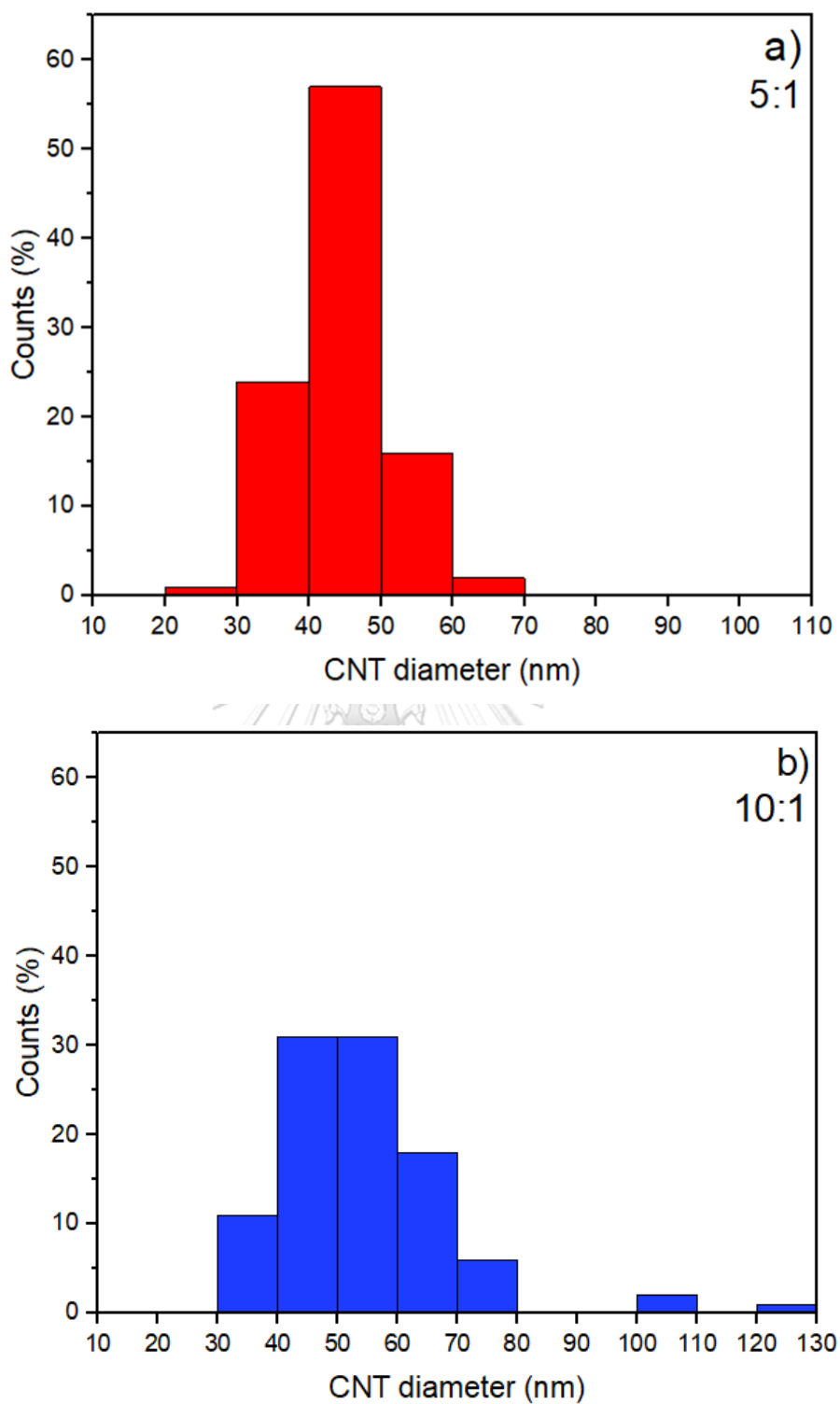


Fig. 55 CNT diameter distributions of as-synthesized products by use of different eucalyptus oil to catalyst molar ratio of a) 5:1 and b) 10:1

Generally, mechanism of MCNT formation in co-pyrolysis method induced by catalyst particles involves decomposition, mass transfer of carbon cluster to catalyst,

diffusion, and precipitation process [22, 23]. Eucalyptus oil and 4:1 ferrocene impregnated with nickel nitrate were vaporized and decomposed after when they were fed at synthesis temperature. Carbon and metal clusters were carried by nitrogen gas to heating zone of tubular reactor. The carbon cluster is important for the CNT synthesis. While metal cluster condensed to nanoparticles on the quartz reactor surface, carbon cluster would be transferred to these particles by concentration driving force. Then the carbon would be dissolved or catalyzed to carbon atom with the FeNi_3 catalyst particles. When the carbon dissolution reached saturated point, the graphitic carbon would precipitate and enclose the FeNi_3 nanoparticles. As the results, CNTs with FeNi_3 nanoparticles could be obtained, and residue gas was purged with carrier gas to atmosphere.

According to CNT formation mechanism, it can be suggested that an increase in molar ratio of eucalyptus oil to catalyst. The higher mass transfer rate and diffusion rate of carbon cluster could be expected. For 2:1 molar ratio, carbon cluster amount transferred to catalyst particles was low. The mass transfer step was slow, and then the following steps of CNT formation were obstructed. This reason could be confirmed by outlet gas flowrate profile as shown in **Fig. 56**. The gas flowrate of 2:1 molar ratio was the least, consistent with the lowest carbon cluster concentration. Therefore, there were no CNT structure in the product as SEM analysis.

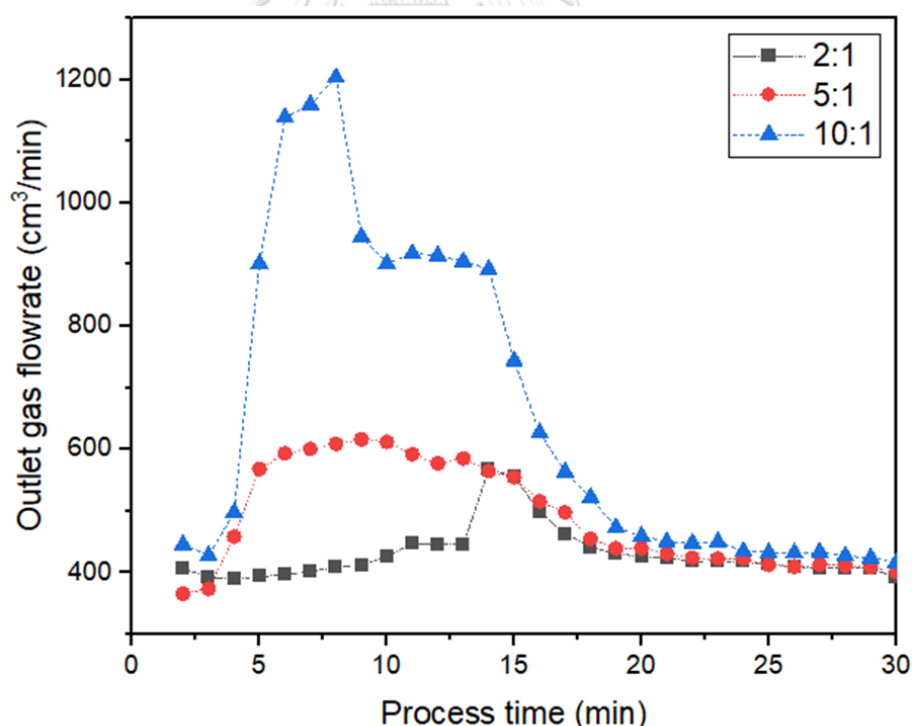


Fig. 56 Outlet gas flowrate from the reactor at different molar ratio of eucalyptus oil to catalyst

To increase the molar ratio from 5:1 to 10:1, excessive amount of carbon cluster could not be dissolved or catalyzed with catalyst particles because carbon dissolution of catalyst particles reached a saturated point. Some remaining carbon cluster was decomposed and formed into amorphous carbon instead. SEM images indicated the result.

Some previous works reported studies of effect molar ratio of carbon precursor to catalyst on CNT structure. Tripathi et al. [45] reported that the diameter ranges of CNTs increased from 12-38 nm to 45-60 nm and 85-94 nm when the molar ratio of C₂H₂ to Ni catalyst was increased from 1.3:1 to 1.9:1 and 3.2:1. Venkatesan et al. [46] indicated that the average diameter of CNTs was 20 nm, 32 nm, and 46 nm when the molar ratio of C₂H₂ to Ni was 3.5:1, 4.9:1, and 6.3:1, respectively. Their results indicated that more amorphous carbon was deposited on CNT structure; therefore, the molar ratio of carbon precursor to catalyst affected the increment of CNT diameter.

4.4.2 Thermal stability of MCNTs synthesized from different molar ratio of eucalyptus oil to 4:1 ferrocene impregnated with nickel nitrate

The thermal stability of synthesized carbon could be observed by Thermogravimetric analyzer (TGA) under O₂ atmosphere. TGA and DTG curves of synthesized NCNTs at different molar ratio of eucalyptus oil to catalyst are shown in **Fig. 57a-57b**, respectively. TGA curves were plotted between the weight percentage of sample against oxidation temperature. DTG curves were plotted between the derivative sample weight percentage against oxidation temperature. Significant weight loss at 430-600 °C was obtained from the degradation of synthesized MCNTs [43]. **Fig. 57a** represents that those synthesized products started to decompose at 486°C to 473°C and 455°C when the molar ratio was increased from 2:1 to 5:1 and 10:1. Also, DTG analysis was employed to figure out a peak temperature with maximum weight loss rate, as shown in **Fig. 57b**. The peaks indicated at 578 °C, 559 °C, and 551 °C for as-synthesized carbon, which were produced using the molar ratio of eucalyptus oil to catalyst of 2:1, 5:1, and 10:1, respectively. TGA and DTG results indicated worse thermal stability of products when molar ratio was increased. To enhance the molar ratio from 2:1 to 10:1, the reduction of thermal stability accorded to increasing amount of amorphous carbon in the product as characterization results from SEM.

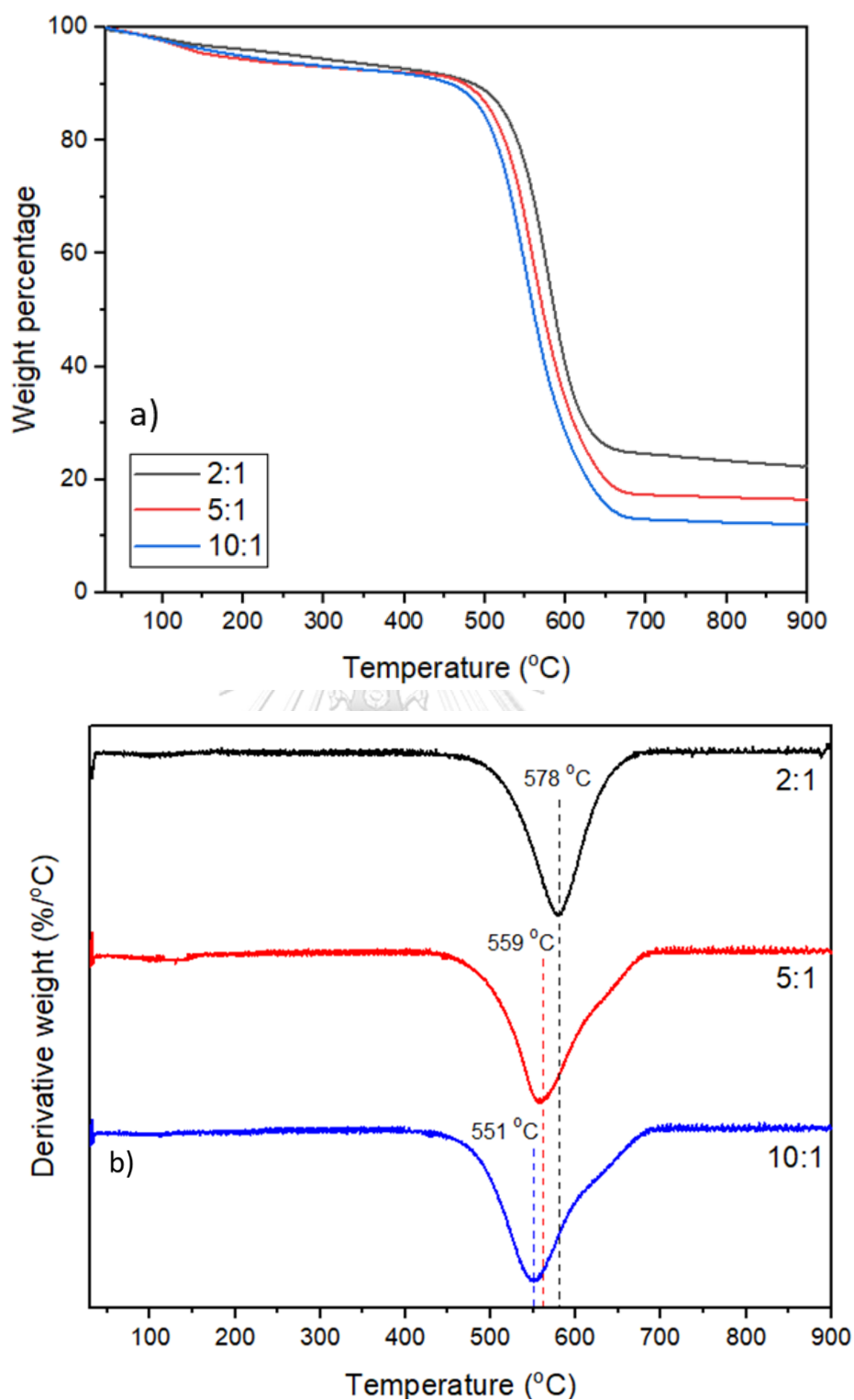


Fig. 57 a) TGA curves and b) DTG curves of as-synthesized carbon from different molar ratio of eucalyptus oil to catalyst

4.4.3 Crystallinity of MCNTs synthesized from different molar ratio of eucalyptus oil to 4:1 ferrocene impregnated with nickel nitrate

Crystallinity of synthesized carbon at different molar ratio of eucalyptus oil to catalyst could be observed from Raman spectra as shown in **Fig. 58**. D-band at a Raman shift of $1,335\text{ cm}^{-1}$ corresponds to the vibration of non- sp^2 bonded carbon atom. This peak is used to identify amorphous or deflected carbon. G-band at Raman shift of $1,585\text{ cm}^{-1}$ can be assigned to the vibration of sp^2 bonded carbon atom. The band is applied to specify CNTs [56]. From this experiment, $I_{\text{D}}/I_{\text{G}}$ decreased from 1.01 to 0.83 when the molar ratio was increased from 2:1 to 5:1. The crystallinity of the MCNTs was improved as molar ratio was raised. An enhancement of crystallinity was obtained from an increase of CNT structure in synthesized product which was also supported by the characterization results from SEM. Nevertheless, $I_{\text{D}}/I_{\text{G}}$ ratio enhanced from 0.83 to 1.08 when the molar ratio was raised from 5:1 to 10:1. The reduction of crystallinity of MCNTs was caused by an increment of amorphous carbon amount in MCNT product. These results were supported by the characterization results from SEM and TGA.

Some previous studies reported the effect of molar ratio of carbon precursor to catalyst. From Tripathi et al. [45], $I_{\text{D}}/I_{\text{G}}$ ratio was 0.808 to 0.807 when increased in acetylene to nickel catalyst molar ratio from 0.6:1 to 1.3:1. Nevertheless, Increment of $I_{\text{D}}/I_{\text{G}}$ from 0.807 to 0.878 was observed when raised in the molar ratio from 1.3:1 to 3.2:1. The decreased $I_{\text{D}}/I_{\text{G}}$ could be attributed to higher amount of CNT structure in product. However, in case of exorbitant molar ratio of carbon precursor to catalyst, an increase in $I_{\text{D}}/I_{\text{G}}$ could be assigned to deflect of CNT structure due to amorphous carbon generation.



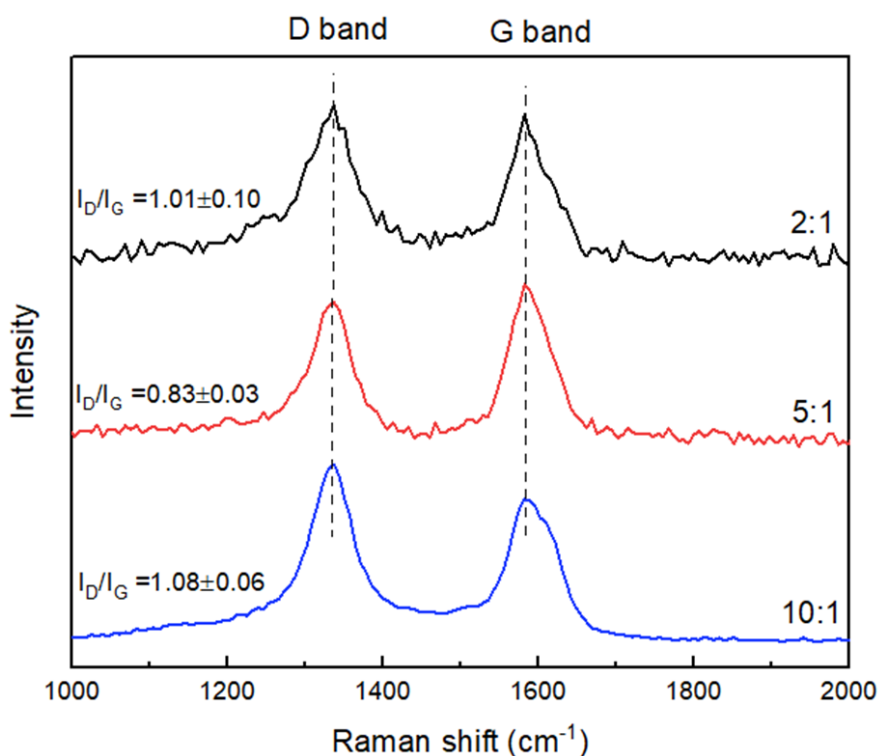


Fig. 58 Raman spectra of as-synthesized carbon from different molar ratio of eucalyptus oil to catalyst

4.4.4 Total mass yield of MCNTs synthesized from different molar ratio of eucalyptol to 4:1 ferrocene impregnated with nickel nitrate

Total mass yields by weight of synthesized products were calculated by **Eq 2**. Weight of eucalyptus oil and 4:1 ferrocene impregnated with nickel nitrate from **Eq C1** and **Eq C2** in **Appendix C**, respectively. Total mass yield of each condition is shown in **Fig. 59**. For synthesis by increasing in eucalyptus oil to catalyst molar ratio from 2:1 to 5:1, total mass yield increased from $16.2 \pm 1.5\%$ to $17.1 \pm 1.7\%$, respectively. However, total mass yield reduced from $17.1 \pm 1.7\%$ to $6.7 \pm 0.4\%$ when increased in molar ratio from 5:1 to 10:1. The decreasing total mass yield would attribute by two impossible reasons: (i) lower space time and (ii) different flow of oil droplet.

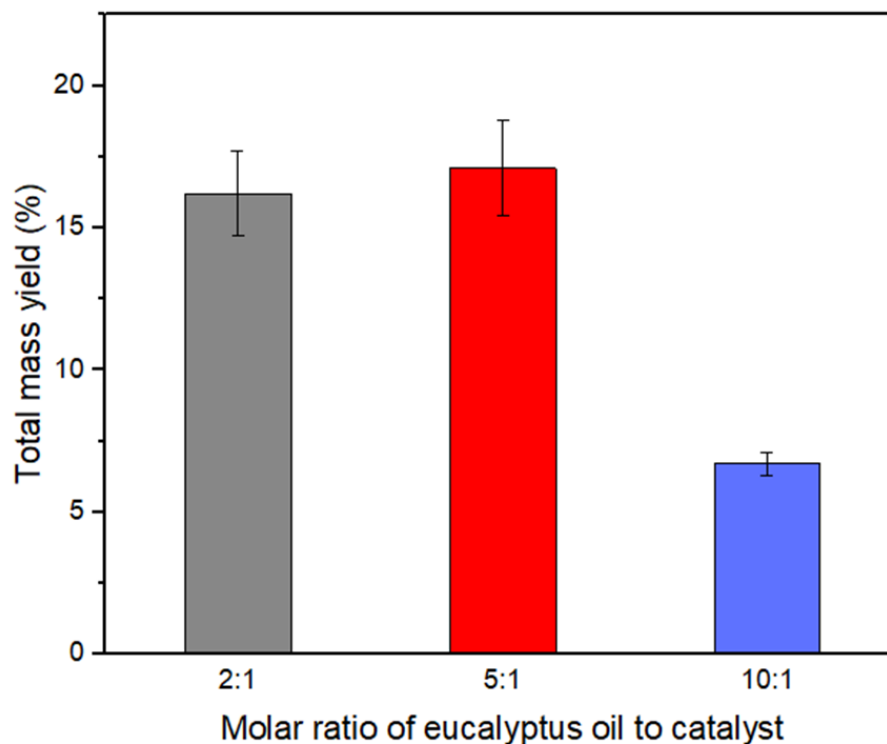


Fig. 59 Total mass yield of as-synthesized carbon products from different eucalyptus oil to catalyst molar ratio

The increment of total mass yield happened by increasing in the molar ratio from 2:1 to 5:1 because of enhancement of carbon cluster transfer rate through FeNi_3 catalyst particles. The rate increment resulted in higher rate of diffusion of carbon cluster to dissolve or catalyze to carbon atom for CNT formation (see **section 4.3.1** for more detail). The enhancement of carbon weight product from 0.25 g to 0.49 g could be referred to the more CNT growth which was confirmed by characterization results from SEM and Raman.

For the reduction of total mass yield in the increase in 5:1 to 10:1 molar ratio, the first possible reason was lower space time. When eucalyptus oil flow rate is increased, the space time of vapors within the reactor becomes shorter. The **Eq 4** is employed to calculate the space time of the gas in the reactor.

$$\tau = \frac{V}{v_0} \quad \text{Equation 4}$$

Where τ is space time.

V is volume of heating zone of the quartz tube.

v_0 is total inlet volumetric flowrate of nitrogen gas and eucalyptus oil.

V can be calculated directly from its dimension as shown in **Eq 5**,

$$V = \frac{\pi d^2}{4} h \quad \text{Equation 5}$$

Where d is inner diameter of quartz tube (4.2 cm).

h is length of heating zone (62 cm).

From the **Eq 5**, volume of heating zone of quartz tube can be calculated about 859.0 cm³. **Table 5** summarizes the space time in the reactor at different molar ratio of eucalyptus oil to catalyst.

Table 5 Space time of different molar ratio of eucalyptus oil to catalyst

Molar ratio of eucalyptus oil to catalyst	Eucalyptus oil flow rate (cm ³ /min)	Space time (min)
5:1	0.18	1.68
10:1	0.37	1.31

From the observed phenomena during the MCNT production at 10:1 molar ratio of eucalyptus oil to catalyst, there was sticky brown liquid attached on inner surface of quartz tube at outlet zone. Meanwhile, there was no liquid on the surface when synthesized using the 5:1 molar ratio. The as-synthesized MCNTs weight also reduced from 0.49 g to 0.38 g when increased in eucalyptus oil to catalyst from 5:1 to 10:1. These results would support that some oil vapor could not decompose completely and then condensed to liquid because there was not enough time to transform to carbon product as shown in **Table 5**. The longer space time at molar ratio of 5:1 could be achieved to provide the synthesized MCNTs with higher total mass yield than the production using 10:1 molar ratio.

The second possible reason of the decreasing in total mass yield could be described by different flowed oil droplet. The observed phenomena during eucalyptus oil flow out with nitrogen gas from T-junction tube to quartz reactor at room temperature. None of visible droplet flowed out when eucalyptus oil was fed at 5:1 molar ratio. Meanwhile, the eucalyptus oil droplet was noticeable from outlet of T-junction tube when eucalyptus oil was fed at 10:1 molar ratio. From this observation, there is difference of eucalyptus oil droplet size when increased in molar ratio of eucalyptus oil to catalyst.

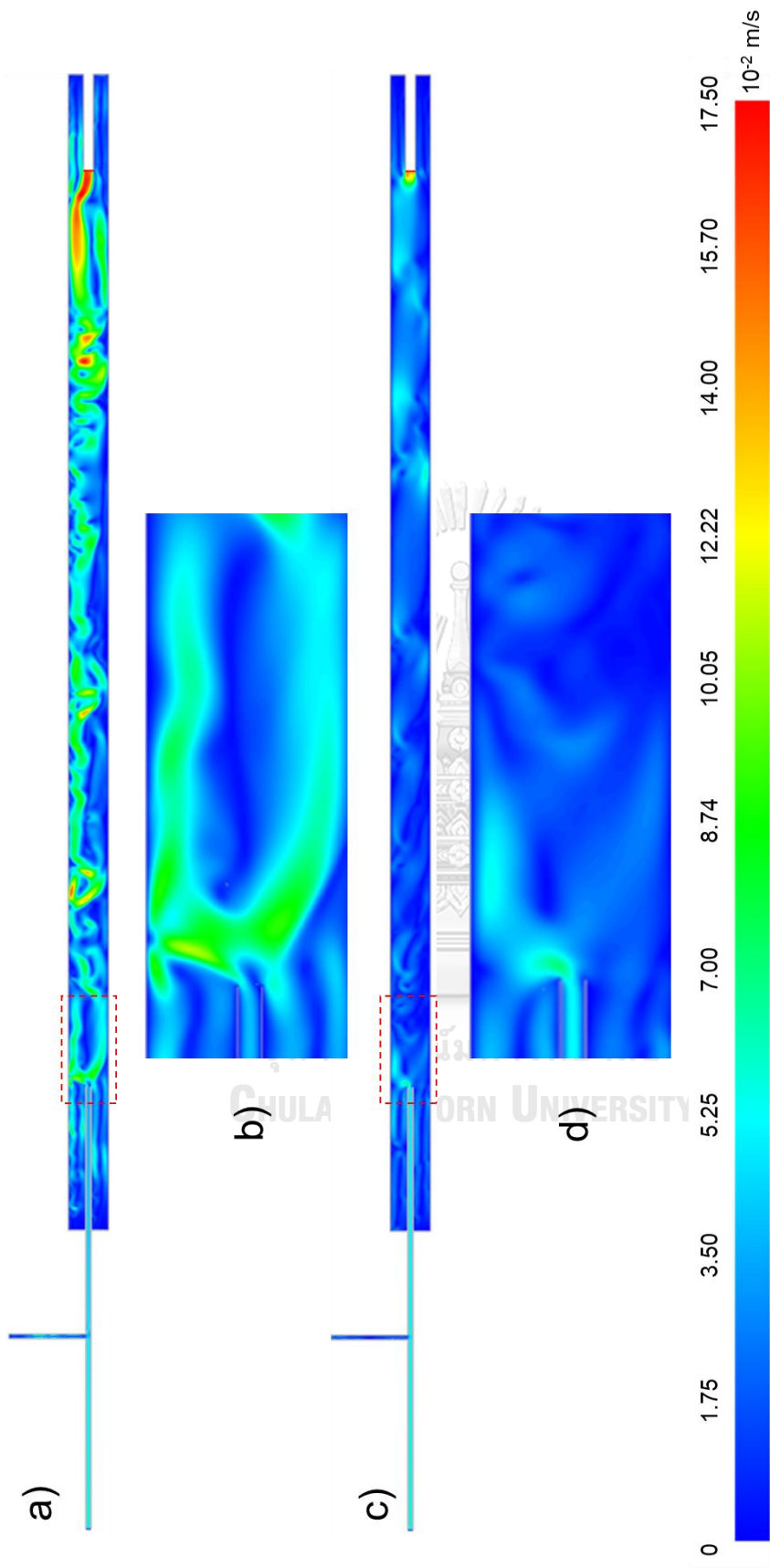


Fig. 60 Contour of velocity magnitude (10^{-2} m/s) at eucalyptus oil to catalyst molar ratio of a)-b) 5:1 and c)-d) 10:1

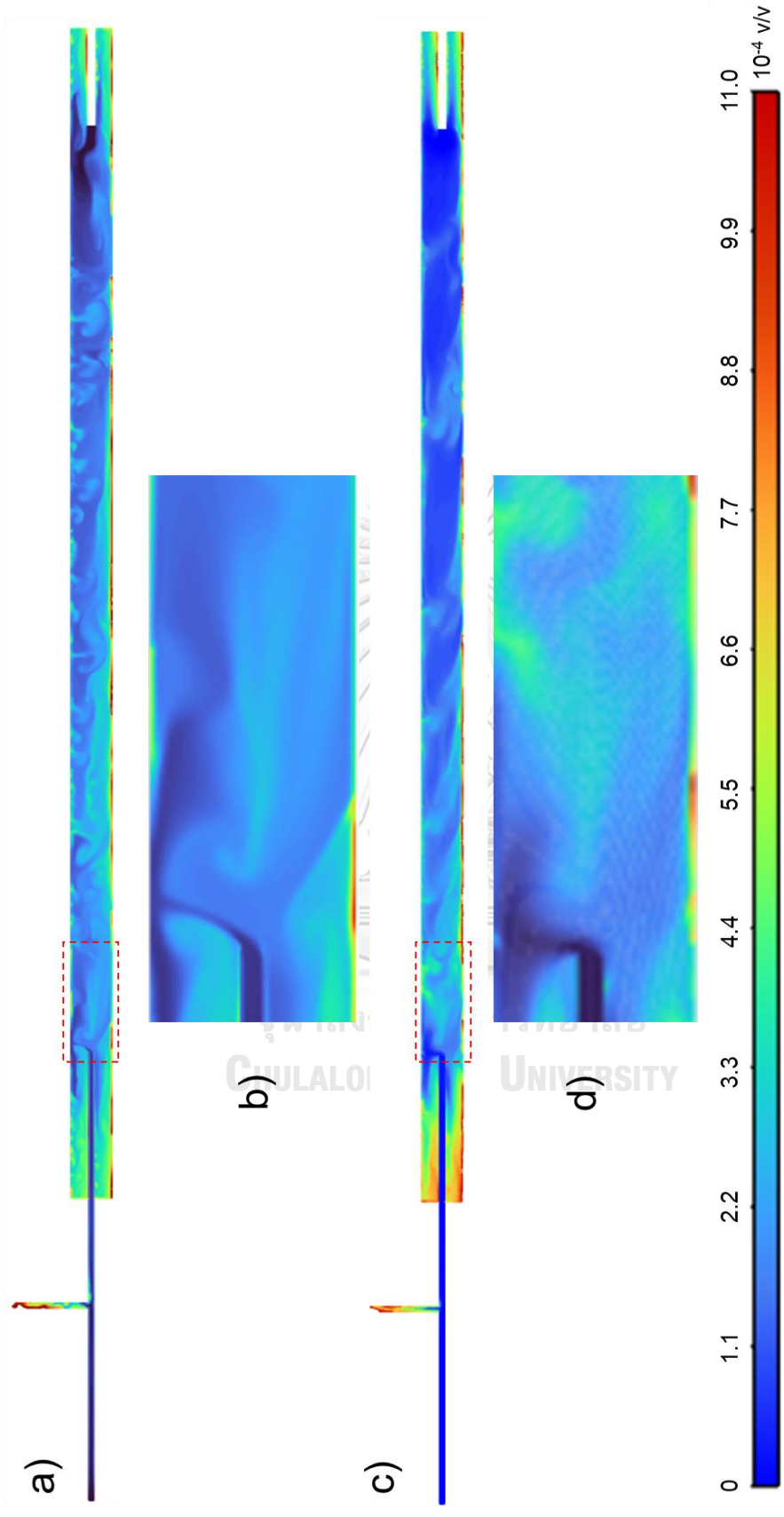


Fig. 61 Contour of eucalyptus oil volume fraction at eucalyptus oil to catalyst molar ratio of a)-b) 5:1 and c)-d) 10:1

The simulation results show magnitude velocity contours for the eucalyptus oil feeding at molar ratio of eucalyptus oil to catalyst of 5:1 and 10:1 in room temperature as shown in **Fig. 60a-60b** and **Fig.60c-60d**, respectively. Eucalyptus oil was flowed from T-junction pipe to the quartz tube reactor and flowed out to outlet. The velocity of 5:1 molar ratio condition was higher than velocity of 10:1 molar ratio condition. From the results, increasing in flow rate of eucalyptus oil could reduce magnitude velocity because the making formation of droplets would be more difficult [73]. Nitrogen gas would disintegrate eucalyptus oil stream to droplet due to the disruptive forces provided by high velocity of gas acting on the oil surface. When increasing the flowrate of eucalyptus oil, the forces was insufficient to disturb eucalyptus oil to droplet as a result of the phenomena observation.

Fig. 61a-61d also demonstrate eucalyptus oil volume fraction along the system at conditions of 5:1 and 10:1 molar ratio of eucalyptus oil to catalyst for comparison with each velocity profile. For 5:1 molar ratio, **Fig. 61a-61b** illustrate good eucalyptus oil volume fraction distribution along the reactor. Meanwhile, the contours of 10:1 molar ratio from **Fig. 61c-61d** show lower uniformity. These results confirmed that simulating eucalyptus oil droplet could not be appropriately dispersed when using the molar ratio of 10:1 due to insufficient disruptive force from nitrogen gas flow. Additionally, when the MCNT synthesis was in process, heat transfer rate from heated tube to eucalyptus oil droplet would reduce because of decreasing surface area to volume ratio of oil droplet [74, 75]. The large droplet resulted in reduction in decomposition rate and decrease in total mass yield.

To confirm the effect of molar ratio on MCNT synthesis, MCNTs were produced using eucalyptus oil amount as the condition of 10:1. However, the eucalyptus oil feed flowrate was equal to the flowrate of 5:1 condition. The space time and oil droplet characteristic were similarity to 5:1 condition. Total mass yield increased from 6.7% to 24.4%, and weight of product also enhanced from 0.38 g to 1.37 g. These results supported that the space time and different oil droplets could result in the total mass yield.

From previous study of effect molar ratio of carbon precursor to catalyst, Tripathi et al. [45] reported that an increase in molar ratio of C_2H_2 to Ni in catalyst from 0.6:1 to 1.3:1 raised CNT yields. However, CNT yield decreased when the molar ratio was increased from 1.3:1 to 3.2:1. The yield increment was attributed to the increase in the diffusion rate of carbon through the catalyst particles for CNT formation. When the molar ratio was too high, the decomposition rate of C_2H_2 became higher than diffusion rate of carbon to CNT growth. Remaining carbon deposited on CNT surface in amorphous form and covered catalyst surface. Therefore, the catalyst activity and CNT formation rate would be reduced. Thus, optimal molar ratio of carbon precursor to catalyst in CNT synthesis is necessary to obtain good quality product.

4.4.5 Magnetic properties of MCNTs synthesized from different molar ratio of eucalyptus oil to 4:1 ferrocene impregnated with nickel nitrate

VSM was used to measure the hysteresis loops of carbon samples at room temperature of all magnetic carbon nanoparticles (MCNPs) synthesized from different molar ratio of eucalyptus oil to catalyst. **Fig. 62a-62b** show all hysteresis loops for the MCNTs. The all shape of the hysteresis loop indicated ferromagnetic state at room temperature. M_s values of MCNPs were 30.3 emu/g, 20.7 emu/g, and 16.7 emu/g when 2:1, 5:1, and 10:1 molar ratio of eucalyptus oil to catalyst was used in the production. One possible cause of M_s value reduction was higher carbon content in MCNPs, which could lead to diamagnetic influence [47]. These results were supported by residue percentage from TGA. Low residue content suggested high content of carbon in sample. The weight percentage of metal decreased from 22.4% to 16.5% and 12.0% when increased in eucalyptus oil to catalyst from 2:1 to 5:1 and 10:1, respectively. The effect of molar ratio of carbon precursor to catalyst on magnetization of MCNPs had been reported by Kerdnawee et al. [50] and Sajitha et al. [51]. Kerdnawee et al. studied the effect of the molar ratio of glycerol to ferrocene on magnetic susceptibility (χ). χ values are the proportion of magnetization to magnetic field, and the values are also depended on M_s [76]. They observed χ values of MCNPs from high glycerol to ferrocene ratio were low with the reducing proportion of Fe. This effect resulted in lower M_s of MCNPs because of low presence of Fe nanoparticles embedded inside the MCNPs. For Sajitha et al. research, they reported M_s decreased from 20.2 emu/g to 9.9 emu/g when maleic anhydride to ferrocene molar ratio was increased from 2:1 to 20:1 because of lower magnetic phase proportion of MCNP product. The metal weight percentage in MCNP synthesis increased from 20.5% to 4.9%, respectively.

The H_c of all samples were determined from magnetic hysteresis curves. For increase the molar ratio of 2:1 to 5:1, H_c values increased from 115 G to 201 G, respectively. Carbon product which produced from the molar ratio of 5:1 was MCNTs. The carbon structure could encapsulate $FeNi_3$ and arrange the particles. It could provide large coercivity due to the arrangement of particles in a quasi-one-dimensional manner in MCNT structure [48]. Additionally, MCNT structure can support stabilization of magnetic order against thermal fluctuations in such reduced dimensions [70]. However, when the molar ratio was increased from 5:1 to 10:1, H_c values of MCNTs reduced from 201 G to 192 G, respectively. Both values were not different significantly. The higher coercivity could be related to the alignment of $FeNi_3$ particles in CNT structure of samples [72]. The effect of molar ratio of carbon precursor to catalyst on magnetic property of MCNPs had been reported by Sajitha et al. [51]. They reported H_c of MCNPs reduced from 388 G and 270 G when increased in maleic anhydride to ferrocene molar ratio in MCNP synthesis from 2:1 to 20:1, respectively. From their results, 20:1_MCNP had lower H_c than 2:1_MCNP because H_c exhibits involving Fe particle diameter and carbon structure where Fe particles were embedded.

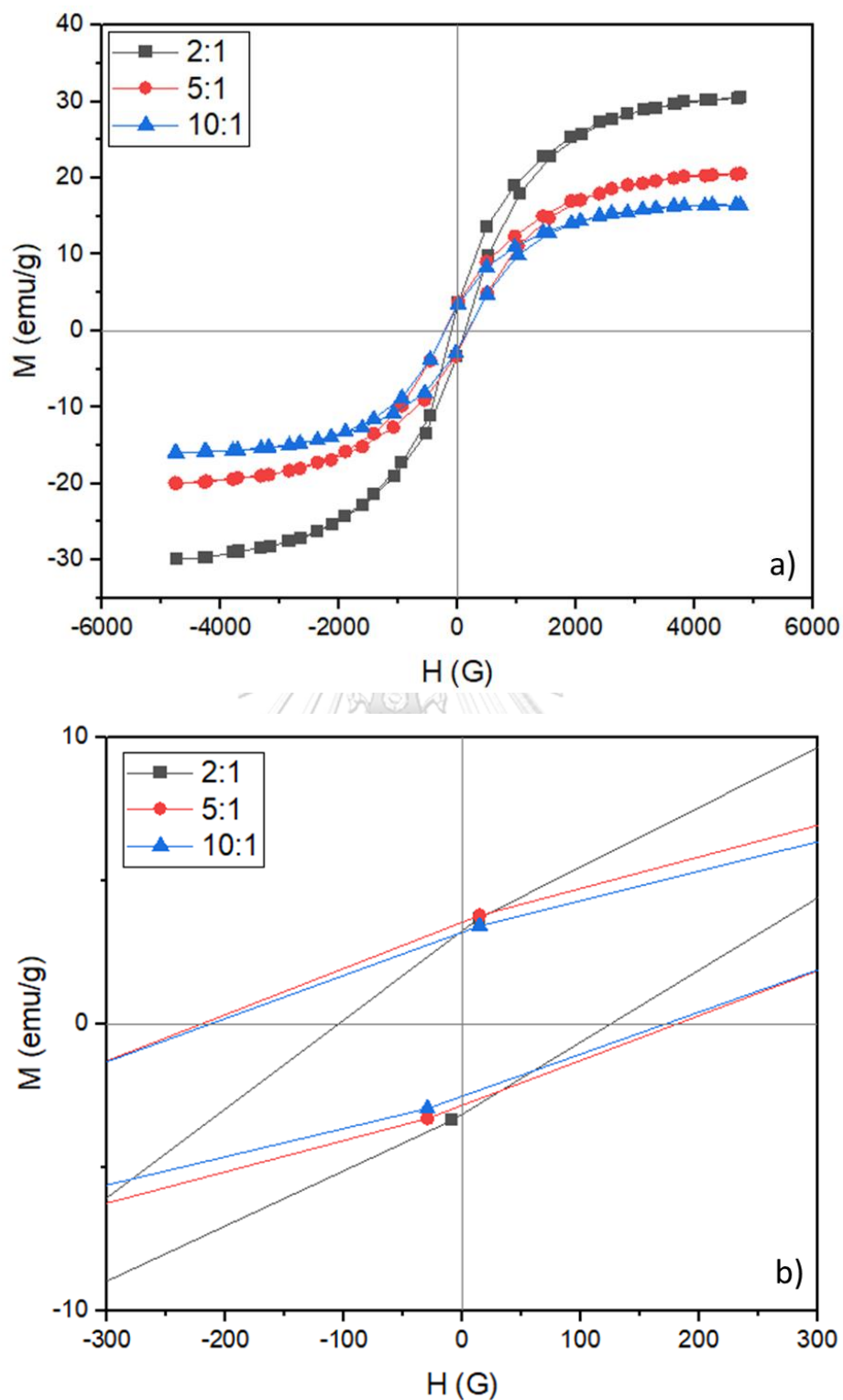


Fig. 62 Magnetic hysteresis loops of as-synthesized carbon from different molar ratio of eucalyptus oil to catalyst at room temperature in a) a whole range and b) magnified range of -300 G to 300 G

Effect of molar ratio of eucalyptus oil to catalyst on MCNT properties was studied. Inlet flowrate of eucalyptus oil was manipulated in each condition. From our results, the flowrate significantly affected on carbon structure in product. 5:1 molar ratio of eucalyptus oil to catalyst provided good quality MCNTs, high crystallinity, and high total mass yield. For other cases, low quality of MCNTs was obtained. If eucalyptus oil flowrate was too low as case of the molar ratio of 2:1. The synthesis could not obtain CNT structure because of low concentration driving force of carbon cluster to catalyst particle. MCNT formation would be prohibited. Meanwhile, in case of too high molar ratio as 10:1 molar ratio, MCNTs still could be formed. However, amorphous carbon was also generated by excessive carbon cluster decomposition because carbon dissolution of catalyst was reached to saturated point. Therefore, the optimal molar ratio in MCNT synthesis would provide high quality of MCNTs.



CHAPTER 5

CONCLUSIONS AND RECOMMENDATIONS

This chapter provides key finding summary of this study. There are 3 main parts of investigations as follows: (i) the study of effect of synthesis temperature, (ii) the study effect of different catalyst, and (iii) the study effect of molar ratio of eucalyptus oil to catalyst. Finally, some valuable suggestions were provided as further investigation guidelines during the study.

5.1 Conclusions

Magnetic carbon nanotubes (MCNTs) have been one of interested material due to their promising properties. They would be used in many applications. For example, CNTs have high specific area and chemical stability which are appropriate for antibiotic removal or surface functionalization. Furthermore, CNT structure could embed magnetic particles. The structure contributes to the improved stability of magnetic property and prolonged shelf-life due to the stability of MCNTs. Therefore, many researchers have been developed magnetic MCNT production to increase in MCNT yield and their quality. Because catalyst plays important role for MCNT formation, catalyst improvement has been interested to study.

In this study, new catalyst for MCNT synthesis, ferrocene impregnated with nickel nitrate, was introduced. The catalyst was developed for reducing cost of catalyst support material such as alumina, magnesium oxide, and silica oxide. Moreover, the cost of support material removal is also decreased because they are essentially removed for collecting MCNT product. Ferrocene is powder and one of preferable catalysts for MCNT production. Thus, ferrocene was used as alternative support material. Nickel nitrate is general and low-cost nickel source. Nickel catalyst is also good for MCNT formation. Also, it could improve graphitization. Therefore, new bimetallic Ni-Fe catalyst was introduced. Ferrocene impregnated with nickel nitrate were prepared by simple method as wet impregnation of nickel nitrate solution on pure ferrocene. From our experiment, MCNT synthesis from the catalyst could achieved. Ferrocene impregnated with nickel nitrate also could improve quality of MCNTs and increase in yield of MCNTs.

5.1.1 Effect of catalyst

In this study, use of ferrocene impregnated with nickel nitrate was compared with use of ferrocene and nickel nitrate in MCNT synthesis by co-pyrolysis of eucalyptus oil with each catalyst. Then, different molar ratio of Fe to Ni of new catalyst preparation was also investigated. As the results, 4:1 ferrocene impregnated with nickel nitrate was the best catalyst in this work. There are two main reasons to explain obtaining the best quality and the highest total mass yield of MCNTs. First, H₂ from

decomposed ferrocene in the catalyst could help to reduce NiO to forming high activity catalyst for MCNT formation. For explaining role of H₂, 1:1 ferrocene impregnated with nickel nitrate was used as catalyst. Total mass yield was less than the use of 4:1 ferrocene impregnated with nickel nitrate and ferrocene because of lower activity of catalyst. Lack of H₂ from decomposed ferrocene for the reduction was a possible cause. Additionally, **bimetallic Fe-Ni catalyst** could reduce amorphous carbon generation and support formation of MCNTs. Thus, 4:1 ferrocene impregnated with nickel nitrate could provide high crystallinity of MCNTs. However, crystallinity of MCNTs from using 1:1 ferrocene impregnated with nickel nitrate was worse than the use of 4:1 ferrocene impregnated with nickel nitrate because of lower performance catalyst.

From results of magnetic properties of MCNTs synthesized from different catalysts, Ni addition could attribute higher M_s because there was high metal content in MCNTs and magnetic moment may be extended along MCNT structure. In case of using 4:1 ferrocene impregnated with nickel nitrate and 1:1 ferrocene impregnated with nickel nitrate. The addition could also reduce H_c due to increasing metal crystalline size and resulting in particle diameter. The particle could become magnetic multi-domain.

5.1.2 Effect of synthesis temperature

Synthesis temperature was the second variable examined in this thesis. Its effect on quality of MCNT products was investigated. Based on all analytical results, synthesis temperature of 800 °C was the optimal condition for MCNT synthesis. The lower synthesis temperature (700 °C) could result in MCNTs with a large amount of amorphous carbon. This result would be ascribed to lower decomposition rate and MCNT formation rate. For higher synthesis temperature (900 °C), MCNT product had low crystallinity due to high decomposed carbon cluster. The reason would result in more carbon deposited on CNT structure and low uniformity.

For magnetic properties of MCNTs, the M_s was decreased when synthesis temperature was increased from 700 °C to 900 °C due to influence of diamagnetic from carbon. For increasing synthesis temperature of 700 °C to 800 °C, H_c raised because magnetic particles were arranged in MCNT structure. The results could indicate retaining magnetization of MCNTs. However, H_c decreased when synthesis temperature increased from 800 °C to 900 °C because the high temperature could induce aggregation of metal particles, and then caused the multi-domain properties.

5.1.3 Effect of molar ratio of eucalyptus oil to catalyst

In the study of effect, eucalyptus oil feed was adjusted inlet flowrate and fed to quartz tube reactor within 15 minutes. The different carbon cluster concentration from decomposed eucalyptus oil could result in formation of MCNTs. In the case of 2:1 molar ratio, MCNTs were not formed because there was insufficient carbon cluster. The low concentration also caused low driving force to catalyst surface and then MCNT

formation procedure was prohibited. For 5:1 molar ratio, MCNTs were produced because the sufficient carbon cluster concentration raised the driving force. The MCNT formation could happen. However, when eucalyptus oil was fed as case of 10:1 molar ratio, saturated carbon cluster dissolution of catalyst particles was reached. Amorphous carbon could be generated because of some remaining carbon cluster decomposition. Additionally, the increasing molar ratio could reduce space time of vapor in reactor for MCNT synthesis. In condition of 10:1 molar ratio, both of yield and amount of product were lower than case of 5:1 molar ratio. First, some oil vapor was flown out from reactor before thermal decomposition. Second, the larger droplet of oil when eucalyptus oil fed at 10:1 also reduced the heat transfer rate to oil droplet for decomposition, resulting in low total mass yield. The CFD simulation of eucalyptus oil flowing in pipe also supported the results.

Magnetic properties of MCNTs synthesized from different eucalyptus oil to catalyst influenced by metal embed different carbon structures and proportion of carbon in product. M_s of synthesized carbon product was decreased when fed eucalyptus oil to catalyst molar ratio in MCNT production because of low proportion of metal. H_c of MCNPs from 2:1 molar ratio was significantly lower than H_c of MCNT products synthesized from the molar ratio of 5:1 to 10:1. These results confirmed that MCNT structure could stabilize their magnetization.

5.2 Recommendations

From our experiment, the amount of MCNT products from co-pyrolysis of eucalyptus oil and ferrocene impregnated with nickel nitrate was about 0.5 g per batch. In our opinion, there are 2 suggestions of improving the production to obtain more yields. First, the process should be scaled up, more synthesized MCNTs would be obtained which would be reduce the time for synthesis. Next, ferrocene may be impregnated with other metal compounds to produce more activity catalysts for increasing the amount of product such as molybdenum and cobalt compounds.

REFERENCES



จุฬาลงกรณ์มหาวิทยาลัย
CHULALONGKORN UNIVERSITY

1. WatElectronics. *What are Ferromagnetic Materials : Magnetization & Their Applications*. 2020; Available from: <https://www.watelectronics.com/what-are-ferromagnetic-materials-magnetization-their-applications/>.
2. *Superparamagnetism*. 2020; Available from: [https://eng.libretexts.org/Bookshelves/Materials_Science/Supplemental_Modules_\(Materials_Science\)/Magnetic_Properties/Superparamagnetism](https://eng.libretexts.org/Bookshelves/Materials_Science/Supplemental_Modules_(Materials_Science)/Magnetic_Properties/Superparamagnetism).
3. Zhu, M. and G. Diao, *Review on the progress in synthesis and application of magnetic carbon nanocomposites*. *Nanoscale*, 2011. **3**(7): p. 2748-67.
4. Sanchez-Ramirez, J., et al., *Cellulases immobilization on chitosan-coated magnetic nanoparticles: application for Agave Atrovirens lignocellulosic biomass hydrolysis*. *Bioprocess Biosyst Eng*, 2017. **40**(1): p. 9-22.
5. Faaliyan, K., et al., *Magnetite-silica nanoparticles with core-shell structure: single-step synthesis, characterization and magnetic behavior*. *Journal of Sol-Gel Science and Technology*, 2018. **88**(3): p. 609-617.
6. Seo, W.S., et al., *FeCo/graphitic-shell nanocrystals as advanced magnetic-resonance-imaging and near-infrared agents*. *Nat Mater*, 2006. **5**(12): p. 971-6.
7. Sun, Z., et al., *Fabrication and characterization of magnetic carbon nanotube composites*. *Journal of Materials Chemistry*, 2005. **15**(42).
8. Su, J., et al., *Fe₃O₄-Graphene Nanocomposites with Improved Lithium Storage and Magnetism Properties*. *The Journal of Physical Chemistry C*, 2011. **115**(30): p. 14469-14477.
9. Lee, J., et al., *Simple synthesis of mesoporous carbon with magnetic nanoparticles embedded in carbon rods*. *Carbon*, 2005. **43**(12): p. 2536-2543.
10. Carole E. Baddour, C.B., *CNT synthesis : A review*. *International Journal of Chemical Reactor Engineering*, 2005. **3**.
11. Li, K., et al., *Catalytic Preparation of Carbon Nanotubes from Waste Polyethylene Using FeNi Bimetallic Nanocatalyst*. *Nanomaterials (Basel)*, 2020. **10**(8).
12. Ratkovic, S., E. Kiss, and G. Boskovic, *Synthesis of high-purity carbon nanotubes over alumina and silica supported bimetallic catalysts*. *Chemical Industry and Chemical Engineering Quarterly*, 2009. **15**(4): p. 263-270.
13. Dijith, K.S., et al., *Polyol derived Ni and NiFe alloys for effective shielding of electromagnetic interference*. *Materials Chemistry Frontiers*, 2018. **2**(10): p. 1829-1841.
14. Wack, M., M. Volk, and Q. Wei, *Magnetic Properties of the Iron-Nickel System: Pressure, Composition, and Grain Size*, in *Magnetic Fields in the Solar System*. 2018. p. 383-406.
15. Tumanski, S., *Magnetic Materials*, in *Handbook of Magnetic Measurements*. 2011, CRC Press. p. 117-158.
16. Luís, Â., et al., *Chemical composition, antioxidant, antibacterial and anti-quorum sensing activities of Eucalyptus globulus and Eucalyptus radiata essential oils*. *Industrial Crops and Products*, 2016. **79**: p. 274-282.
17. Zhang, W., Z. Zhang, and Y. Zhang, *The application of carbon nanotubes in target drug delivery systems for cancer therapies*. *Nanoscale Research Letters*, 2011. **6**: p. 555.

18. Ribeiro, B., et al., *Carbon nanotube buckypaper reinforced polymer composites: a review*. *Polímeros*, 2017. **27**(3): p. 247-255.
19. Jonathan C. Acomb, C.W., Paul T. Williams, *Effect of growth temperature and feedstock:catalyst ratio on the production of carbon nanotubes and hydrogen from the pyrolysis of waste plastics*. *Journal of Analytical and Applied Pyrolysis*, 2015. **113**: p. 231-238.
20. Esteves, L.M., H.A. Oliveira, and F.B. Passos, *Carbon nanotubes as catalyst support in chemical vapor deposition reaction: A review*. *Journal of Industrial and Engineering Chemistry*, 2018. **65**: p. 1-12.
21. Ghiazza, M., G. Vietti, and I. Fenoglio, *Carbon nanotubes: properties, applications, and toxicity*, in *Health and Environmental Safety of Nanomaterials*. 2014. p. 147-174.
22. Nessim, G.D., *Properties, synthesis, and growth mechanisms of carbon nanotubes with special focus on thermal chemical vapor deposition*. *Nanoscale*, 2010. **2**(8): p. 1306-23.
23. Kumar, M., *Carbon Nanotubes - Synthesis, Characterization, Applications*. 2011, InTech.
24. Persson, A.I., et al., *Solid-phase diffusion mechanism for GaAs nanowire growth*. *Nat Mater*, 2004. **3**(10): p. 677-81.
25. *Hysteresis*. 2013; Available from: <https://www.britannica.com/science/hysteresis>.
26. Indeck, R.S. and M.W. Muller, *Magnetic Recording Measurements*, in *Encyclopedia of Materials: Science and Technology*, K.H.J. Buschow, et al., Editors. 2002, Elsevier: Oxford. p. 1-14.
27. Khan, H.R., *Ferromagnetism*, in *Encyclopedia of Physical Science and Technology (Third Edition)*, R.A. Meyers, Editor. 2003, Academic Press: New York. p. 759-768.
28. Krishnan, K.M., *Fundamentals and Applications of Magnetic Materials*. 2016, United States of America: Oxford University Press.
29. Cullity, B.D. and C.D. Graham, *Diamagnetism and Paramagnetism*, in *Introduction to Magnetic Materials*. 2008. p. 87-114.
30. Cullity, B.D. and C.D. Graham, *Ferromagnetism*, in *Introduction to Magnetic Materials*. 2008. p. 115-149.
31. *Antiferromagnetism*, in *Introduction to Magnetic Materials*. 2008. p. 151-173.
32. Cullity, B.D. and C.D. Graham, *Ferrimagnetism*, in *Introduction to Magnetic Materials*. 2008. p. 175-195.
33. *Classification of Magnetic Materials*. Available from: <https://www.birmingham.ac.uk/Documents/college-eps/metallurgy/research/Magnetic-Materials-Background/Magnetic-Materials-Background-4-Classification-of-Magnetic-Materials.pdf>.
34. Cullity, B.D. and C.D. Graham, *Fine Particles and Thin Films*, in *Introduction to Magnetic Materials*. 2008. p. 359-408.
35. Mohapatra, J. and J.P. Liu, *Rare-Earth-Free Permanent Magnets: The Past and Future*, in *Handbook of Magnetic Materials*. 2018. p. 1-57.
36. Srisraththa, P., *Synthesis of Multi-walled Carbon Nanotubes from C6 Hydrocarbon Compounds with Different Heat Supplying Patterns*, in

- Chemical engineering*. 2019, Chulalongkorn University: Chulalongkorn University.
37. Kusriani, E., et al., *The Effect of Mass Ratio of Ferrocene to Camphor as Carbon Source and Reaction Time on the Growth of Carbon Nanotubes*. E3S Web of Conferences, 2018. **67**.
 38. Mitina, A.A., A.N. Redkin, and E.E. Yakimov, *New way of the nickel catalyst preparation for carbon nanotubes synthesis by pyrolysis of ethanol vapor*. Fullerenes, Nanotubes and Carbon Nanostructures, 2019. **28**(2): p. 112-117.
 39. Yao, D., et al., *Co-production of hydrogen and carbon nanotubes from catalytic pyrolysis of waste plastics on Ni-Fe bimetallic catalyst*. Energy Conversion and Management, 2017. **148**: p. 692-700.
 40. Fazle Kibria, A.K.M., Y.H. Mo, and K.S. Nahm, *Synthesis of carbon nanotubes over nickel–iron catalysts supported on alumina under controlled condition*. Catalysis Letters, 2001. **71**(3/4): p. 229-236.
 41. Yao, D. and C.-H. Wang, *Pyrolysis and in-line catalytic decomposition of polypropylene to carbon nanomaterials and hydrogen over Fe- and Ni-based catalysts*. Applied Energy, 2020. **265**.
 42. Mongkolsamai, P., *Treatment of Wastewater Contaminated with Antibiotics Using Magnetic Carbon Nanoparticles*, in *Chemical Engineering*. 2013, Chulalongkorn University: Chulalongkorn University. p. 88.
 43. Lee, C., et al., *Temperature effect on the growth of carbon nanotubes using thermal chemical vapor deposition*. Chemical Physics Letters, 2001. **343**: p. 33-38.
 44. Shamsudin, M.S., et al., *Effect of Synthesis Temperature on the Growth Iron-Filled Carbon Nanotubes as Evidenced by Structural, Micro-Raman, and Thermogravimetric Analyses*. Advances in Condensed Matter Physics, 2012. **2012**: p. 1-7.
 45. Tripathi, N., et al., *Fine-tuning control on CNT diameter distribution, length and density using thermal CVD growth at atmospheric pressure: an in-depth analysis on the role of flow rate and flow duration of acetylene (C₂H₂) gas*. Applied Nanoscience, 2014. **5**(1): p. 19-28.
 46. Venkatesan, S., et al., *Effect of chemical vapor deposition parameters on the diameter of multi-walled carbon nanotubes*. International Nano Letters, 2018. **8**(4): p. 297-308.
 47. Xu, M.H., et al., *Highly stable Fe–Ni alloy nanoparticles encapsulated in carbon nanotubes: Synthesis, structure and magnetic properties*. Journal of Alloys and Compounds, 2010. **495**(1): p. 200-204.
 48. Liu, Q., et al., *Synthesis of different magnetic carbon nanostructures by the pyrolysis of ferrocene at different sublimation temperatures*. Carbon, 2008. **46**(14): p. 1892-1902.
 49. Dong, X.L., et al., *Characterization of Fe–Ni(C) nanocapsules synthesized by arc discharge in methane*. Journal of Materials Research, 1999. **14**(5): p. 1782-1790.
 50. Kerdnawee, K., et al., *Controlled synthesis of magnetic carbon nanoparticles via glycerol/ferrocene co-pyrolysis with magnetic induction*. Particuology, 2018. **37**: p. 9-16.

51. Sajitha, E.P., et al., *Synthesis and characteristics of iron nanoparticles in a carbon matrix along with the catalytic graphitization of amorphous carbon*. Carbon, 2004. **42**(14): p. 2815-2820.
52. Leonhardt, A., et al., *Synthesis, Properties, and Applications of Ferromagnetic-Filled Carbon Nanotubes*. Chemical Vapor Deposition, 2006. **12**(6): p. 380-387.
53. Brockner, W., C. Ehrhardt, and M. Gjika, *Thermal decomposition of nickel nitrate hexahydrate, Ni(NO₃)₂·6H₂O, in comparison to Co(NO₃)₂·6H₂O and Ca(NO₃)₂·4H₂O*. Thermochimica Acta, 2007. **456**(1): p. 64-68.
54. Tan, J.M., et al., *A Review on Characterizations and Biocompatibility of Functionalized Carbon Nanotubes in Drug Delivery Design*. Journal of Nanomaterials, 2014. **2014**: p. 1-20.
55. Li, Q., et al., *Effect of hydrocarbons precursors on the formation of carbon nanotubes in chemical vapor deposition*. Carbon, 2004. **42**(4): p. 829-835.
56. Le, G.T.T., et al., *Bio-based production of carbon nanotubes via co-pyrolysis of eucalyptus oil and ferrocene*. Journal of Analytical and Applied Pyrolysis, 2021. **158**.
57. He, L., et al., *Promoting effects of Fe-Ni alloy on co-production of H₂ and carbon nanotubes during steam reforming of biomass tar over Ni-Fe/α-Al₂O₃*. Fuel, 2020. **276**.
58. Cai, N., et al., *Bimetallic carbon nanotube encapsulated Fe-Ni catalysts from fast pyrolysis of waste plastics and their oxygen reduction properties*. Waste Manag, 2020. **109**: p. 119-126.
59. Batakliiev, T., et al., *Effects of Graphene Nanoplatelets and Multiwall Carbon Nanotubes on the Structure and Mechanical Properties of Poly(lactic acid) Composites: A Comparative Study*. Applied Sciences, 2019. **9**(3).
60. Yao, D., et al., *Hydrogen production from catalytic reforming of the aqueous fraction of pyrolysis bio-oil with modified Ni–Al catalysts*. International Journal of Hydrogen Energy, 2014. **39**(27): p. 14642-14652.
61. Yao, D., et al., *Impact of temperature on the activity of Fe-Ni catalysts for pyrolysis and decomposition processing of plastic waste*. Chemical Engineering Journal, 2021. **408**.
62. Kanamori, J., K. Terakura, and K. Yamada, *The Approximate Expression of Green's Function for the Calculation of Electronic Structure in Metals and Alloys*. Progress of Theoretical Physics, 1969. **41**(6): p. 1426-1437.
63. Wang, H., et al., *The effect of methane decomposition on the formation and magnetic properties of iron carbide prepared from oolitic hematite*. RSC Advances, 2017. **7**(7): p. 3921-3927.
64. He, X., et al., *Size dependence of the magnetic properties of Ni nanoparticles prepared by thermal decomposition method*. Nanoscale Research Letters, 2013. **8**: p. 446.
65. Wang, J., et al., *Giant magnetic moment enhancement of nickel nanoparticles embedded in multiwalled carbon nanotubes*. Physical Review B, 2010. **82**(19).
66. Nirouei, M., A. Jafari, and K. Boustani, *Magnetic and Structural Study of FeNi₃ Nanoparticles: Effect of Calcination Temperature*. Journal of Superconductivity and Novel Magnetism, 2014. **27**(12): p. 2803-2811.

67. Sajitha, E.P., et al., *Size-dependent magnetic properties of iron carbide nanoparticles embedded in a carbon matrix*. Journal of Physics: Condensed Matter, 2007. **19**(4).
68. Yan, S.J., et al., *Microwave absorption properties of FeNi₃ submicrometre spheres and SiO₂@FeNi₃ core-shell structures*. Journal of Physics D: Applied Physics, 2010. **43**(24).
69. Choudhury, P.K., et al., *Variations in magnetic properties of nanostructured nickel*. J Nanosci Nanotechnol, 2013. **13**(12): p. 8162-6.
70. Geng, F. and H. Cong, *Fe-filled carbon nanotube array with high coercivity*. Physica B: Condensed Matter, 2006. **382**(1-2): p. 300-304.
71. Lafdi, K., et al., *Cobalt-doped carbon nanotubes: Preparation, texture, and magnetic properties*. Journal of Applied Physics, 1996. **79**(8).
72. Leonhardt, A., et al., *Enhanced magnetism in Fe-filled carbon nanotubes produced by pyrolysis of ferrocene*. Journal of Applied Physics, 2005. **98**(7).
73. Kang, B.-S. and K.-J. Choi, *Cooling of a heated surface with an impinging water spray*. KSME International Journal, 1998. **12**(4): p. 734-740.
74. Mahesh, N.S., et al., *Modeling of droplet dynamic and thermal behaviour during spray deposition*. Bulletin of Materials Science, 2003. **26**(3): p. 355-364.
75. Wen, R., et al., *Droplet dynamics and heat transfer for dropwise condensation at lower and ultra-lower pressure*. Applied Thermal Engineering, 2015. **88**: p. 265-273.
76. Batsaikhan, E., et al., *Largely Enhanced Ferromagnetism in Bare CuO Nanoparticles by a Small Size Effect*. ACS Omega, 2020. **5**(8): p. 3849-3856.
77. Hazra, A., et al., *Characterization of Some Essential Oils and Their Key Components: Thermoanalytical techniques*. Journal of Thermal Analysis and Calorimetry, 2004. **75**: p. 317-330.



APPENDICES

จุฬาลงกรณ์มหาวิทยาลัย
CHULALONGKORN UNIVERSITY

APPENDIX A

Eucalyptus Oil Specification

EUCALYPTUS OIL											
British Pharmacopoeia Standard (B.P.)											
COMMODITY	EUCALYPTUS OIL	PHARMARCEUTICAL STANDARD									
BATCH NUMBER	20190902	MANUFACTURING DATE	SEPTEMBER 02, 2019								
QUANTITY	480 DRUMS	EXPIRY DATE	SEPTEMBER 02, 2023								
CERTIFICATE OF ANALYSIS AND SPECIFICATION											
TEST ITEMS	SPECIFICATION	TEST RESULT									
APPEARANCE	Colorless or light yellow liquid	Qualified									
Aroma	Fresh camphoraceous odour	Qualified									
SPECIFIC GRAVITY (20/20°C)	0.909-0.919	0.915									
REFRACTIVE INDEX (20°C)	1.4590—1.4650	1.4618									
OPTICAL ROTATION (20°C)	-10 -- +10	+2.046									
Eucalyptol Content (Cineol content)	80% Min	80.33%									
SOLUBILITY (20°C)	1 ML sample soluble completely in 5ML 70% (v/v) Alcohol	Qualified									
Safrole Content (GC,%)	Non-existent	Qualified									
AS content (%)	Less than 0.0003	Qualified									
Heavy Metal (Pb) content (%)	Less than 0.001	Qualified									
CONCLUSION:	Fully compliant with British Pharmacopoeia (B.P.)										
<table style="width: 100%; border: none;"> <tr> <td style="width: 40%;">CHEMICAL NAME</td> <td>: Eucalyptus oil</td> </tr> <tr> <td>CAS REGISTRY NUMBER</td> <td>: 8000-48-4</td> </tr> <tr> <td>SYNONYMS/TRADE NAMES :</td> <td></td> </tr> <tr> <td></td> <td> <ul style="list-style-type: none"> • Dinkum oil • Eucalyptus citriodora oil • Eucalyptus oel • Oil of eucalyptus </td> </tr> </table>				CHEMICAL NAME	: Eucalyptus oil	CAS REGISTRY NUMBER	: 8000-48-4	SYNONYMS/TRADE NAMES :			<ul style="list-style-type: none"> • Dinkum oil • Eucalyptus citriodora oil • Eucalyptus oel • Oil of eucalyptus
CHEMICAL NAME	: Eucalyptus oil										
CAS REGISTRY NUMBER	: 8000-48-4										
SYNONYMS/TRADE NAMES :											
	<ul style="list-style-type: none"> • Dinkum oil • Eucalyptus citriodora oil • Eucalyptus oel • Oil of eucalyptus 										

Fig A1 Eucalyptus oil specification information from Chanjao Longevity, Thailand

APPENDIX B

Preparation of Ferrocene Impregnated with Nickel Nitrate

Different molar ratio of Fe to Ni in ferrocene impregnated with nickel nitrate could be calculated based on 0.75 g of ferrocene. Ferrocene and nickel (II) nitrate hexahydrate were used as metal precursors, while solvent would be ethanol. The calculation of nickel nitrate hexahydrate (Ni precursor) requirement was shown in **Eq. B1**.

$$\text{Molar ratio of Fe to Ni} = \frac{\text{mol}_{Fe}}{\text{mol}_{Ni}} = \frac{\text{mol}_{fer}}{\text{mol}_{Ni \text{ precursor}}} = \frac{\frac{W_{fer}}{MW_{fer}}}{\frac{W_{Ni \text{ precursor}}}{MW_{Ni \text{ precursor}}}}$$

$$W_{Ni \text{ precursor}} = \frac{W_{fer} \times MW_{Ni \text{ precursor}}}{MW_{fer} \times \frac{\text{mol}_{Fe}}{\text{mol}_{Ni}}} \quad \text{Equation B1}$$

Where

$W_{Ni \text{ precursor}}$ = weight of nickel (II) nitrate hexahydrate (g)

$MW_{Ni \text{ precursor}}$ = molecular weight of nickel (II) nitrate hexahydrate (290.80 g/mol)

$\frac{\text{mol}_{Fe}}{\text{mol}_{Ni}}$ = molar ratio of Fe to Ni (1 or 4)

W_{fer} = weight of ferrocene (0.75 g)

MW_{fer} = molecular weight of ferrocene (186.03 g/mol)

MW metal atom in precursor = molecular weight of Fe in ferrocene or Ni in nickel (II) nitrate hexahydrate (55.85 g/mol and 58.69 g/mol respectively)

Example calculation of nickel (II) nitrate hexahydrate requirement for preparation of 4:1 ferrocene impregnated with nickel nitrate

$$\text{Nickel nitrate hexahydrate requirement} = W_{Ni \text{ precursor}} = \frac{0.75 \times 290.80}{186.03 \times 4} = 0.2931 \text{ g}$$

Table B1 Weight of nickel (II) nitrate hexahydrate requirement for each Fe to Ni molar ratio in ferrocene impregnated with nickel nitrate

Fe to Ni molar ratio in ferrocene impregnated with nickel nitrate	Nickel (II) nitrate hexahydrate (g)
4:1	0.29
1:1	1.17

Table B2 Percentage of Fe-Ni which analyzed from EDS and XRF of each ferrocene impregnated with nickel nitrate catalyst

Catalyst	EDS			XRF		
	Fe (mol%)	Ni (mol%)	Fe:Ni molar ratio	Fe (mol%)	Ni (mol%)	Fe:Ni molar ratio
4:1 ferrocene impregnated with nickel nitrate	1.6	3.6	0.44:1	16.8	10.4	1.6:1
1:1 ferrocene impregnated with nickel nitrate	1.2	3.3	0.36:1	9.4	15.8	0.6:1

Both actual molar ratio of Fe to Ni from 4:1 ferrocene impregnated with nickel nitrate and 1:1 ferrocene impregnated with nickel nitrate were indicated by EDS and XRF as shown in **Table B2**. From EDS spectra of 4:1 ferrocene impregnated with nickel nitrate and 1:1 ferrocene impregnated with nickel nitrate as shown in **Fig. B1-B2**. Both spectra indicated peaks of C and Fe, which are atomic components of ferrocene, and specified peaks of O, N, and Ni, which are atomic elements of nickel nitrate.

Fe to Ni molar ratio of 4:1 ferrocene impregnated with nickel nitrate from EDS and XRF was different. Because EDS analysis mainly measures catalyst surface contents while XRF characterization penetrates relatively deep into the catalyst sample. Therefore, Ni content could be more detected in case of EDS. It could also confirm that impregnation of nickel nitrate onto ferrocene was success. However, Fe to Ni molar ratio of catalyst should be assure by XRF due to deeper measurement.

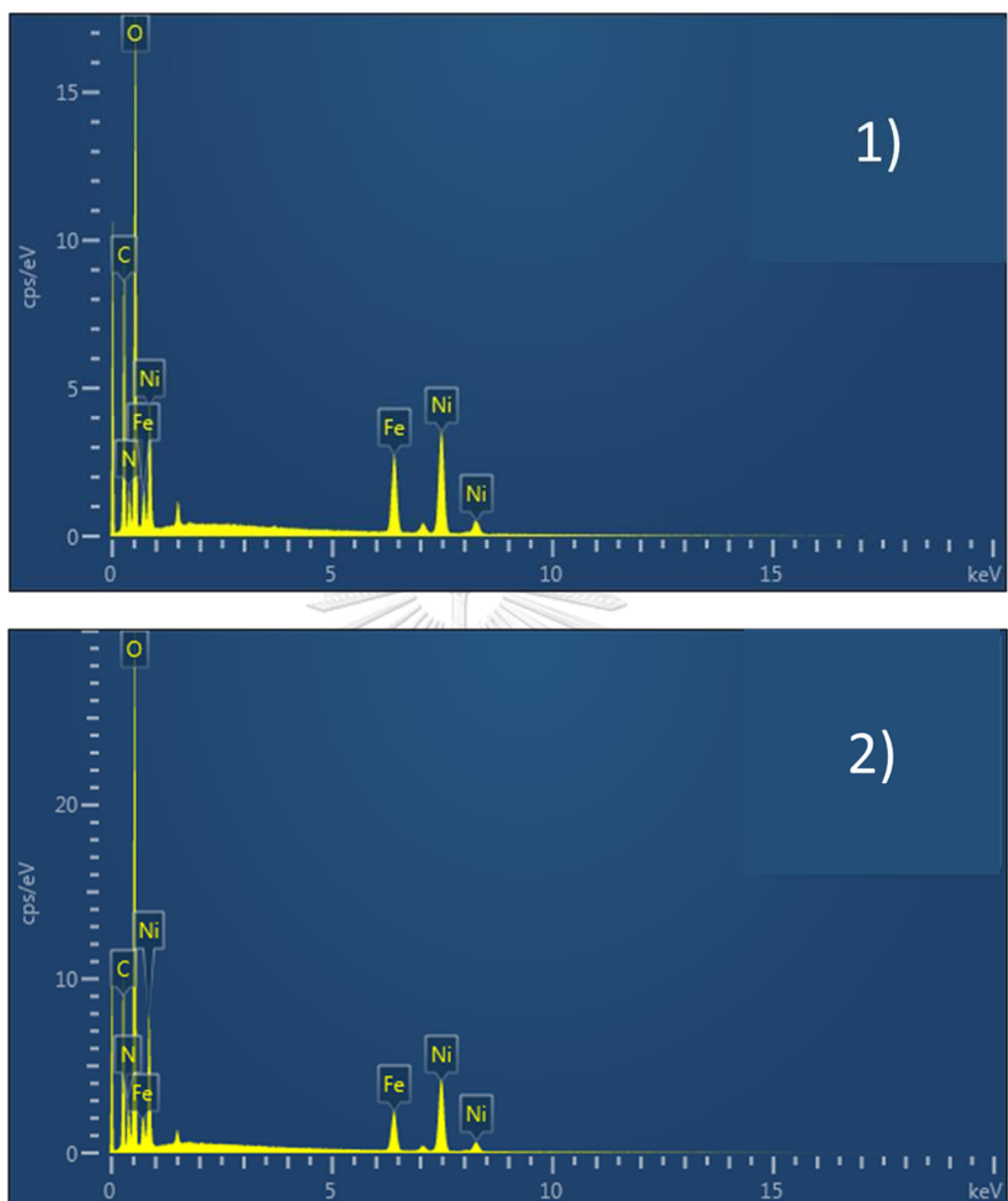


Fig. B1 EDS spectra of 1) 4:1 ferrocene impregnated with nickel nitrate and 2) 1:1 ferrocene impregnated with nickel nitrate

APPENDIX C

Total Mass Yield of Synthesized CNTs

Total mass yield of synthesized CNTs at different synthesis temperature, catalyst, and molar ratio of eucalyptus oil to catalyst were calculated by **Eq 2** respectively. Due to the different catalyst, each metal precursor weight used in the synthesis of CNTs was calculated by **Eq.C1** and is shown in **Table C1**. The eucalyptus oil volume of each molar ratio was calculated by **Eq.C2** and is shown in **Table C2**.

Calculation of catalyst precursor weight

$$\text{Total metal weight} = W_{\text{Fe}} + W_{\text{Ni}} = \text{mol}_{\text{Fe}}MW_{\text{Fe}} + \text{mol}_{\text{Ni}}MW_{\text{Ni}}$$

$$\text{Weight of metal precursor} = \frac{W_{\text{metal}} \times MW_{\text{metal precursor}}}{MW_{\text{metal atom}}} \quad \text{Equation C1}$$

Where

Total metal weight = total weight of metal loading in catalyst precursor (0.15 g)

W_{Fe} = weight of Fe in metal precursor

mol_{Fe} = mole of Fe in metal precursor

MW_{Fe} = molecular weight of Fe (55.85 g/mol)

W_{Ni} = weight of Ni in metal precursor

mol_{Ni} = mole of Ni in metal precursor

MW_{Ni} = molecular weight of Ni (58.69 g/mol)

W_{metal} = weight of Fe or Ni in metal precursor

$MW_{\text{metal precursor}}$ = molecular weight of ferrocene or nickel (II) nitrate hexahydrate (186.03 g/mol and 290.80 g/mol)

$MW_{\text{metal atom}}$ = molecular weight of Fe in ferrocene or Ni in nickel (II) nitrate hexahydrate (55.85 g/mol and 58.69 g/mol, respectively)

Example calculation of used weight of 4:1 ferrocene impregnated with nickel nitrate

- Calculation weight of Fe and Ni in the catalyst precursor

$$0.15 = \text{mol}_{\text{Fe}}MW_{\text{Fe}} + \text{mol}_{\text{Ni}}MW_{\text{Ni}} = (4\text{mol}_{\text{Ni}} \times 55.85) + (\text{mol}_{\text{Ni}} \times 58.69)$$

$$\text{mol}_{\text{Ni}} = 5.317 \times 10^{-4} \text{ mole}, \quad W_{\text{Ni}} = 0.03 \text{ g}, \quad W_{\text{Fe}} = 0.15 - 0.03 = 0.12 \text{ g}$$

- Calculation weight of ferrocene, nickel (II) nitrate hexahydrate, and Catalyst

$$\text{Weight of ferrocene} = \frac{0.12 \times 186.03}{55.85} = 0.40 \text{ g}$$

$$\text{Weight of nickel (II) nitrate hexahydrate} = \frac{0.03 \times 290.80}{58.69} = 0.15 \text{ g}$$

$$\text{Weight of metal precursor} = 0.40 + 0.15 = 0.55 \text{ g}$$

Table C1 Weight of Fe, Ni, metal precursors and catalyst requirement for each various catalyst precursors

Catalyst	Fe to Ni molar ratio	Fe (g)	Ni (g)	Total mole of Fe and Ni (mmole)	Metal precursor		Catalyst weight (g)
					Ferrocene (g)	Nickel (II) nitrate hexahydrate (g)	
Ferrocene	1:0	0.15	-	2.69	0.50	-	0.50
4:1 ferrocene impregnated with nickel nitrate	4:1	0.12	0.03	2.66	0.40	0.15	0.55
1:1 ferrocene impregnated with nickel nitrate	1:1	0.07	0.08	2.62	0.24	0.38	0.62
Nickel nitrate	0:1	-	0.15	2.56	-	0.74	0.74

Calculation of eucalyptus oil volume

$$\text{Molar ratio of eucalyptus oil to catalyst} = \frac{\text{mol}_{\text{eu}}}{\text{mol}_{\text{catalyst}}} = \frac{\frac{W_{\text{eu}}}{MW_{\text{eu}}}}{\frac{W_{\text{Fe}}}{MW_{\text{Fe}}} + \frac{W_{\text{Ni}}}{MW_{\text{Ni}}}}$$

$$= \frac{X_{\text{eu}} \times \rho_{\text{oil}} \times V_{\text{oil}}}{MW_{\text{eu}}}$$

$$= \frac{\text{mol}_{\text{Fe}} + \text{mol}_{\text{Ni}}}{\text{mol}_{\text{Fe}} + \text{mol}_{\text{Ni}}}$$

$$V_{\text{oil}} = \frac{\frac{\text{mol}_{\text{eu}}}{\text{mol}_{\text{catalyst}}} \times MW_{\text{eu}} \times (\text{mol}_{\text{Fe}} + \text{mol}_{\text{Ni}})}{X_{\text{eu}} \times \rho_{\text{oil}}}$$

Equation C2

Although total mole of Fe and Ni ($\text{mol}_{\text{Fe}} + \text{mol}_{\text{Ni}}$) in each catalyst were different as shown in **Table C1**, in calculation of molar ratio of eucalyptus oil to catalyst, the mole of catalyst was assumed to their average value (2.63 mmol) because quality and quantity of CNTs depended on total amount of eucalyptus oil although feed flowrate was fixed [56]. Therefore, amount of eucalyptus oil feed was fixed in the study effect of catalyst.

Where

V_{oil} = volume of eucalyptus oil

$\frac{mol_{eu}}{mol_{catalyst}}$ = molar ratio of eucalyptus oil to catalyst (2, 5, or 10)

$mol_{Fe} + mol_{Ni}$ = total mole of Fe and Ni in catalyst (2.63 mmol)

X_{eu} = purity of eucalyptol in eucalyptus oil (0.8033)

W_{eu} = weight of eucalyptol

MW_{eu} = molecular weight of eucalyptol (154.25 g/mol)

ρ_{oil} = density of eucalyptus oil (0.915 g/cm³)

Example calculation of eucalyptus oil volume and oil feed flowrate at 5:1 molar ratio of eucalyptus oil to catalyst (15 minutes feeding time)

$$V_{oil} = \frac{5 \times 154.25 \times 0.00263}{0.8033 \times 0.915} = 2.76 \text{ cm}^3$$

$$\text{Oil feed flowrate} = \frac{2.76}{15} = 0.18 \text{ cm}^3/\text{min}$$

Table C2 Volume and weight of eucalyptus oil and their feed flowrate used in the synthesis of MCNTs at different molar ratio of eucalyptus oil to catalyst

Molar ratio of eucalyptus oil to catalyst	V_{oil} (cm ³)	Eucalyptus oil weight (g)	Oil feed flowrate (cm ³ /min)
2:1	1.10	1.01	0.07
5:1	2.76	2.53	0.18
10:1	5.52	5.05	0.37

CHULALONGKORN UNIVERSITY

In study of effect of catalyst, the weight of eucalyptus oil, weight of each catalyst, and weight of product demonstrate in **Table C3**. Then, total mass yield shows in **Table C4**.

Table C3 Weight of eucalyptus oil, catalyst, and weight of product at 800 °C of synthesis temperature

Catalyst	Weight of eucalyptus oil (g)	Weight of catalyst (g)	Weight of product (g)
Ferrocene	2.53	0.5048	0.4288
		0.5023	0.4576
		0.5068	0.3819
4:1 ferrocene impregnated with nickel nitrate		0.5518	0.4370
		0.5574	0.5384
		0.5537	0.4894
1:1 ferrocene impregnated with nickel nitrate		0.6279	0.4426
		0.6252	0.4026
		0.6259	0.3759
Nickel nitrate		0.7460	0.2657
	0.7434	0.2037	
	0.7445	0.1803	

Table C4 Total mass yield (%) of synthesized MCNTs at synthesis temperature of 800 °C and using 5:1 molar ratio of eucalyptus oil to catalyst

Repeatability	Total mass yield at different catalysts			
	CNT_F1N0	CNT_F1N0.25	CNT_F1N1	CNT_F0N1
Run 1	15.28	18.80	15.12	8.73
Run 2	16.32	15.32	13.77	6.70
Run 3	13.60	17.14	12.82	5.93
Average	15.60	17.09	13.90	7.72
Standard Deviation	1.37	1.74	1.15	1.45

In study of effect of synthesis temperature, the weight of eucalyptus oil, weight of 1:1 ferrocene impregnated with nickel nitrate, and weight of product demonstrate in **Table C5**. Then, total mass yield shows in **Table C6**.

Table C5 Weight of eucalyptus oil, 1:1 ferrocene impregnated with nickel nitrate, and weight of product at different synthesis temperature

Synthesis temperature (°C)	Weight of eucalyptus oil (g)	Weight of 1:1 ferrocene impregnated with nickel nitrate (g)	Weight of product (g)
700	2.53	0.6252	0.2929
		0.6259	0.2856
		0.6264	0.2146
800		0.6279	0.4426
		0.6252	0.4026
		0.6259	0.3759
900		0.6278	0.4874
		0.6292	0.5445
		0.6262	0.5076

Table C6 Total mass yield (%) of synthesized MCNTs by using 1:1 ferrocene impregnated with nickel nitrate and 5:1 molar ratio of eucalyptus oil to catalyst

Repeatability	Total mass yield at different synthesis temperature (°C)		
	700	800	900
Run 1	10.01	15.12	18.59
Run 2	9.76	13.77	17.32
Run 3	7.33	12.82	16.65
Average	9.04	13.90	17.52
Standard Deviation	1.48	1.15	0.99

In study of effect of molar ratio of eucalyptus oil to catalyst, the weight of eucalyptus oil, weight of each catalyst, and weight of product was shown in **Table C7**. Then, total mass yield was shown in **Table C8**.

Table C7 Weight of eucalyptus oil, 4:1 ferrocene impregnated with nickel nitrate, and weight of product at 800 °C of synthesis temperature and different molar ratio of eucalyptus oil to catalyst

Molar ratio of eucalyptus oil to catalyst	Weight of eucalyptus oil (g)	Weight of 4:1 ferrocene impregnated with nickel nitrate (g)	Weight of product (g)
2:1	1.01	0.5554	0.2862
		0.5559	0.2291
		0.5554	0.2455
5:1	2.53	0.5518	0.4370
		0.5574	0.5384
		0.5537	0.4894
10:1	5.05	0.5567	0.3994
		0.5545	0.3847
		0.5535	0.3427

Table C8 Total mass yield (%) of synthesized MCNTs by at 800 °C of synthesis temperature and using 4:1 ferrocene impregnated with nickel nitrate at different molar ratio of eucalyptus oil to catalyst

Repeatability	Total mass yield at different molar ratio of eucalyptus oil to catalyst		
	2:1	5:1	10:1
Run 1	18.28	18.80	7.12
Run 2	14.63	15.32	6.86
Run 3	15.89	17.14	6.12
Average	16.20	17.09	6.70
Standard Deviation	1.54	1.74	0.43

APPENDIX D

CNT Diameter Distribution

Table D1 Diameter of CNTs synthesized from eucalyptus oil and different catalyst

Counts	CNT diameter (nm)			
	CNT_F1N0	CNT_F1N0.25	CNT_F1N1	CNT_F0N1
1	26.2	23.8	17.3	41.0
2	26.2	33.7	23.1	41.0
3	26.6	33.7	24.5	43.4
4	26.6	34.7	24.5	46.5
5	26.6	34.7	24.5	46.6
6	27.3	35.2	24.5	47.0
7	28.5	36.6	25.9	47.3
8	28.5	36.6	25.9	48.0
9	28.7	36.6	28.9	48.4
10	28.9	36.6	28.9	48.4
11	28.9	37.0	28.9	49.1
12	28.9	37.0	28.9	49.2
13	28.9	37.0	28.9	49.2
14	28.9	37.0	31.1	50.6
15	28.9	37.0	31.1	51.1
16	28.9	37.0	32.7	51.1
17	29.8	38.8	32.7	51.6
18	30.2	38.8	33.7	51.9
19	30.7	38.8	33.7	52.0
20	30.8	38.8	34.7	52.0
21	30.8	38.8	35.2	52.1
22	30.8	38.8	37.0	52.3
23	30.8	38.8	37.0	53.1
24	31.3	38.8	37.0	53.8
25	31.3	38.8	38.8	54.2
26	31.3	40.9	38.8	54.3
27	32.0	40.9	38.8	54.8
28	32.4	40.9	38.8	54.8
29	32.4	40.9	40.5	55.5
30	32.4	40.9	40.5	55.7
31	32.7	41.7	40.5	55.8
32	33.0	41.7	40.5	56.0
33	33.0	41.7	40.5	56.1
34	33.0	41.7	40.9	56.7
35	33.0	41.7	40.9	57.2
36	33.0	41.7	40.9	57.4

37	33.0	41.7	40.9	57.4
38	33.8	41.7	41.7	57.4
39	34.7	42.1	41.7	57.6
40	34.7	42.1	41.7	58.4
41	34.8	42.1	41.7	59.5
42	34.8	42.1	41.7	59.5
43	34.8	42.1	42.1	59.5
44	34.9	44.0	42.1	60.3
45	34.9	44.0	44.0	61.2
46	34.9	44.0	44.0	61.9
47	34.9	44.0	46.2	62.2
48	35.0	44.0	46.6	62.3
49	35.0	44.0	46.6	62.5
50	35.3	44.0	46.6	62.5
51	35.3	44.0	46.6	63.3
52	35.7	45.1	47.7	63.3
53	36.2	45.1	47.7	64.1
54	36.2	45.1	49.0	64.9
55	36.3	45.1	49.0	64.9
56	36.6	45.1	49.4	65.8
57	36.8	46.2	49.4	65.9
58	36.8	46.2	49.4	66.4
59	37.0	46.2	49.4	66.7
60	37.6	46.2	49.7	67.3
61	37.6	46.2	49.7	67.5
62	37.6	46.6	49.7	68.5
63	37.7	46.6	51.7	68.5
64	37.7	46.6	51.7	68.7
65	37.7	46.6	52.0	68.7
66	37.7	46.6	52.0	69.7
67	37.7	46.6	52.3	70.2
68	37.7	46.6	53.3	71.3
69	38.8	46.6	53.3	71.5
70	38.8	47.7	53.3	72.3
71	38.8	47.7	53.3	73.1
72	38.9	47.7	54.5	73.7
73	38.9	47.7	54.8	74.6
74	39.4	47.7	54.8	75.2
75	39.4	47.7	56.9	75.3
76	39.4	49.0	57.2	75.8
77	40.3	49.0	57.2	75.9
78	40.3	49.4	57.2	76.7

79	40.3	49.4	57.8	77.0
80	40.5	49.7	57.8	77.1
81	40.5	49.7	57.8	77.1
82	40.5	49.7	58.1	77.8
83	40.9	51.7	58.9	78.6
84	40.9	51.7	60.3	78.9
85	40.9	51.7	60.3	79.4
86	40.9	51.7	60.3	80.0
87	40.9	51.7	61.4	81.7
88	41.4	52.3	62.5	81.8
89	42.1	52.3	64.6	82.3
90	42.7	53.3	64.6	83.1
91	42.7	53.3	64.6	84.4
92	43.0	53.3	65.4	87.4
93	43.0	53.3	65.9	87.9
94	43.4	56.9	67.4	89.5
95	43.4	57.2	67.4	90.0
96	43.7	58.1	67.7	91.7
97	44.1	58.9	68.4	95.4
98	44.9	58.9	69.6	95.6
99	45.7	61.4	70.6	98.0
100	49.5	61.4	74.0	99.7
Average	35.6	44.6	46.6	65.1
Standard deviation	5.2	6.7	12.9	13.8

Table D2 Diameter of CNTs synthesized from eucalyptus oil and 1:1 ferrocene impregnated with nickel nitrate at different synthesis temperature of 700 °C to 900 °C

Counts	CNT diameter (nm)		
	700 °C	800 °C	900 °C
1	11.6	17.3	58.3
2	18.3	23.1	58.3
3	20.8	24.5	59.5
4	20.8	24.5	60.9
5	20.8	24.5	62.0
6	20.8	24.5	62.8
7	23.1	25.9	66.1
8	23.1	25.9	67.4
9	23.1	28.9	68.2
10	23.8	28.9	70.5
11	24.5	28.9	71.2

12	24.5	28.9	71.5
13	24.5	28.9	75.6
14	25.9	31.1	75.8
15	25.9	31.1	75.8
16	25.9	32.7	75.8
17	25.9	32.7	76.0
18	25.9	33.7	78.4
19	28.9	33.7	78.8
20	28.9	34.7	78.8
21	28.9	35.2	79.3
22	28.9	37.0	81.0
23	28.9	37.0	81.2
24	28.9	37.0	81.2
25	28.9	38.8	82.5
26	28.9	38.8	82.9
27	28.9	38.8	83.5
28	28.9	38.8	84.4
29	28.9	40.5	87.0
30	28.9	40.5	87.0
31	29.5	40.5	88.3
32	29.5	40.5	88.5
33	29.5	40.5	88.8
34	31.1	40.9	89.2
35	31.1	40.9	90.0
36	31.1	40.9	90.2
37	31.1	40.9	90.5
38	32.7	41.7	91.3
39	32.7	41.7	92.2
40	32.7	41.7	93.5
41	32.7	41.7	94.4
42	32.7	41.7	94.9
43	33.7	42.1	95.1
44	33.7	42.1	96.2
45	33.7	44.0	96.5
46	33.7	44.0	97.2
47	33.7	46.2	98.6
48	34.7	46.6	99.1
49	34.7	46.6	99.1
50	35.2	46.6	99.3
51	35.2	46.6	99.3
52	36.6	47.7	99.8
53	36.6	47.7	100.3

54	37.0	49.0	104.2
55	37.0	49.0	104.2
56	37.0	49.4	104.5
57	37.0	49.4	104.5
58	37.0	49.4	104.7
59	38.8	49.4	105.1
60	38.8	49.7	105.2
61	40.5	49.7	107.8
62	40.5	49.7	108.5
63	40.5	51.7	108.9
64	40.5	51.7	108.9
65	40.9	52.0	108.9
66	40.9	52.0	109.4
67	40.9	52.3	109.6
68	41.7	53.3	110.1
69	41.7	53.3	112.0
70	42.1	53.3	114.2
71	42.1	53.3	115.9
72	42.1	54.5	116.1
73	44.0	54.8	116.5
74	44.0	54.8	116.7
75	44.0	56.9	116.8
76	45.1	57.2	117.2
77	45.1	57.2	117.4
78	45.1	57.2	117.4
79	46.2	57.8	119.4
80	46.6	57.8	119.5
81	46.6	57.8	120.6
82	46.6	58.1	121.7
83	46.6	58.9	122.3
84	46.6	60.3	124.5
85	47.7	60.3	125.9
86	47.7	60.3	127.1
87	49.0	61.4	127.3
88	49.0	62.5	127.7
89	49.7	64.6	129.1
90	49.7	64.6	129.6
91	52.0	64.6	133.5
92	52.0	65.4	133.8
93	52.3	65.9	135.6
94	53.3	67.4	137.8
95	53.3	67.4	138.3

96	53.3	67.7	140.6
97	53.3	68.4	145.3
98	54.5	69.6	149.2
99	56.9	70.6	157.8
100	60.3	74.0	157.8
Average	36.5	46.6	100.8
Standard deviation	10.1	12.9	23.2

Table D3 Diameter of CNTs synthesized from different molar ratio of eucalyptol to 4:1 ferrocene impregnated with nickel nitrate of 5:1 and 10:1

Counts	CNT diameter (nm)	
	5:1	10:1
1	23.8	32.4
2	33.7	33.0
3	33.7	33.9
4	34.7	35.0
5	34.7	36.9
6	35.2	37.1
7	36.6	37.6
8	36.6	38.9
9	36.6	38.9
10	36.6	38.9
11	37.0	39.0
12	37.0	41.1
13	37.0	42.1
14	37.0	43.0
15	37.0	43.0
16	37.0	43.4
17	38.8	43.5
18	38.8	44.0
19	38.8	44.2
20	38.8	44.3
21	38.8	44.3
22	38.8	45.1
23	38.8	45.1
24	38.8	45.3
25	38.8	46.7
26	40.9	46.7
27	40.9	46.8
28	40.9	47.0
29	40.9	47.1

30	40.9	47.5
31	41.7	47.5
32	41.7	48.2
33	41.7	48.2
34	41.7	48.2
35	41.7	49.1
36	41.7	49.1
37	41.7	49.5
38	41.7	49.5
39	42.1	49.6
40	42.1	49.8
41	42.1	49.9
42	42.1	49.9
43	42.1	50.5
44	44.0	50.6
45	44.0	51.3
46	44.0	51.5
47	44.0	51.6
48	44.0	52.0
49	44.0	52.1
50	44.0	52.1
51	44.0	52.2
52	45.1	52.8
53	45.1	53.3
54	45.1	53.8
55	45.1	54.1
56	45.1	54.8
57	46.2	55.1
58	46.2	55.6
59	46.2	55.6
60	46.2	56.1
61	46.2	56.2
62	46.6	57.0
63	46.6	57.0
64	46.6	57.8
65	46.6	57.8
66	46.6	58.0
67	46.6	58.2
68	46.6	58.2
69	46.6	58.2
70	47.7	58.5
71	47.7	58.5

72	47.7	58.5
73	47.7	58.7
74	47.7	60.2
75	47.7	60.9
76	49.0	61.3
77	49.0	61.4
78	49.4	61.4
79	49.4	61.4
80	49.7	61.5
81	49.7	63.6
82	49.7	63.8
83	51.7	64.9
84	51.7	65.4
85	51.7	65.9
86	51.7	66.0
87	51.7	66.0
88	52.3	66.8
89	52.3	67.7
90	53.3	69.6
91	53.3	69.9
92	53.3	70.4
93	53.3	71.5
94	56.9	73.1
95	57.2	74.5
96	58.1	76.4
97	58.9	76.8
98	58.9	102.9
99	61.4	105.4
100	61.4	120.8
Average	44.6	54.8
Standard deviation	6.7	14.1

APPENDIX E

Calculation of Outlet Gas Flowrate from Reactor

During MCNT synthesis, flowrates of outlet gas were measured by soap-film meter which are shown in **Table E1-E2**. A soap-film meter had an inner diameter ($2r$) of 0.019 m and the time that soap-film moved for height (h) of 0.15 m, Lapse time, was measured.

Therefore, the volume (V) which gas flown,

$$V = \pi r^2 h = \pi \left(\frac{0.019}{2}\right)^2 (0.15) = 4.25 \times 10^{-5} m^3$$

After that, flowrate of outlet gases (F) was calculated by dividing the volume with lapse time. For example, at synthesis temperature of 900 °C, lapse time was equal to 5.27 second

$$F = \frac{V (m^3)}{\text{Lapse time (s)}} = \frac{4.25 \times 10^{-5}}{5.27} = 8.07 \times 10^{-6} m^3/s$$

Converting to cm^3/min unit,

$$F = 8.07 \times 10^{-6} \frac{m^3}{s} \times \frac{10^6 cm^3}{m^3} \times \frac{60 s}{min} = 484 cm^3/min$$

Table E1 Flowrate of outlet gases in MCNT synthesis at different synthesis temperature

Process time (min)	700 °C		800 °C		900 °C	
	Lapse times (s)	Flowrate (cm ³ /min)	Lapse times (s)	Flowrate (cm ³ /min)	Lapse times (s)	Flowrate (cm ³ /min)
1	Clock time < 2s					
2	6.18	412.9	6.07	420.4	5.27	484.2
3	6.41	398.1	6.49	393.2	5.60	455.7
4	7.03	363.0	6.21	410.9	6.03	423.2
5	6.79	375.8	5.22	488.8	5.97	427.4
6	5.53	461.4	4.72	540.6	5.45	468.2
7	4.98	512.4	4.27	597.6	4.15	614.9
8	4.88	522.9	4.07	627.0	3.99	639.5
9	4.89	521.8	3.68	693.4	3.88	657.7
10	4.88	522.9	3.63	703.0	3.66	697.2
11	4.91	519.7	3.55	718.8	3.48	733.3
12	4.92	518.7	3.68	693.4	3.42	746.1
13	4.88	522.9	3.80	671.5	3.31	770.9
14	4.92	518.7	3.83	666.3	3.40	750.5
15	4.87	524.0	4.60	554.7	3.65	699.1
16	4.97	513.4	5.17	493.6	4.39	581.3
17	5.08	502.3	5.50	464.0	4.80	531.6
18	5.95	428.9	6.27	407.0	5.06	504.3
19	6.29	405.7	6.44	396.2	5.24	487.0
20	6.32	403.8	6.52	391.4	5.36	476.1
21	6.46	395.0	6.63	384.9	5.37	475.2
22	6.61	386.0	6.71	380.3	5.45	468.2
23	6.52	391.4	6.80	375.3	5.47	466.5
24	6.71	380.3	6.87	371.4	5.52	462.3
25	6.57	388.4	6.89	370.4	5.57	458.1
26	6.59	387.2	6.87	371.4	5.72	446.1
27	6.80	375.3	6.87	371.4	5.74	444.6
28	6.93	368.2	6.95	367.2	5.78	441.5
29	6.76	377.5	6.99	365.1	5.80	440.0
30	6.76	377.5	7.04	362.5	5.89	433.2

Table E2 Flowrate of outlet gases in MCNT synthesis at different molar ratio of eucalyptus oil to catalyst

Process time (min)	2:1		5:1		10:1	
	Lapse times (s)	Flowrate (cm ³ /min)	Lapse times (s)	Flowrate (cm ³ /min)	Lapse times (s)	Flowrate (cm ³ /min)
1	Clock time < 2s					
2	6.27	407.0	6.98	365.6	5.73	445.3
3	6.51	392.0	6.83	373.6	5.97	427.4
4	6.56	389.0	5.57	458.1	5.13	497.4
5	6.48	393.8	4.49	568.3	2.83	901.7
6	6.44	396.2	4.30	593.4	2.24	1,139.2
7	6.36	401.2	4.25	600.4	2.20	1,159.9
8	6.24	408.9	4.19	609.0	2.12	1,203.7
9	6.19	412.2	4.14	616.4	2.70	945.1
10	5.99	426.0	4.17	611.9	2.83	901.7
11	5.71	446.9	4.31	592.1	2.78	917.9
12	5.73	445.3	4.42	577.3	2.79	914.6
13	5.72	446.1	4.36	585.3	2.82	904.9
14	4.49	568.3	4.52	564.5	2.86	892.2
15	4.59	555.9	4.60	554.7	3.43	744.0
16	5.12	498.4	4.95	515.5	4.07	627.0
17	5.51	463.1	5.13	497.4	4.53	563.3
18	5.78	441.5	5.61	454.9	4.89	521.8
19	5.92	431.0	5.81	439.2	5.40	472.5
20	6.00	425.3	5.81	439.2	5.56	459.0
21	6.01	424.6	5.93	430.3	5.67	450.0
22	6.10	418.3	6.02	423.9	5.70	447.7
23	6.09	419.0	6.04	422.5	5.67	450.0
24	6.11	417.6	6.04	422.5	5.87	434.7
25	6.18	412.9	6.19	412.2	5.90	432.5
26	6.22	410.3	6.23	409.6	5.91	431.8
27	6.28	406.3	6.18	412.9	5.89	433.2
28	6.26	407.6	6.20	411.6	5.97	427.4
29	6.28	406.3	6.25	408.3	6.02	423.9
30	6.50	392.6	6.36	401.2	6.13	416.3

APPENDIX F

Effect of Fe to Ni Molar Ratio on Resultant CNTs

This section is study of molar ratio of Fe to Ni on synthesized MCNT properties. Ferrocene impregnated with nickel nitrate were prepared at 4:1 and 1:1 molar ratio of Fe to Ni. The catalysts were called 4:1 ferrocene impregnated with nickel nitrate and 1:1 ferrocene impregnated with nickel nitrate, respectively. MCNTs were produced from co-pyrolysis of eucalyptus oil and the catalysts.

SEM images of MCNTs synthesized from eucalyptus oil with 4:1 ferrocene impregnated with nickel nitrate and eucalyptus oil with 1:1 ferrocene impregnated with nickel nitrate is demonstrated in **Fig F1a-F1b**. CNTs synthesized from each catalyst were labeled as CNT_F1N0.25 and CNT_F1N1, respectively. **Fig F1a** shows lower amount of irregular shape carbon in sample than **Fig F1b**. Additionally, their CNT diameter ranges were 45 ± 7 nm and 47 ± 13 nm as shown in CNT diameter distribution in **Fig F2a-F2b**. The results suggested the addition nickel nitrate could be enhanced CNT diameter.

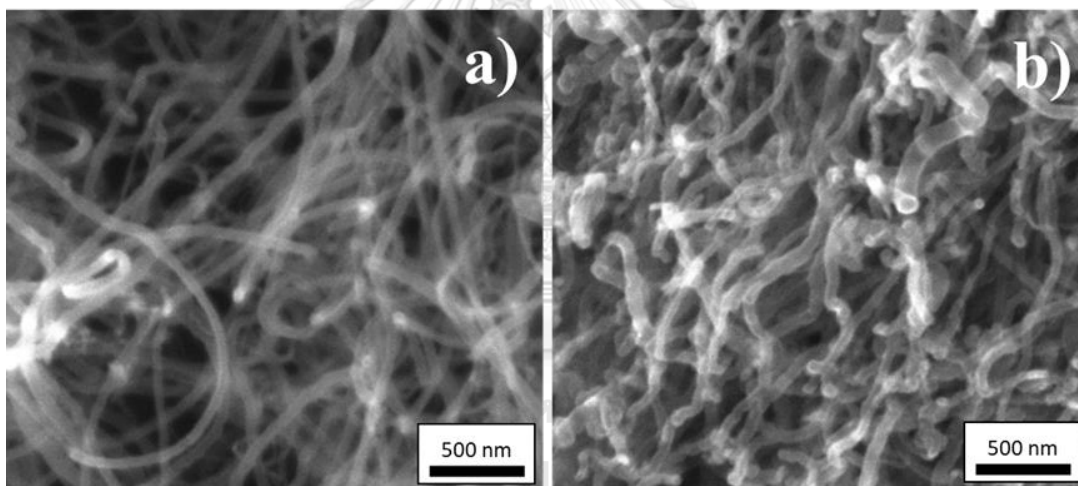


Fig. F1 SEM images of MCNTs synthesized by using eucalyptus oil and a) 4:1 ferrocene impregnated with nickel nitrate and b) 1:1 ferrocene impregnated with nickel nitrate

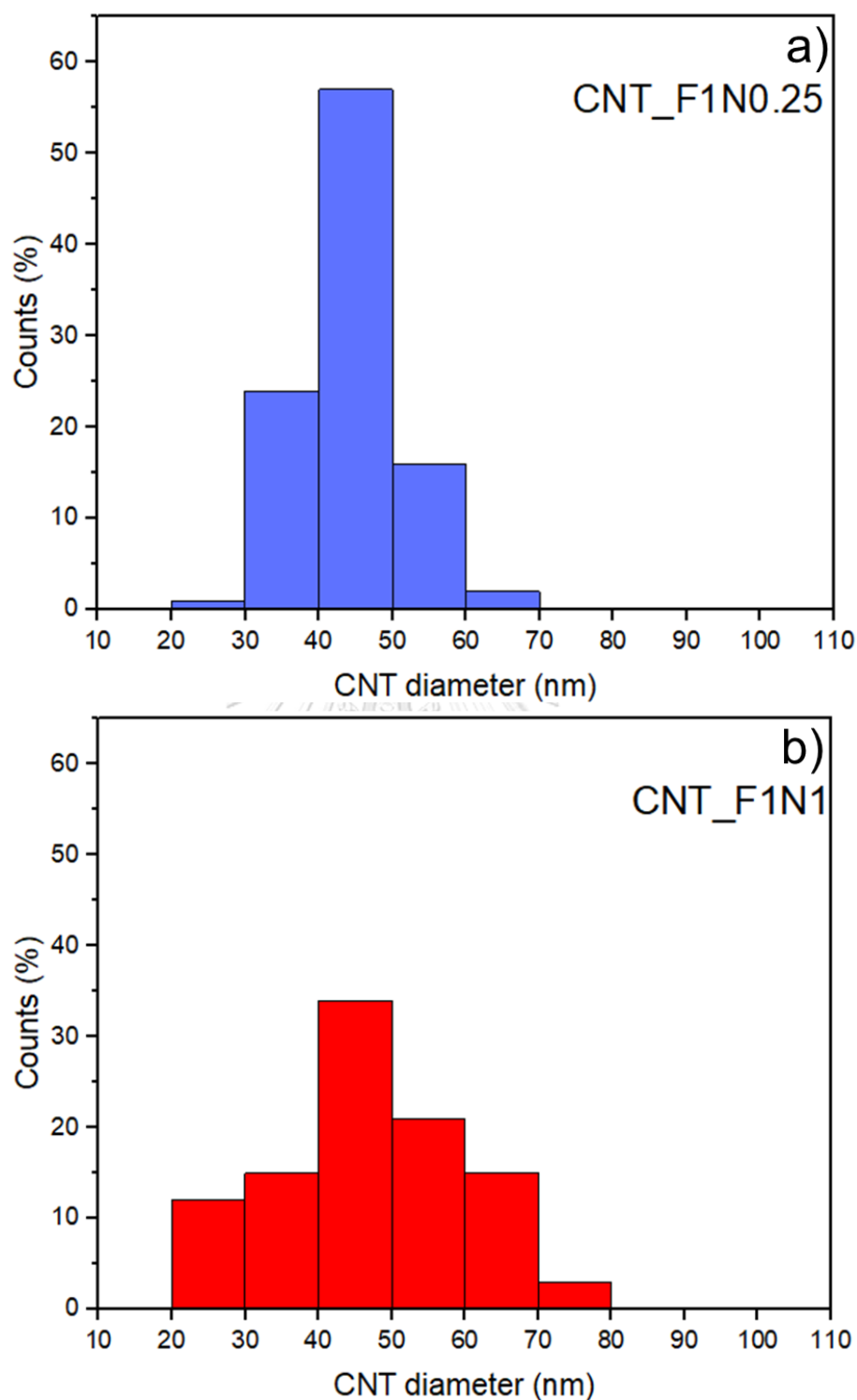


Fig. F2 CNT diameter distribution of MCNTs synthesized using eucalyptus oil and a) 4:1 ferrocene impregnated with nickel nitrate and b) 1:1 ferrocene impregnated with nickel nitrate

TGA curves and DTG curves are shown in **Fig F3a-F3b**. **Fig. F3a** reveals that CNT_F1N0.25 and CNT_F1N1 were started to decompose at temperature of 467 °C and 473 °C respectively. Additionally, **Fig. F3b**, illustrates DTG curves of

CNT_F1N0.25 and CNT_F1N1 indicated the peaks at oxidation temperature of 559 °C and 579 °C. These results suggested that a high proportion of nickel nitrate in catalyst could be increased thermal stability of CNTs. The results could confirm more Ni content could improve thermal stability of CNTs.

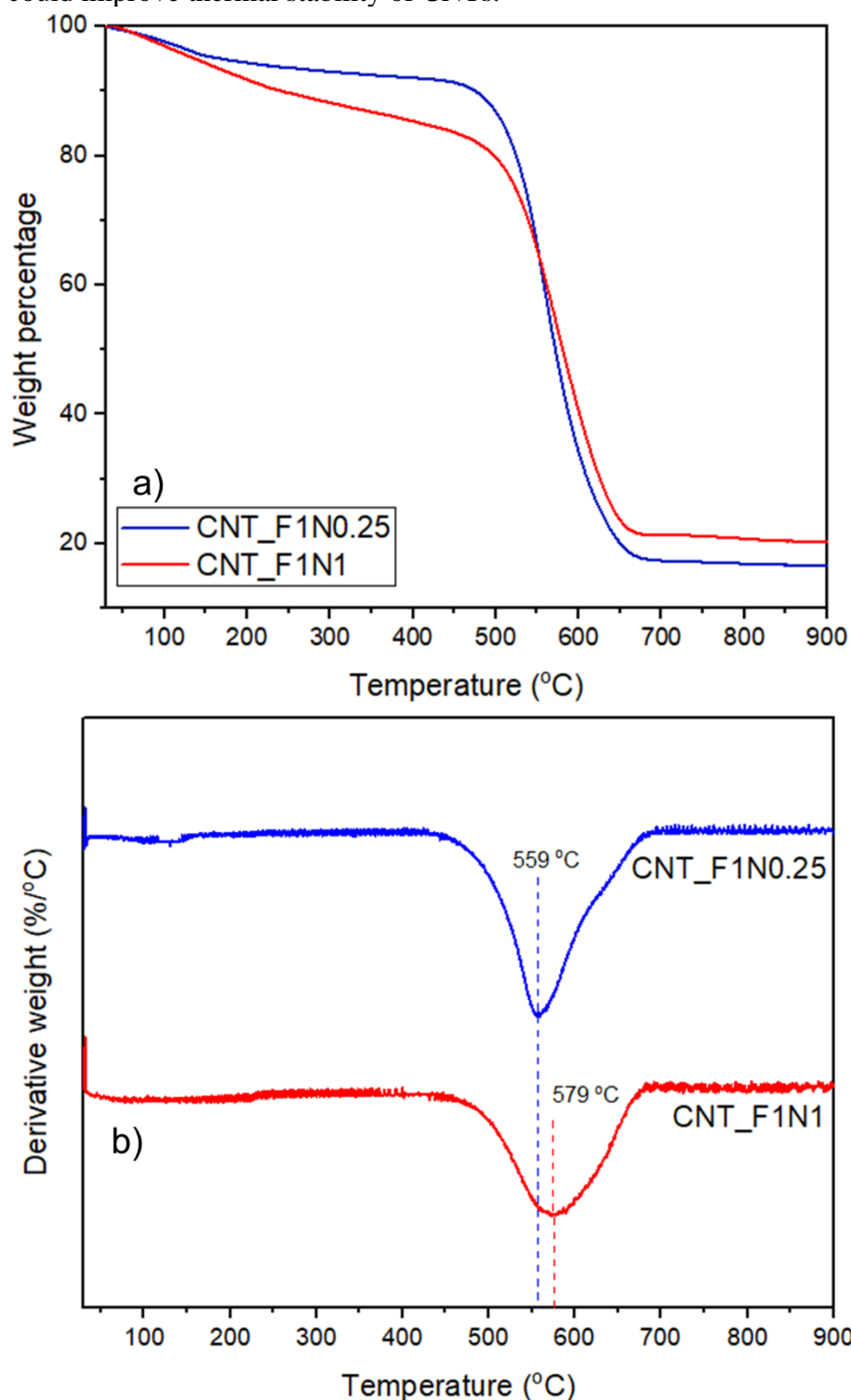


Fig. F3 a) TGA curves and b) DTG curves of CNTs synthesized from eucalyptus oil and ferrocene impregnated nickel nitrate at different Fe to Ni molar ratio

Raman spectra of CNT_F1N0.25 and CNT_F1N1 is illustrated in **Fig. 54**. D-band at Raman shift $1,323\text{ cm}^{-1}$ attributes the vibration of non- sp^2 bonded carbon atom. The band is applied to identify amorphous carbon or defect structure. G-band at Raman shift $1,588\text{ cm}^{-1}$ assigns to the vibration of sp^2 bonded carbon atom. The band is used to identify CNT structure [56]. I_D/I_G ratio was used to indicate crystallinity of MCNTs. I_D/I_G ratio increased from 0.83 to 1.05 because of lack of H_2 resource in catalyst. These results could be supported by Mitina et al. [38]. The I_D/I_G ratio of CNTs raised from 0.95 to 1.55 when did not added ethanol as hydrogen precursor in nickel nitrate catalyst. H_2 from decomposed ethanol would not supply for nickel nitrate reduction to nickel catalyst. From these results, the reduction process was essential to produce catalyst for adequate MCNT formation.

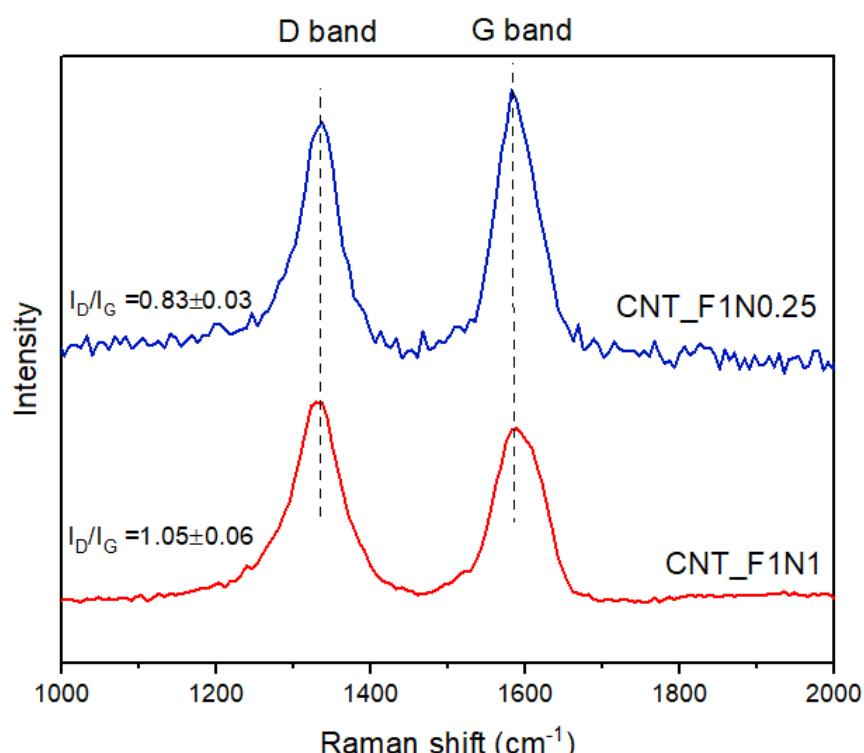


Fig. F4 Raman spectra of CNTs synthesized by using eucalyptus oil and ferrocene impregnated nickel nitrate with different Fe to Ni molar ratio

Total mass yield was decreased from $17.1 \pm 1.7\%$ to $13.9 \pm 1.2\%$ when 4:1 ferrocene impregnated with nickel nitrate and 1:1 ferrocene impregnated with nickel nitrate were used, respectively. The reduction in total mass yield could be originated by (i) agglomeration of catalyst particles and (ii) lack of H_2 precursor in catalyst.

XRD patterns of CNT_F1N0.25 and CNT_F1N1 are demonstrated in **Fig. 55**. The crystallinity peaks of CNT_F1N0.25 and CNT_F1N1 indicate diffraction peak of graphite at $2\theta = 26.5^\circ$ which can be assigned to (002) planes of CNTs (PDF 03-065-6212). FeNi_3 peaks also show at $2\theta = 44.3^\circ$, 51.6° , and 75.7° which match with (111), (200), and (222) planes of the bimetallic Ni-Fe (PDF 00-038-0419). These peaks of FeNi_3 could confirm interaction between Fe and Ni. The Scheler equation was then

applied to calculate the crystallite size of FeNi_3 . For CNT_F1N0.25 and CNT_F1N1, FeNi_3 crystallite size increased from 13.0 nm to 14.3 nm, respectively. These results could support that average diameter of CNT_F1N0.25 and CNT_F1N1 was increased from 45 nm to 47 nm due to FeNi_3 particle size enhancement from addition of nickel nitrate. Thus, the increment of crystalline size could be attributed to a reduction in surface area from an agglomeration of FeNi_3 catalysts.

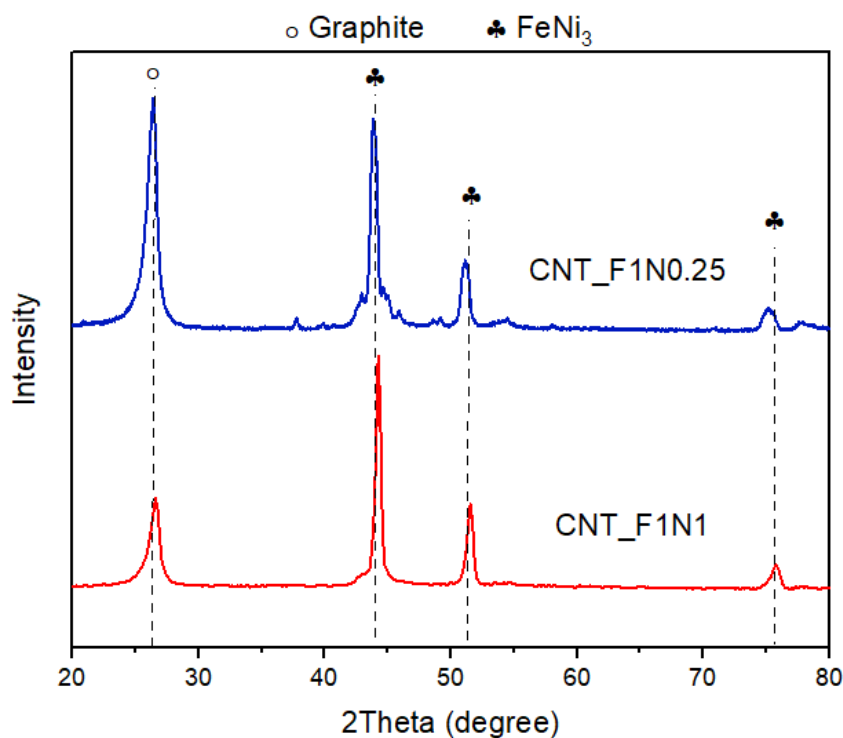


Fig. F5 XRD patterns of CNTs synthesized by using eucalyptus oil and ferrocene impregnated nickel nitrate with different Fe to Ni molar ratio

From discussion in **section 4.1.5**, H_2 was essential oxidizing agent for NiO reduction to active Ni catalyst. The decrease in ferrocene proportion of catalyst could result in reduction of total mass yield. The results were in good agreement with Mitina et al. [38], suggesting that hydrogen precursor in nickel nitrate catalyst (or ethanol in their experiment) would provide higher activity catalyst. CNT yield was increased when ethanol was added to the catalyst from 17.5% to 25.0%. However, the uses of 1:1 ferrocene impregnated with nickel nitrate could obtain lower total mass yield because lower H_2 source from ferrocene reduced NiO.

Magnetic property of MCNTs could be measured by VSM. Hysteresis loops of CNT_F1N0.25 and CNT_F1N1 demonstrate in **Fig F6a-F6b**. The all shapes of the hysteresis loop indicated ferromagnetic properties at room temperature. M_s values of CNT_F1N0.25 and CNT_F1N1 were 20.6 emu/g and 33.0 emu/g. The results suggested that adding nickel nitrate of catalyst could enhance M_s of MCNTs. In the cases of this study, the addition of Ni content to the Fe-rich region enhances electron distribution

because the number of positive-spin electrons was raised and hence a decline of magnetic moment [62]. Another possible reason of the M_s increment is low diamagnetic effect from carbon because influence of carbon atoms could be rearrangement of magnetic moment [71]. There are some studies of effect of Fe to Ni molar ratio on magnetic properties. From Xu et al. [47], the M_s of MCNTs was increased from 3.32 emu/g to 8.32 emu/g when used 3:1 to 2:2 molar ratio of Fe to Ni molar ratio of catalyst, respectively. From Dong et al. [49], the M_s of MCNPs was enhanced from 34.3 emu/g to 55.6 emu/g and 109.1 emu/g when Fe to Ni molar ratio of catalyst used was reduced from 6.0:1 to 2.5:1 and 1.3:1. These results indicated increasing in Ni content in Fe catalyst with low carbon content of MCNPs affected increment of M_s .

H_c values of CNT_F1N0.25 and CNT_F1N1 were 200.7 G and 118.0 G, respectively. The results suggested that decreasing proportion of ferrocene of catalyst could reduce H_c of MCNTs. For CNT_F1N0.25 and CNT_F1N1, $FeNi_3$ crystallite size increased from 13.0 nm to 14.3 nm, respectively. The increase in crystalline size is consistent with average diameter enhancement from 45 nm to 47 nm for CNT_F1N0.25 and CNT_F1N1, respectively. Both of results confirmed larger $FeNi_3$ particles of CNT_F1N1 than CNT_F1N0.25. The decrease in H_c was caused multi-domain properties of particles [34, 35]. These results compare with H_c value of Bulk $FeNi_3$ is 66 G [68], the enhanced value of H_c was obtained in case of CNT_F1N0.25 and CNT_F1N1. The high H_c could relate to the magnetic particle alignment and nanotube structure of samples [72]. From Xu et al. [47], H_c values of MCNTs decreased from 207 G to 68 G when CNTs were synthesized by use of less Fe content from 3:1 to 2:2 molar ratio of Fe to Ni. Crystalline size of bimetallic Ni-Fe also increased from 13.9 nm to 27.9 nm. These results indicated the increment of Fe proportion in bimetallic Ni-Fe could be induced H_c .

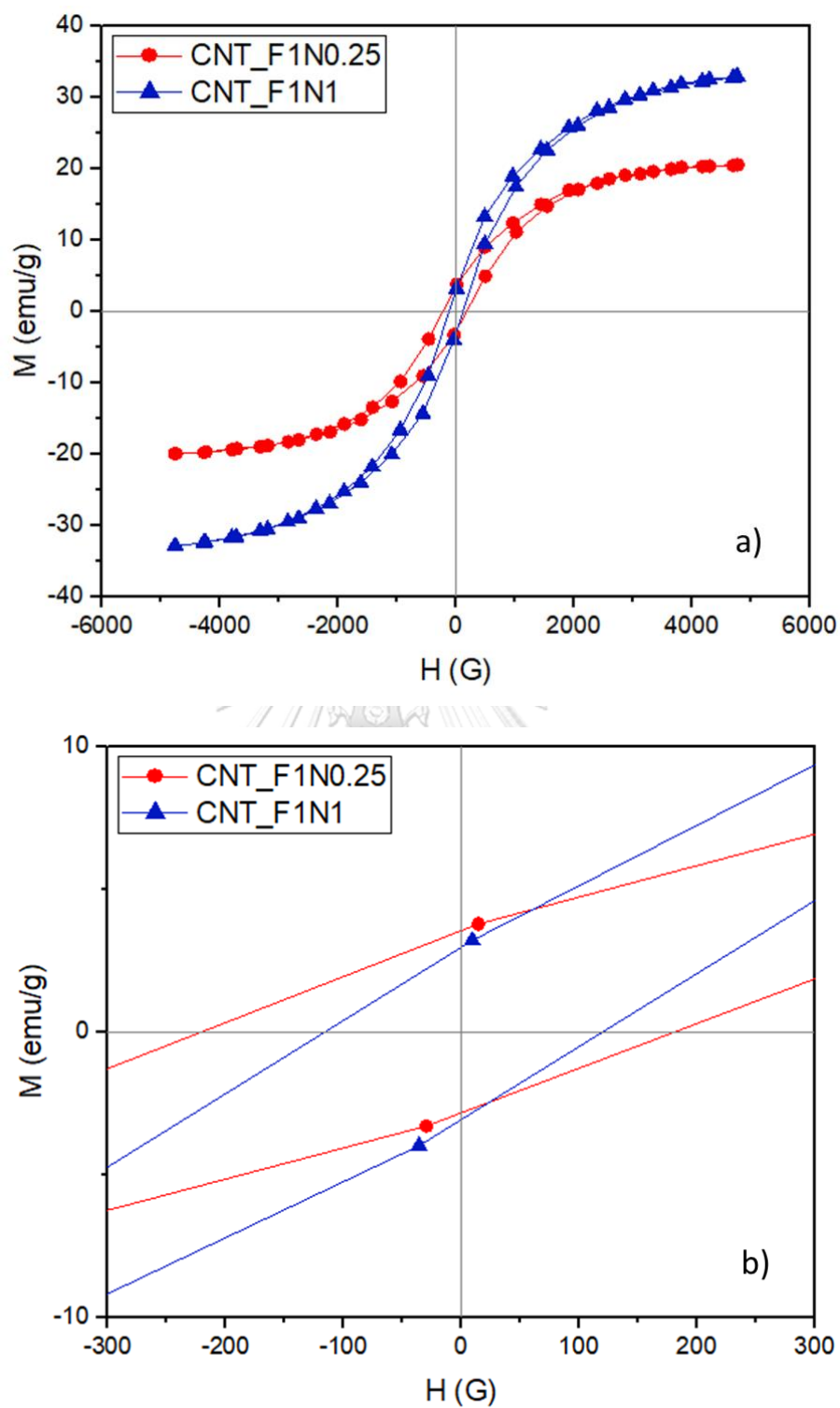


Fig. F6 Magnetic hysteresis loops of as-synthesized CNTs by using eucalyptus oil ferrocene impregnated nickel nitrate with different Fe to Ni molar ratio in a) a whole range and b) magnified range of -300 G to 300 G

Consideration on total mass yield with respect to catalyst could not clearly provide a viewpoint of MCNT synthesis improvement. Focuses of yield from eucalyptus oil and unit mass of catalyst would suggest performance of catalyst. Yield from eucalyptus oil could be calculated from **Eq F1**. Product yield per unit mass of catalyst was determined based on **Eq F2**.

$$\text{Yield from eucalyptus oil} = \frac{W_P - W_{P,cat}}{W_{oil}} \times 100 \quad \text{Equation F1}$$

$$\text{Product yield per unit mass of catalyst} = \frac{W_P}{W_{cat}} \quad \text{Equation F2}$$

Where

W_P = weight of synthesized product from eucalyptus oil and catalyst

$W_{P,cat}$ = weight of synthesized product from catalyst

W_{oil} = weight of eucalyptus oil

W_{cat} = weight of catalyst

Table F1 demonstrates results of weight of pyrolyzed catalyst and product weight from MCNT production at synthesis temperature of 800 °C at 5:1 molar ratio of eucalyptus oil to catalyst. Yield calculation is also shown in this table. 4:1 ferrocene impregnated with nickel nitrate could provide the highest total mass yield of 17.1%, indicating its catalyst performance of eucalyptus oil consumption to carbon in MCNT synthesis. The highest yield from eucalyptus oil of 17.9% could confirm this evidence. Product yield per unit mass of catalyst was also the highest value of 0.89, illustrating there was the highest MCNT production. These results could assure 4:1 ferrocene impregnated with nickel nitrate catalyst was the best catalyst in these experimental.

Table F1 Weight of pyrolyzed catalysts, products, total mass yield, yield from eucalyptus oil, and product yield per unit mass of catalyst

Catalyst	$W_{P,cat}$ (g)	W_P (g)	Total mass yield (%)	Yield from eucalyptus oil (%)	Carbon product/Catalyst (w/w)
Ferrocene	0.0293	0.4228	15.60	15.56	0.8456
4:1 ferrocene impregnated with nickel nitrate	0.0345	0.4883	17.09	17.94	0.8878
1:1 ferrocene impregnated with nickel nitrate	0.0621	0.4070	13.90	13.63	0.6565
Nickel nitrate	0.0945	0.2166	7.72	4.83	0.2927

APPENDIX G

Inlet Gas Volumetric Flowrate Calculation

In study of effect of molar ratio of eucalyptus oil to catalyst on resultant MCNTs, space time was calculated to explain results of total mass yield. Space time was calculated from **Eq 4**. In this part, calculation of total inlet volumetric flowrate of nitrogen gas and eucalyptus oil (v_0) is described in detail. All gas in MCNT synthesis were assumed as ideal gas. Total gas flowrate was calculated from **Eq G1**.

$$v_0 = v_{N_2} + v_{oil} \quad \text{Equation G1}$$

Where

v_{N_2} = inlet volumetric flowrate of nitrogen gas

v_{oil} = inlet volumetric flowrate of eucalyptus oil

For v_{N_2} calculation, it was calculated from **Eq G2**.

$$\frac{P_{in}v_{N_2,in}}{T_{in}} = \frac{Pv_{N_2}}{T} \quad \text{Equation G2}$$

Where

P_{in} = pressure of nitrogen gas feed (2 atm)

P = pressure of system (1 atm)

$v_{N_2,in}$ = feed volumetric flowrate of nitrogen gas (51 cm³/min)

T_{in} = room temperature (298 K)

T = synthesis temperature (1,073 K)

For v_{oil} calculation, it was calculated from **Eq G3**. Vapor pressure of eucalyptus oil at synthesis temperature of 800 °C (1,073 K) was estimated from Clausius Clapeyron equation as shown in **Eq G4**. Vapor pressure at reference temperature for this approximation was calculated from Antonine equation demonstrating at **Eq G5**. Heat of eucalyptus oil vaporization and Antonine constant are referred from Hazra et al [77].

$$P^*v_{oil,in} = Pv_{oil} \quad \text{Equation G3}$$

$$\log\left(\frac{P^*}{P_{ref}^*}\right) = \frac{\Delta H_{vap}}{2.303R} \left(\frac{1}{T_{ref}} - \frac{1}{T}\right) \quad \text{Equation G4}$$

$$P_{ref}^* = A - \frac{B}{T_{ref}+C} \quad \text{Equation G5}$$

Where

P^* = vapor pressure of eucalyptus oil at synthesis temperature of 1,073 K

$v_{oil,in}$ = feed volumetric flowrate of eucalyptus oil (0.18 or 0.37 cm³/min)

P_{ref}^* = vapor pressure of eucalyptus oil at reference temperature (Pascal)

ΔH_{vap} = heat of eucalyptus oil vaporization (39.92 kJ/mol)

R = gas constant (8.3145 J/ mol K)

T_{ref} = reference temperature (410 K)

A, B, C = Antonine constants which are 8.279, 2402.808, and 273.15, respectively (for temperature range of 356-410 K)

Table G1 Inlet volumetric flowrate of nitrogen gas and eucalyptus oil at different molar ratio of eucalyptus oil to catalyst

Molar ratio of eucalyptus oil to catalyst	v_{N_2} (cm ³ /min)	v_{oil} (cm ³ /min)
5:1	367.27	145.46
10:1		290.92

VITA

NAME Tanapat Rodruangnon

DATE OF BIRTH 14 May 1997

PLACE OF BIRTH Songkhla

INSTITUTIONS ATTENDED

M.Eng.
August 2019- Present
Major: Chemical Engineering
Chulalongkorn University, Bangkok, Thailand

B.Eng.
August 2015-May 2019
Major: Chemical Engineering
Prince of Songkla University, Songkhla, Thailand

HOME ADDRESS Songkhla

PUBLICATION

Tanapat Rodruangnon, Giang T. T. Le, Kritapas Laohhasurayotin, Pohnpawee Nontasorn, and Tawatchai Charinpanitkul, "Effect of Weight Ratio of Eucalyptus Oil to Ferrocene on Magnetic Property of Carbon Nanoparticles" Proceeding of the 9th Joint Conference on Renewable Energy and Nanotechnology (JCREN2020), Khon Kaen, Thailand, October 29th, 2020.

Tanapat Rodruangnon, Giang T. T. Le, Samicha Ayukan, Kritapas Laohhasurayotin, Pohnpawee Nontasorn, and Tawatchai Charinpanitkul, "Effect of Ferrocene Impregnated with Nickel Nitrate on Characteristics of Magnetic Carbon Nanoparticles Synthesized from Eucalyptus Oil", Proceeding of the 10th Joint Conference on Renewable Energy and Nanotechnology (JCREN2021), Chiba, Japan, November 27th, 2021.